# Plasmonic excitations in carbon nanostructures: carbon nanotubes and graphene layers*

Pablo Martín-Luna

Email: pablo.martin@uv.es

*Work in collaboration with NOVAS group (ICMUV)

11 MARCH 2025, VALENCIA, SPAIN

# Contents

# 1. Introduction

- The current state-of-the-art of the RF techniques for particle acceleration is limited to gradients on the order of 100 MV/m
- To obtain higher energies, we can increase the length of the accelerators... or use new techniques of acceleration with higher gradients

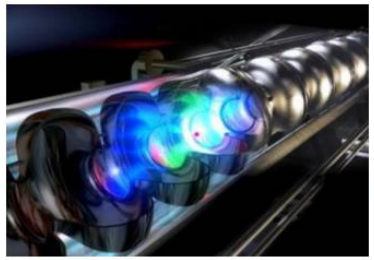

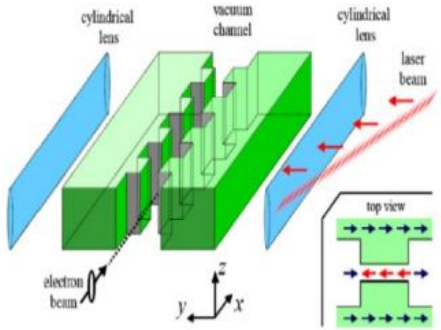


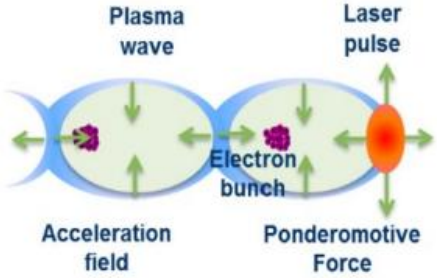


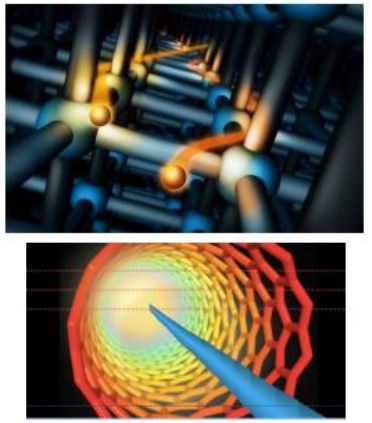

| | Conventional RF cavities | Dielectric laser – driven acceleration (DLA) | Plasma / Laser wakefield acceleration (PWFA / LWFA) | Solid-state plasma wakefield acceleration |
|---|---|---|---|---|
| **Based on** | Normal / superconducting cavities | Quartz / silicon structure | Gaseous plasma | Crystals, nano-channels, CNTs |
| **Max. longitudinal electric field** | $\sim 100$ MV/m | $\sim 10$ GV/m | $\sim 100$ GV/m | $\sim 1 - 100$ TV/m (prediction) |
| **Limitation** | Surface breakdown | Damage threshold | Wave breaking | Wave breaking |

# 1. Introduction

- Plasma-based accelerators → GeV/cm accelerating gradients (wakefield amplitude increases with plasma density):

$$E_0[\mathrm{V/m}] = \frac{m_e c \omega_p}{e} \approx 96\sqrt{n_0[\mathrm{cm^{-3}}]}$$

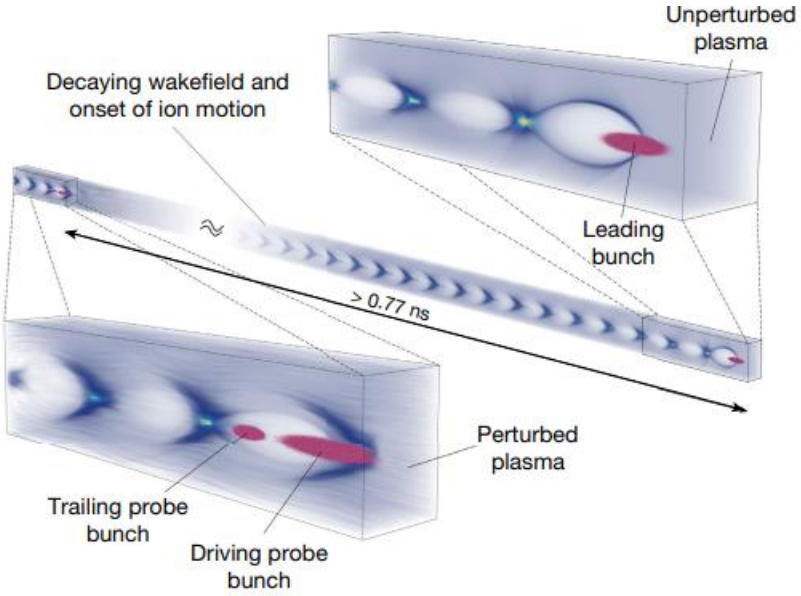


- Density of charge carriers in solids → 4–5 orders of magnitude higher than those in a gaseous plasma
- Solid-based acceleration media, such as crystals or nanostructures, could enable ultra-high gradients, on the order of $E_0$~ 1–10 TV/m

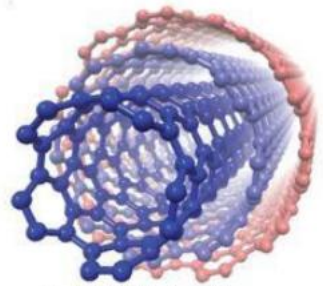

Multi-Walled carbon NanoTube (MWNT)

- If compared to natural crystals, 2D carbon-based structures could help achieving more realistic regimes:
  - larger dimensional flexibility / thermomechanical strength
  - transverse acceptances of up to ~100 nm (3 orders of magnitude higher than a typical silicon channel)
  - lower dechanneling rate
- 2D carbon-based materials (graphene, CNT) are good candidates to be used as ultra-compact accelerating structures

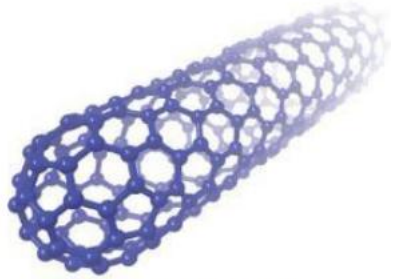

Single-Walled NanoTube (SWNT)

# 1. Introduction

- **Plasmonic acceleration**
  - Excitation of surface plasmonic modes by laser (laser-driven) or charged particle beam (beam-driven)
  - Collective motion of wall electrons acting like a structured plasma
  - To properly excite wakefields laser or beam driving parameters need to be in the time and space scale of the plasmon wave

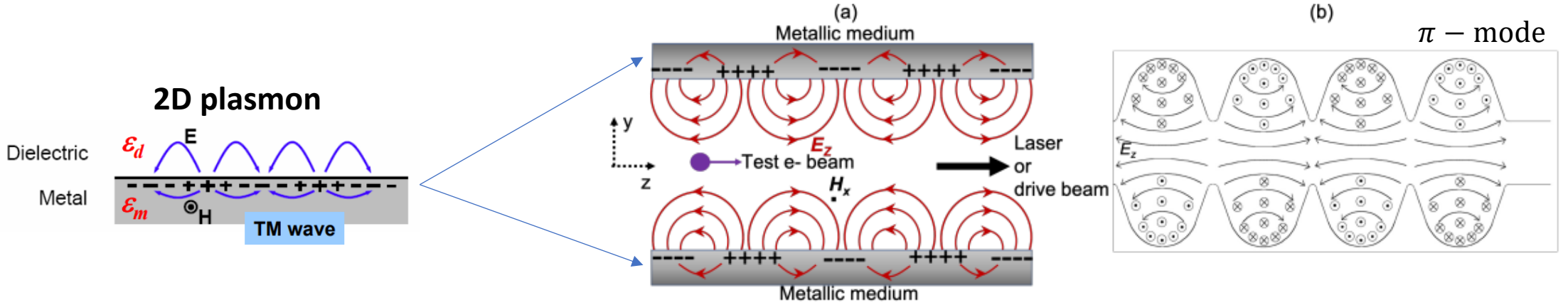


| | Plasmonic acceleration | RF cavities |
|---|---|---|
| Aperture size | ~nm − $\mu$m | ~cm |
| Length | ~mm | ~10cm − m |
| Longitudinal electric field | ~100 GV/m | ~100 MV/m |
| Operation | Travelling wave (TW) | Standing Wave (SW) or TW |

# 1. Introduction

- **Main objectives**
  - Analysis of the excited surface plasmonic modes by a charged particle
  - Optimization of the parameters of the system to obtain the highest longitudinal wakefield
  - Comparison with PIC codes (in progress)

- **I do not study**
  - Acceleration of the witness beam

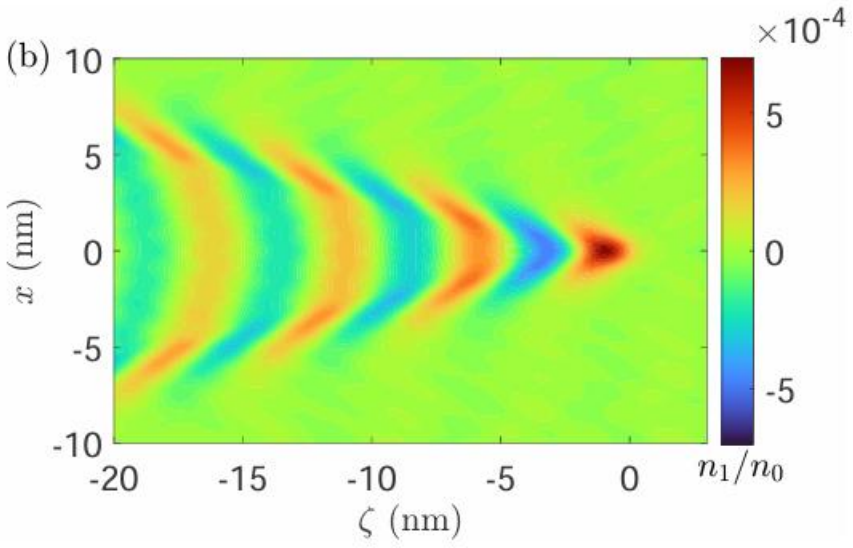


My study

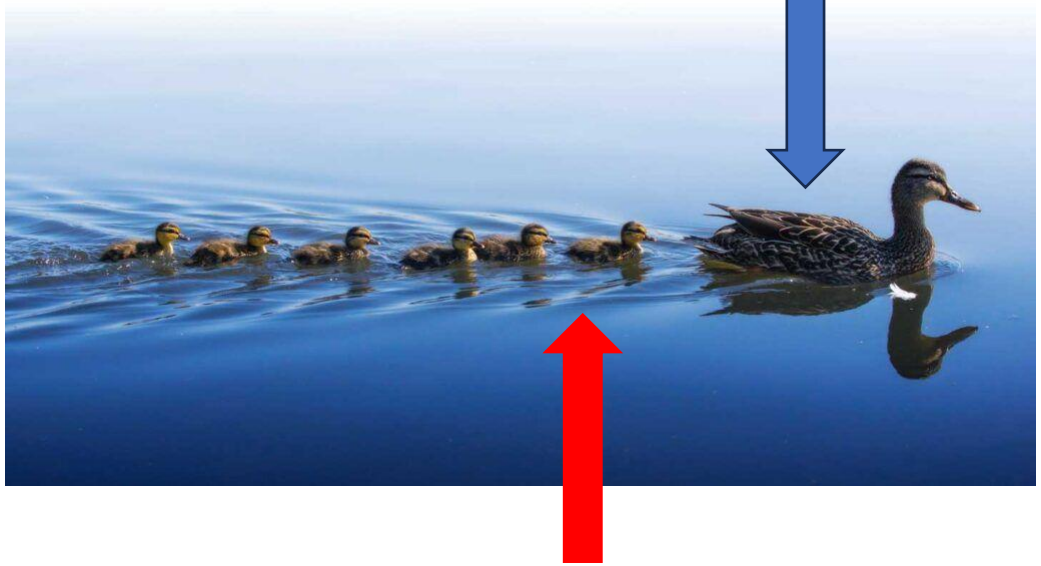

It has to be studied with PIC simulations

# 2. Linearized hydrodynamic model

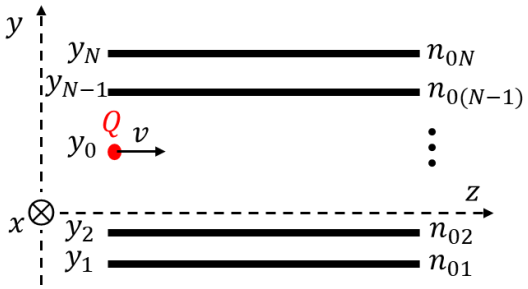


- **Electronic excitation on the j-th wall (linear perturbations):**

(i) the continuity equation

$$\frac{\partial n_j(\mathbf{r_j},t)}{\partial t}+\nabla_j\cdot\left[(n_{0j}+\underbrace{n_j}_{\approx 0})\mathbf{u_j}(\mathbf{r_j},t)\right]\approx\frac{\partial n_j(\mathbf{r_j},t)}{\partial t}+n_{0j}\nabla_j\cdot\mathbf{u_j}(\mathbf{r_j},t)=0$$

$n_j(\mathbf{r_j},t)$: perturbed surface density
$\mathbf{u_j}(\mathbf{r_j},t)$: velocity of the plasma

(ii) the momentum-balance (MB) equation

$$\underbrace{\frac{\partial \mathbf{u_j}(\mathbf{r_j},t)}{\partial t}}_{\approx 0}+\mathbf{u_j}\cdot[\nabla_j\cdot\mathbf{u_j}(\mathbf{r_j},t)]=\nabla_j\cdot\Phi(\mathbf{r_j},t)-\underbrace{\frac{\alpha_j}{n_{0j}}\nabla_j\cdot n_j(\mathbf{r_j},t)}_{\text{Acoustic modes}}+\underbrace{\frac{\beta}{n_{0j}}\nabla_j\left[\nabla_j^2 n_j(\mathbf{r_j},t)\right]}_{\text{Quantum correction}}-\underbrace{\gamma_j\mathbf{u_j}(\mathbf{r_j},t)}_{\text{Frictional force}}$$

$$\Phi=\Phi_0+\Phi_{\text{ind}}$$

$\alpha_j=v_{Fj}^2/2$, with $v_{Fj}=(2\pi n_{0j})^{1/2}$ $\quad\beta=\frac{1}{4}$

$$\Phi_0(\mathbf{r},t)=\frac{Q}{|\mathbf{r}-\mathbf{r_0}|}$$

Driving charge

$$\Phi_{\text{ind}}(\mathbf{r},t)=-\sum_j\int \mathrm{d}^2\mathbf{r_j}\,\frac{n_j(\mathbf{r_j},t)}{|\mathbf{r}-\mathbf{r_j}|}$$

Perturbed densities

We have to obtain $\mathbf{u_j}$ and $n_j$ from (i) and (ii):
2N coupled partial differential eqs

Atomic units ared used thorought

# 2. Linearized hydrodynamic model

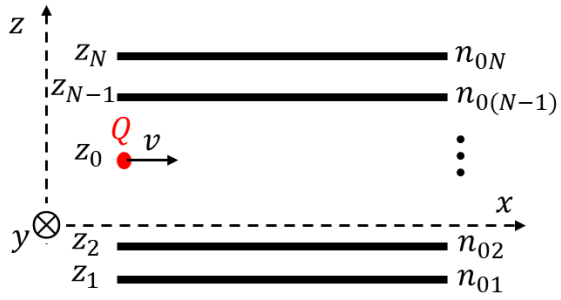


- **Approximations:**
  - Linear approximation: we retain first order terms in $\mathbf{u}_j$ and $n_j$
  - Non-relativistic
  - B-fields are neglected
  - Electrons are constrained to the walls and quasi-free (possible improvement: restoring frequency) BACKUP SLIDES
  - Ion motion is neglected
  - The driver moves at constant velocity

# 2. Linearized hydrodynamic model

- Using the linearized continuity eq., the MB eq. can be expressed in terms of $n_j$:

$$-\left(\frac{\partial^2}{\partial t^2}+\gamma_j\frac{\partial}{\partial t}\right)n_j(\mathbf{r_j},t)=n_{0j}\nabla_j^2\Phi(\mathbf{r_j},t)-\alpha_j\nabla_j^2 n_j(\mathbf{r_j},t)+\beta\nabla_j^2\left[\nabla_j^2 n_j(\mathbf{r_j},t)\right]$$

$$\Phi(\mathbf{r_j},t)=\frac{Q}{|\mathbf{r_j}-\mathbf{r_0}|}-\sum_l\int \mathrm{d}^2\mathbf{r_l}\frac{n_l(\mathbf{r_l},t)}{|\mathbf{r_j}-\mathbf{r_l}|}$$

- To solve it: **Fourier transform**: $t\rightarrow\omega, \mathbf{r_j}\rightarrow\mathbf{k}_\parallel$

$$A(\mathbf{r_j},t)\sim\frac{1}{(2\pi)^3}\int\tilde{A}(\mathbf{k}_\parallel,\omega)e^{-i(\omega t-\mathbf{k}_\parallel\cdot\mathbf{R})}\,\mathrm{d}^2\mathbf{k}_\parallel\mathrm{d}\omega$$

$$S_j(\mathbf{k}_\parallel,\omega)\tilde{n}_j(\mathbf{k}_\parallel,\omega)-\sum_l G_{jl}(\mathbf{k}_\parallel)\tilde{n}_l(\mathbf{k}_\parallel,\omega)=B_j(\mathbf{k}_\parallel,\omega)\propto Q$$

$$\begin{pmatrix} S_1-G_{11} & -G_{12} & \cdots & -G_{1N}\\ -G_{21} & S_2-G_{22} & \cdots & -G_{2N}\\ \vdots & \vdots & \ddots & \vdots\\ -G_{N1} & -G_{N2} & \cdots & S_N-G_{NN}\end{pmatrix}\begin{pmatrix}\tilde{n}_1(\mathbf{k}_\parallel,\omega)\\ \vdots\\ \tilde{n}_N(\mathbf{k}_\parallel,\omega)\end{pmatrix}=\begin{pmatrix}B_1(\mathbf{k}_\parallel,\omega)\\ \vdots\\ B_N(\mathbf{k}_\parallel,\omega)\end{pmatrix}$$

$$M\vec{\tilde{n}}=\vec{B}$$

$\det(M)=0$ if $\gamma_j=0$ gives the dispersion relations $\omega(\mathbf{k}_\parallel)$

→ Obtain $\tilde{n}_j(\mathbf{k}_\parallel,\omega)$ → $n_j(\mathbf{r_j},t)$, or better $\tilde{\Phi}(\mathbf{k}_\parallel,\omega)$ → $\Phi(\mathbf{r_j},t)$ and wakefields

# 3. Carbon nanotubes

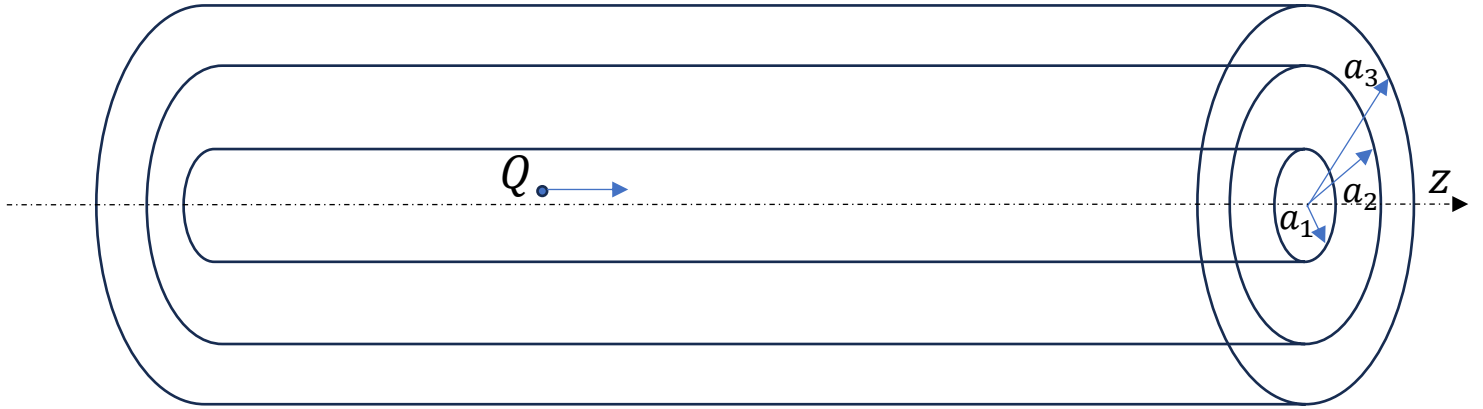


$\mathbf{r_0} = (\mathrm{r}_0, \varphi_0, vt) \qquad \mathbf{r_j} = (a_j, \varphi, z)$

- Fourier definition:

$$A(\varphi, z, t) = \sum_{m=-\infty}^{\infty} \int_{-\infty}^{\infty} \frac{\mathrm{d}k}{(2\pi)^2} \int_{-\infty}^{\infty} \frac{\mathrm{d}\omega}{2\pi} \mathrm{e}^{ikz+im\varphi-i\omega t} \tilde{A}(m, k, \omega)$$

- Using the relation:

$$\frac{1}{\|\mathbf{r} - \mathbf{r}'\|} = \sum_{m=-\infty}^{\infty} \int_{-\infty}^{\infty} \frac{\mathrm{d}k}{(2\pi)^2} \mathrm{e}^{ik(z-z')+im(\varphi-\varphi')} g\left(r, r'; m, k\right) \qquad g\left(r, r'; m, k\right) \equiv 4\pi I_m\left(|k| r_{\min}\right) K_m\left(|k| r_{\max}\right)$$

$$\Phi_0(\mathbf{r}, t) = \frac{Q}{|\mathbf{r} - \mathbf{r_0}|}$$

$$\Phi_{\mathrm{ind}}(\mathbf{r}, t) = -\sum_j \int \mathrm{d}^2\mathbf{r_j} \frac{n_j(\mathbf{r_j}, t)}{|\mathbf{r} - \mathbf{r_j}|}$$

$$\tilde{\Phi}_0(r, m, k, \omega) = 2\pi Q g\left(r, r_0; m, k\right) \delta(\omega - kv) \exp\left(-im\varphi_0\right)$$

$$\tilde{\Phi}_{\mathrm{ind}}\ (r, m, k, \omega) = -\sum_j g\left(r, a_j; m, k\right) a_j \tilde{n}_j(m, k, \omega)$$

# 3. Carbon nanotubes

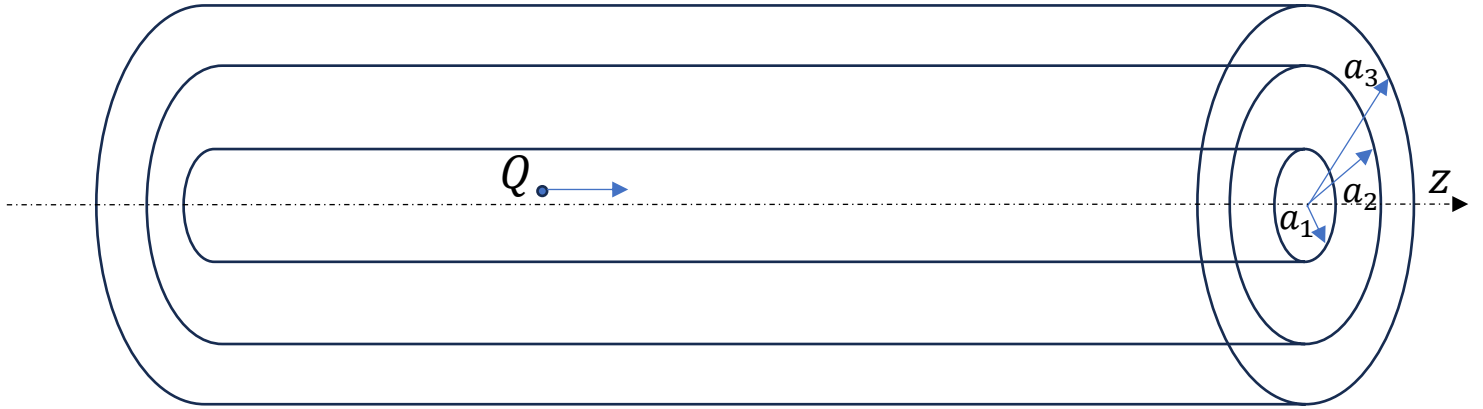


- Matrix equation:

$$\mathbf{r_0} = (\mathrm{r}_0, \varphi_0, vt) \qquad \mathbf{r_j} = (a_j, \varphi, z)$$

$$-\left(\frac{\partial^2}{\partial t^2} + \gamma_j \frac{\partial}{\partial t}\right) n_j(\mathbf{r_j}, t) = n_{0j} \nabla_j^2 \Phi(\mathbf{r_j}, t) - \alpha_j \nabla_j^2 n_j(\mathbf{r_j}, t) + \beta \nabla_j^2 \left[\nabla_j^2 n_j(\mathbf{r_j}, t)\right]$$

$$A(\varphi, z, t) = \sum_{m=-\infty}^{\infty} \int_{-\infty}^{\infty} \frac{\mathrm{d}k}{(2\pi)^2} \int_{-\infty}^{\infty} \frac{\mathrm{d}\omega}{2\pi} \mathrm{e}^{ikz + im\varphi - i\omega t} \tilde{A}(m, k, \omega)$$

$$\Phi(\mathbf{r_j}, t) = \frac{Q}{|\mathbf{r_j} - \mathbf{r_0}|} - \sum_l \int \mathrm{d}^2 \mathbf{r_l} \frac{n_l(\mathbf{r_l}, t)}{|\mathbf{r_j} - \mathbf{r_l}|}$$

$$\nabla_j^2 = \frac{\partial^2}{\partial z^2} + \frac{1}{a_j^2} \frac{\partial^2}{\partial \varphi^2}$$

$$S_j(m, k, \omega) \tilde{n}_j(m, k, \omega) - \sum_l G_{jl}(m, k) \tilde{n}_l(m, k, \omega) = B_j(m, k, \omega)$$

$$S_j(m, k, \omega) = \omega(\omega + i\gamma_j) - \alpha_j \left(k^2 + \frac{m^2}{a_j^2}\right) - \beta \left(k^2 + \frac{m^2}{a_j^2}\right)^2,$$

$$G_{jl}(m, k) = n_{0j} a_l \left(k^2 + \frac{m^2}{a_j^2}\right) g\left(a_j, a_l; m, k\right),$$

$$B_j(m, k, \omega) = -n_{0j} \left(k^2 + \frac{m^2}{a_j^2}\right) \tilde{\Phi}_0\left(a_j, m, k, \omega\right).$$

$$\tilde{n}_j(m, k, \omega)$$

$$\tilde{\Phi}_{\mathrm{ind}}(r, m, k, \omega) = -\sum_j g\left(r, a_j; m, k\right) a_j \tilde{n}_j(m, k, \omega)$$

# 3. Carbon nanotubes

Longitudinal

Transverse

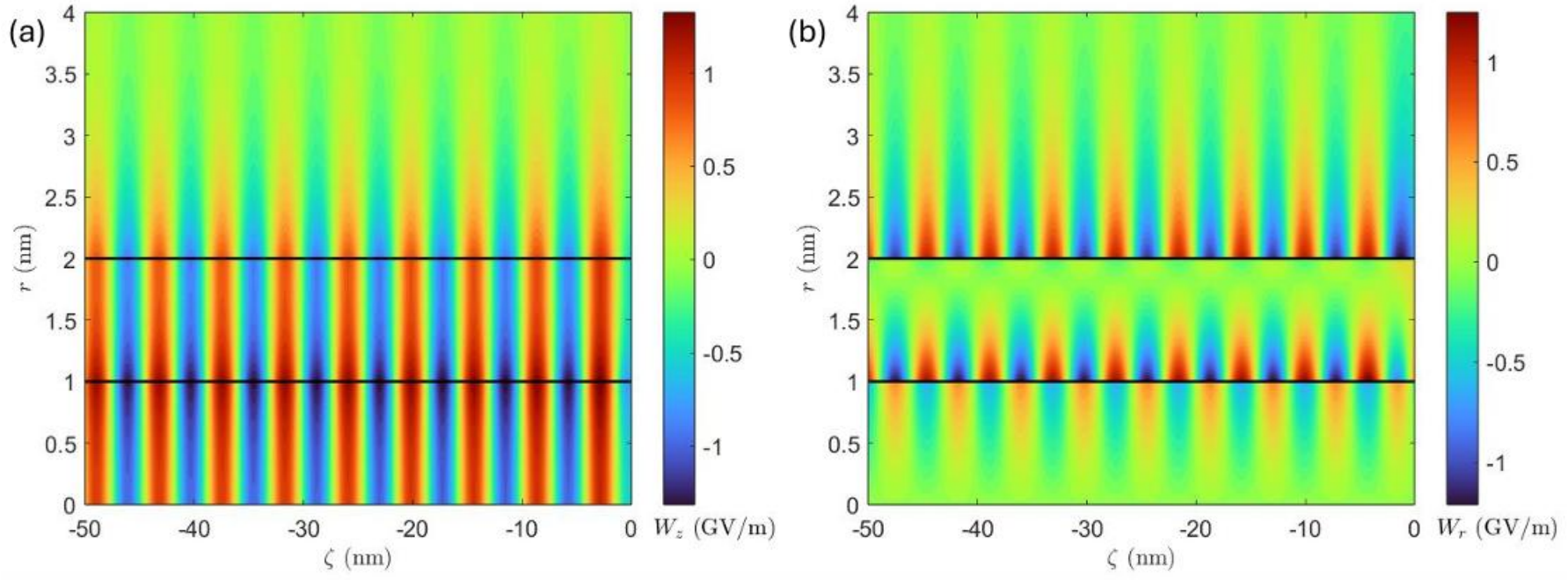


**Figure 6.** Induced (a) longitudinal and (b) transverse wakefield in the $r\zeta$-plane for a proton travelling on axis ($r_0 = 0$) at $v = 0.06c$ along a DWCNT whose radii are $a_1 = 1\,\text{nm}$ and $a_2 = 2\,\text{nm}$. The surface density is $n_{0j} = n_g$ and the friction parameter is $\gamma = 10^{-3}\Omega$, where $\Omega = \sqrt{4\pi n_g/a_1}$. Black horizontal lines indicate the nanotube walls.

# 3. Carbon nanotubes

$$A(\varphi, z, t) = \sum_{m=-\infty}^{\infty} \int_{-\infty}^{\infty} \frac{\mathrm{d}k}{(2\pi)^2} \int_{-\infty}^{\infty} \frac{\mathrm{d}\omega}{2\pi} \mathrm{e}^{ikz+im\varphi-i\omega t} \widetilde{A}(m, k, \omega)$$

- Using that $\mathrm{Re}\left[\widetilde{\Phi}\right]$ is an even function in $k$ and $\mathrm{Im}\left[\widetilde{\Phi}\right]$ odd function, the wakefields are given by:

Longitudinal

$$W_{z,\mathrm{ind}}(r, \varphi, \zeta) = -\frac{\partial \Phi_{\mathrm{ind}}}{\partial z} = \frac{1}{(2\pi)^3} \sum_{m=-\infty}^{+\infty} e^{im\varphi} \int_{-\infty}^{+\infty} \mathrm{d}k\, k \left( \mathrm{Re}\left[\tilde{\Phi}_{\mathrm{ind}}(r, m, k, kv)\right] \sin(k\zeta) \right.$$
$$\left. + \mathrm{Im}\left[\tilde{\Phi}_{\mathrm{ind}}(r, m, k, kv)\right] \cos(k\zeta) \right) = W_{z,\mathrm{Re}} + W_{z,\mathrm{Im}},$$

Comoving coordinate: $\zeta = z - vt$

Transverse

$$W_{r,\mathrm{ind}}(r, \varphi, \zeta) = -\frac{\partial \Phi_{\mathrm{ind}}}{\partial r} = \frac{-1}{(2\pi)^3} \sum_{m=-\infty}^{+\infty} e^{im\varphi} \int_{-\infty}^{+\infty} \mathrm{d}k \left( \mathrm{Re}\left[\partial_r \tilde{\Phi}_{\mathrm{ind}}\,(r, m, k, kv)\right] \cos(k\zeta) \right.$$
$$\left. - \mathrm{Im}\left[\partial_r \tilde{\Phi}_{\mathrm{ind}}\,(r, m, k, kv)\right] \sin(k\zeta) \right) = W_{r,\mathrm{Re}} + W_{r,\mathrm{Im}},$$

# 3. Carbon nanotubes

Behind the driver:

$W_{z,Re} \approx W_{z,Im}$

$W_{r,Re} \approx W_{r,Im}$

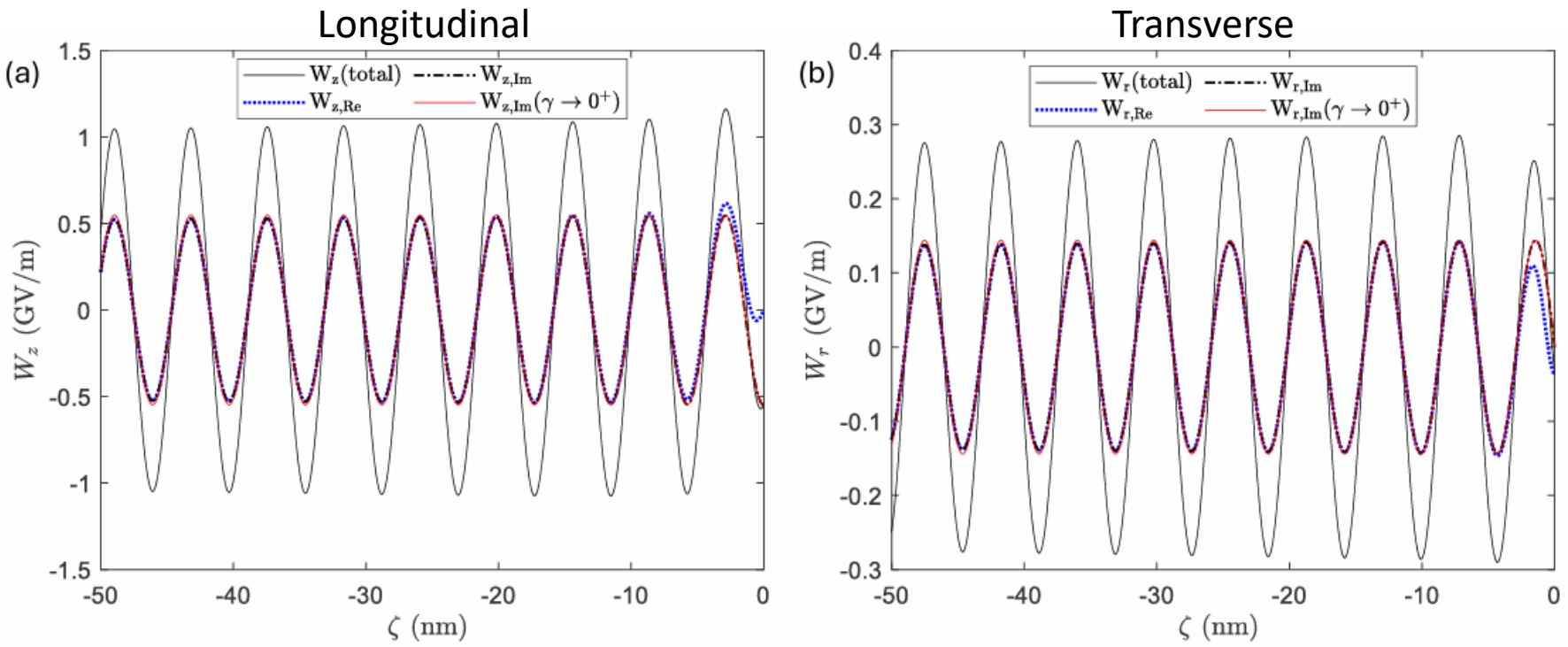


**Figure 4.** (a) Longitudinal wakefield contributions induced on axis ($r = 0$) and (b) transverse wakefield contributions induced at $r = a_1/2$ for a proton moving on axis ($r_0 = 0$) at $v = 0.06c$ along a DWCNT with radii $a_1 = 1\,\text{nm}$ and $a_2 = 2\,\text{nm}$. The surface density is $n_{0j} = n_g$ and the friction parameter is $\gamma = 10^{-3}\Omega$, where $\Omega = \sqrt{4\pi n_g/a_1}$. The red curves depict the approximation for $\gamma \to 0^+$: Eqs. (19)-(20). Note that the driving proton is located at the comoving coordinate $\zeta = 0$.

# 3. Carbon nanotubes

$$M\vec{\tilde{n}} = \vec{B}, \qquad M_{jj} = S_j - G_{jj}, \quad M_{ij} = -G_{ij} \quad (i \neq j)$$

$$\vec{\tilde{n}} = M^{-1}\vec{B}$$

$$M^{-1} = \frac{(\mathrm{Adj}(M))^T}{\det(M)}$$

$$\vec{\tilde{n}}(m,k,\omega) = \frac{\vec{N}(m,k,\omega)}{\det(M)}\delta(\omega - kv)$$

where

$$\vec{N}(m,k,\omega) = \Delta\vec{B}', \quad \vec{B}'(m,k)\delta(\omega - kv) = \vec{B}(m,k,\omega),$$

and $\Delta$ is the classical adjoint matrix of $M$, $\Delta \equiv \mathrm{Adj}(M)$, which satisfies

The determinant can be expressed in terms of the dispersion relations if $\gamma \equiv \gamma_j$:

$$\det(M) = \prod_{j=1}^{N} D_j(m,k,\omega), \quad D_j(m,k,\omega) = \omega(\omega + i\gamma) - \omega_j^2(m,k)$$

# 3. Carbon nanotubes

Compare with waveguides

If $\gamma \to 0^+$:

$$W_{z,\mathrm{Im}}(r,\varphi,\zeta) = \sum_{m=-\infty}^{+\infty} e^{im\varphi} \sum_{j=1}^{N} W_{z,m,j} \cos(k_{m,j}\zeta), \tag{19}$$

$$W_{r,\mathrm{Im}}(r,\varphi,\zeta) = \sum_{m=-\infty}^{+\infty} e^{im\varphi} \sum_{j=1}^{N} W_{r,m,j} \sin(k_{m,j}\zeta), \tag{20}$$

$$\begin{aligned} W_{z,m,j} = {} & \frac{k_{m,j}}{(2\pi)^2} \left( \prod_{l=1,l\neq j}^{N} [Z_{m,l}(k_{m,j}, k_{m,j}v)] \left| \frac{\partial Z_{m,j}}{\partial k} \right|_{k=k_{m,j}} \right)^{-1} \\ & \times \sum_{l=1}^{N} g\,(r, a_l; m, k_{m,j})\, a_l N_l(m, k_{m,j}, k_{m,j}v), \end{aligned} \tag{21}$$

$$\begin{aligned} W_{r,m,j} = {} & \frac{1}{(2\pi)^2} \left( \prod_{l=1,l\neq j}^{N} [Z_{m,l}(k_{m,j}, k_{m,j}v)] \left| \frac{\partial Z_{m,j}}{\partial k} \right|_{k=k_{m,j}} \right)^{-1} \\ & \times \sum_{l=1}^{N} \partial_r g\,(r, a_l; m, k_{m,j})\, a_l N_l(m, k_{m,j}, k_{m,j}v), \end{aligned} \tag{22}$$

where the quantity $Z_{m,j}(k) = \mathrm{Re}[D_j(m,k,kv)] = (kv)^2 - \omega_j^2(m,k)$ is introduced, and $k_{m,j}$ are the positive root of $Z_{m,j}(k)$, i.e. the criterion for plasma resonance $k_{m,j}v = \omega_j(m,k)$. In general, two positive resonances $k_{m,j}$ may exist and their contribution should be summed in Eqs. (19) and (20). However, the contribution from the resonance with a larger value of $k$ is totally negligible (see Appendix). For this reason, for practical purposes, in Eqs. (19)-(22), $k_{m,j}$ refer to the smallest positive root.

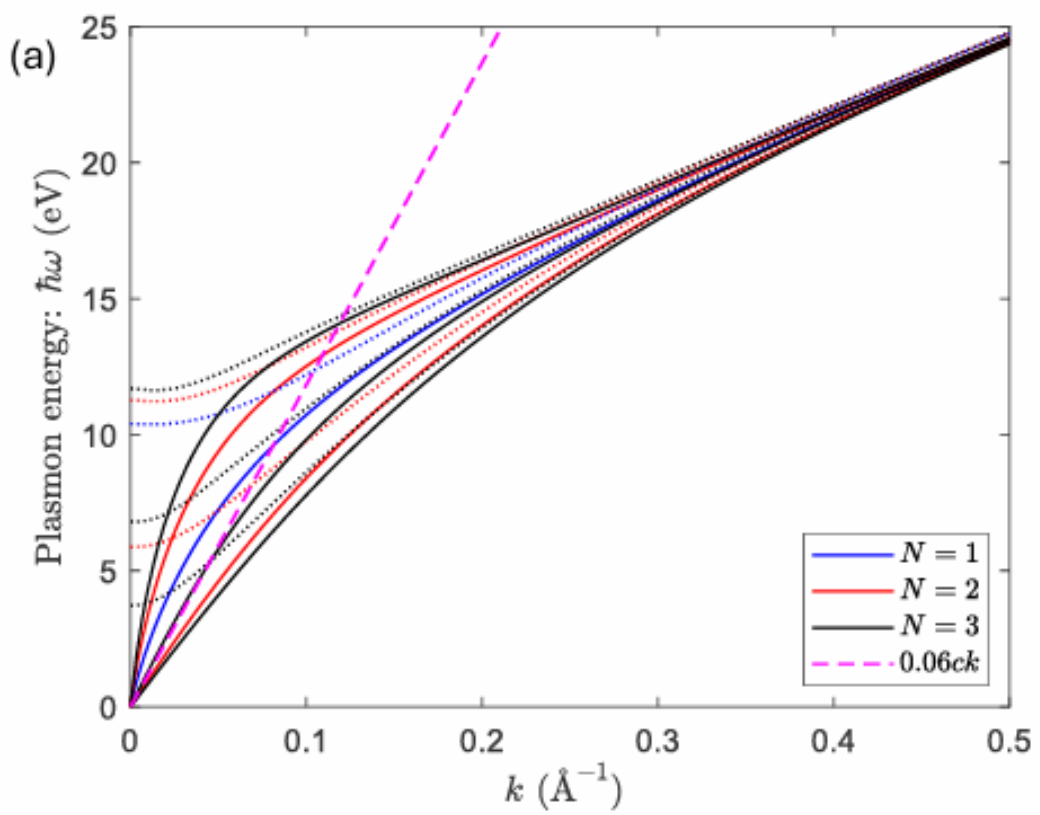


If the driver travels on-axis, m=0 is the only mode that contributes

# 3. Carbon nanotubes

TWCNT

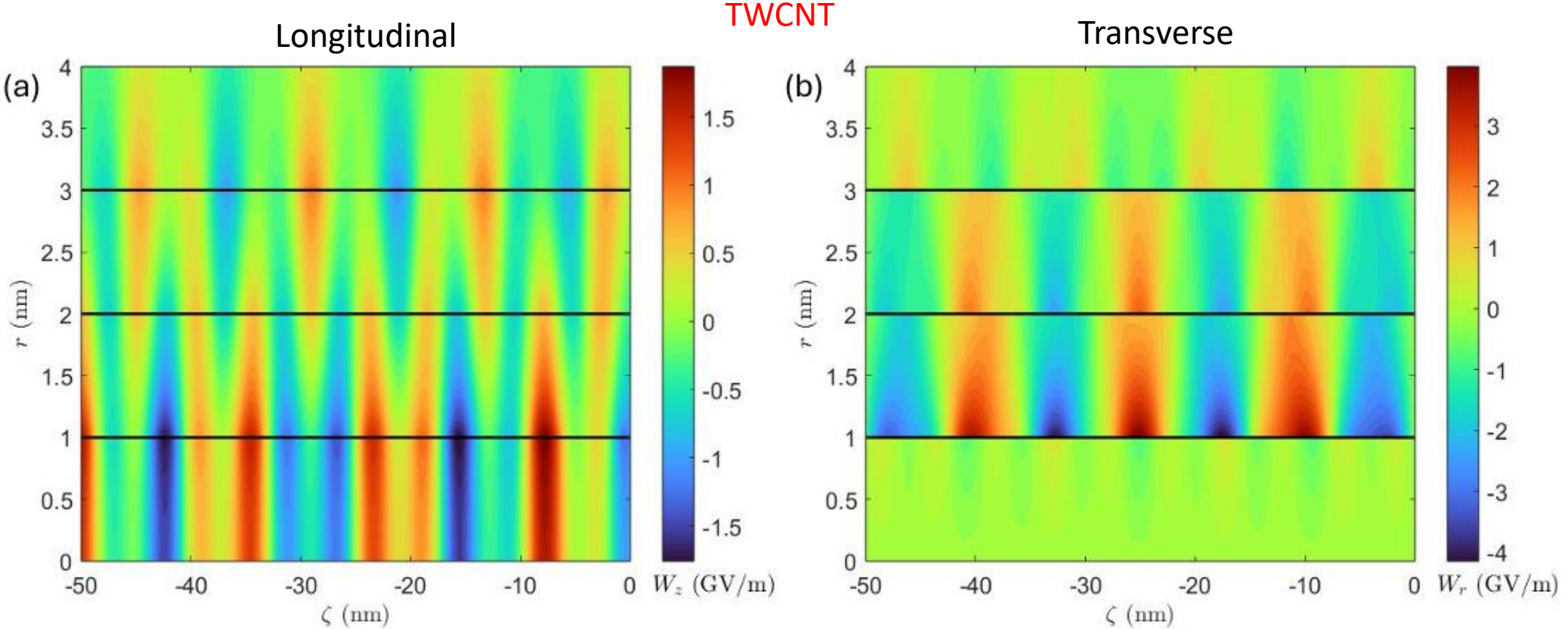


**Figure 7.** Induced (a) longitudinal and (b) transverse wakefield in the $r\zeta$-plane for a proton travelling on axis ($r_0 = 0$) at $v = 0.06c$ along a TWCNT whose radii are $a_1 = 1\,\mathrm{nm}$, $a_2 = 2\,\mathrm{nm}$ and $a_3 = 3\,\mathrm{nm}$. The surface density is $n_{0j} = n_g$ and the friction parameter is $\gamma = 10^{-3}\Omega$, where $\Omega = \sqrt{4\pi n_g/a_1}$. Black horizontal lines indicate the nanotube walls.

# 3. Carbon nanotubes

TWCNT

Longitudinal

Transverse

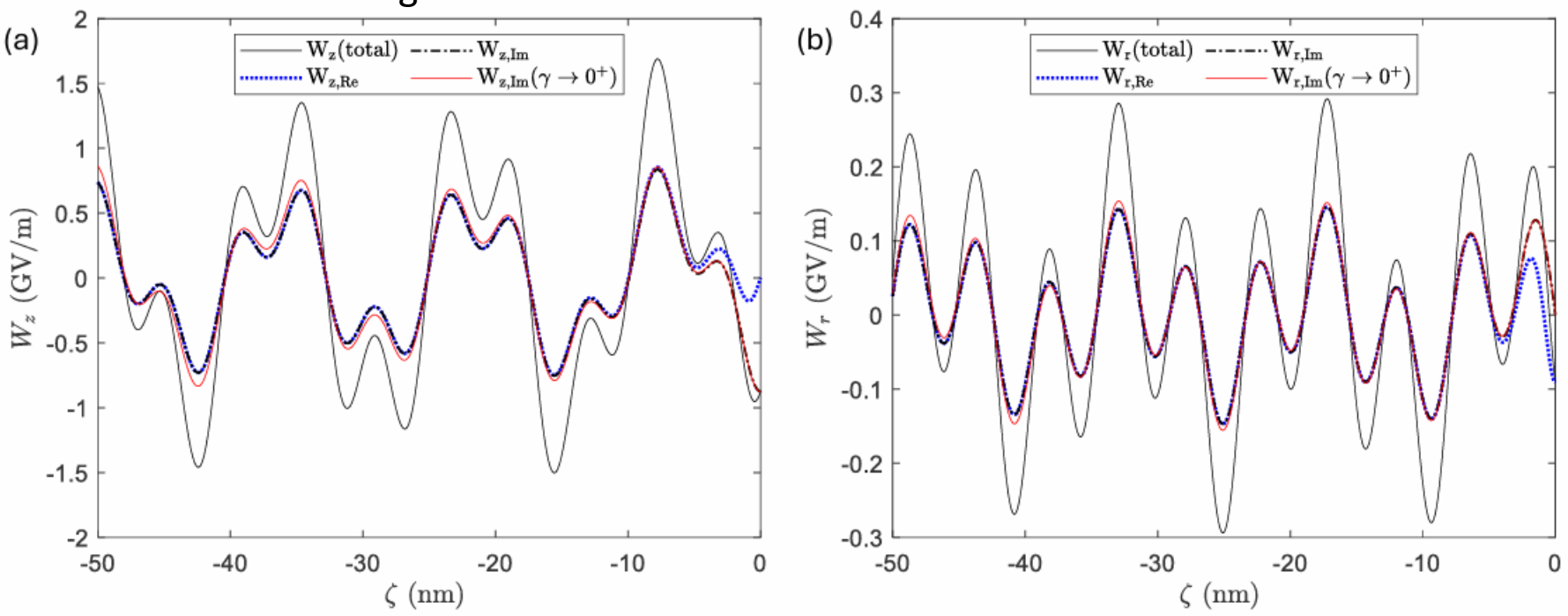


**Figure 5.** (a) Longitudinal wakefield contributions induced on axis ($r = 0$) and (b) transverse wakefield contributions induced at $r = a_1/2$ for a proton moving on axis ($r_0 = 0$) at $v = 0.06c$ along a TWCNT whose radii are $a_1 = 1\,\text{nm}$, $a_2 = 2\,\text{nm}$ and $a_3 = 3\,\text{nm}$. The surface density is $n_{0j} = n_g$ and the friction parameter is $\gamma = 10^{-3}\Omega$, where $\Omega = \sqrt{4\pi n_g/a_1}$. The red curves depict the approximation for $\gamma \to 0^+$: Eqs. (19)-(20).

Two resonant frequencies

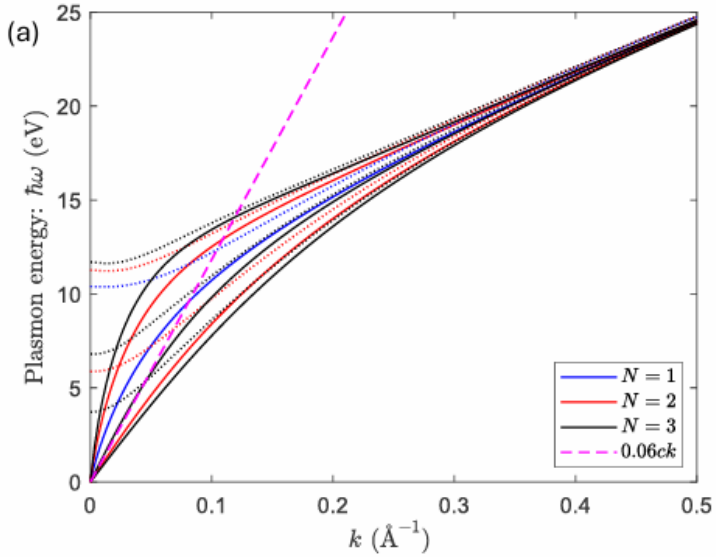

# 3. Carbon nanotubes

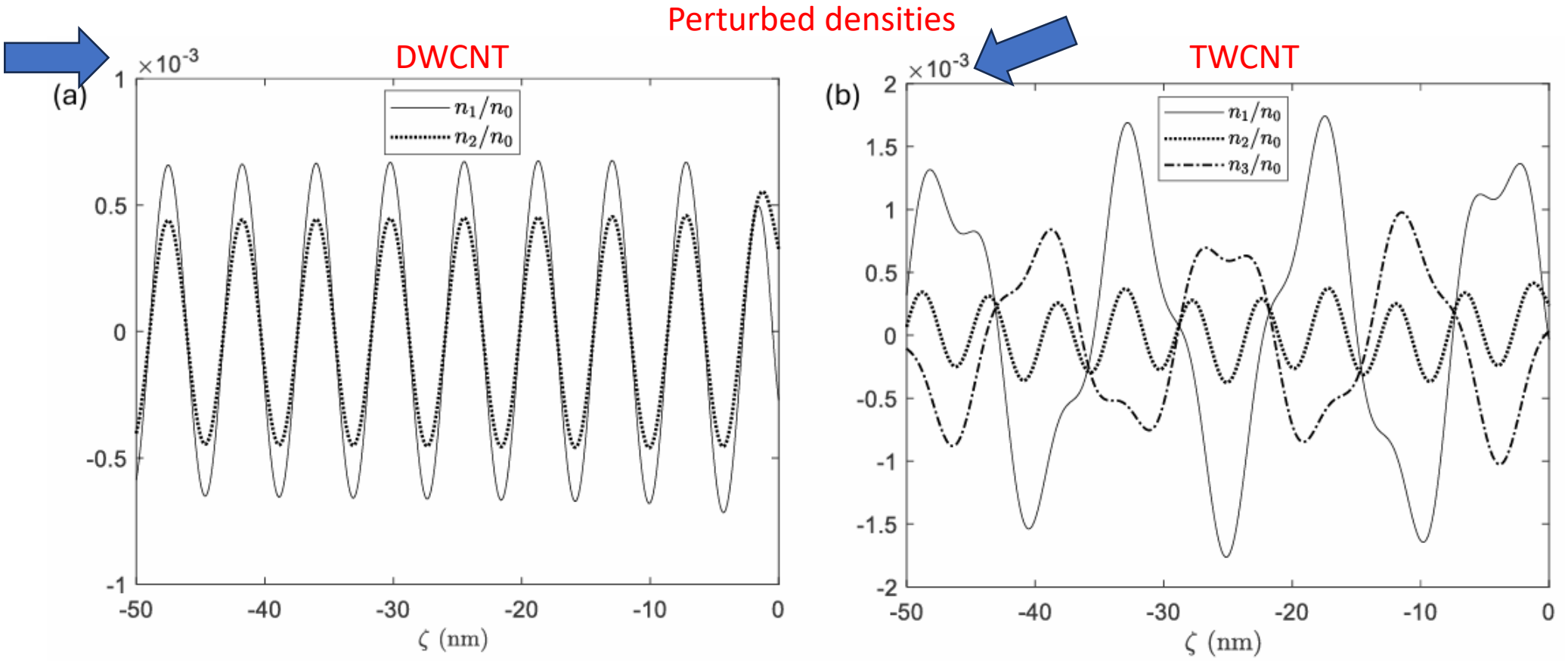


**Figure 8.** Perturbed densities produced by a proton travelling on axis ($r_0 = 0$) at $v = 0.06c$ along a (a) DWCNT whose radii are $a_1 = 1\,\text{nm}$, $a_2 = 2\,\text{nm}$ and (b) a TWCNT whose radii are $a_1 = 1\,\text{nm}$, $a_2 = 2\,\text{nm}$ and $a_3 = 3\,\text{nm}$. The surface density is $n_{0j} = n_g$ and the friction parameter is $\gamma = 10^{-3}\Omega$, where $\Omega = \sqrt{4\pi n_g/a_1}$.

# 3. Carbon nanotubes

Excited modes

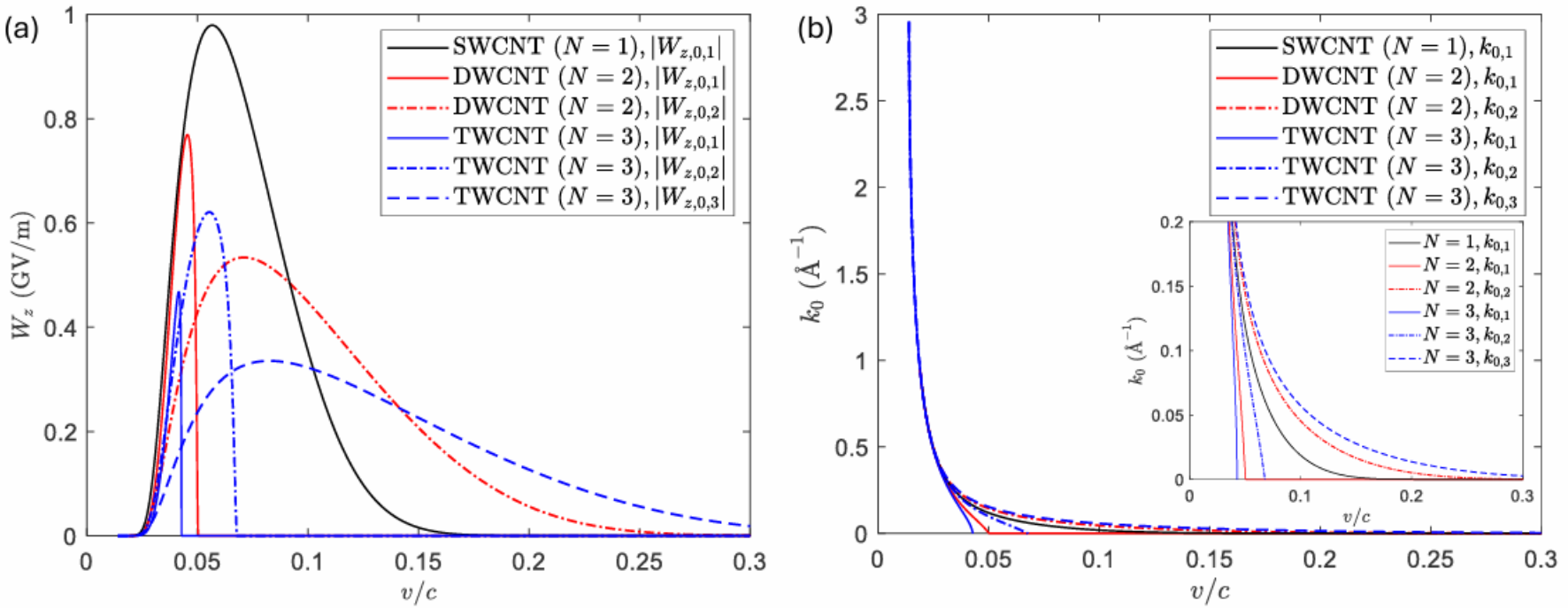


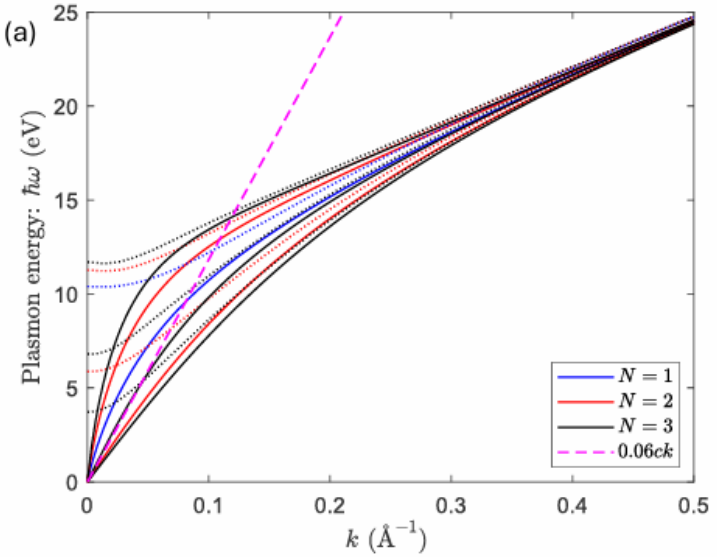


**Figure 9.** (a) Amplitudes $W_z$ of the modes $m = 0$ and (b) corresponding resonant wavenumbers $k_0$ as a function of the velocity for different configurations: SWCNT with $a_1 = 1\,\text{nm}$, DWCNT with $a_1 = 1\,\text{nm}$, $a_2 = 2\,\text{nm}$, and TWCNT with $a_1 = 1\,\text{nm}$, $a_2 = 2\,\text{nm}$, $a_3 = 3\,\text{nm}$. The following parameters are used: $n_{0j} = n_g$ and $r = r_0 = 0$. In (b) it is included a zoomed-in view for small values of $k_0$.

# 3. Carbon nanotubes

Stopping power: $S = -QW_{z,\mathrm{ind}}\big|_{\mathbf{r}=\mathbf{r}_0} = -QW_{z,\mathrm{Im}}\big|_{\mathbf{r}=\mathbf{r}_0}$ → Sum of amplitudes of the modes if $\gamma \to 0$

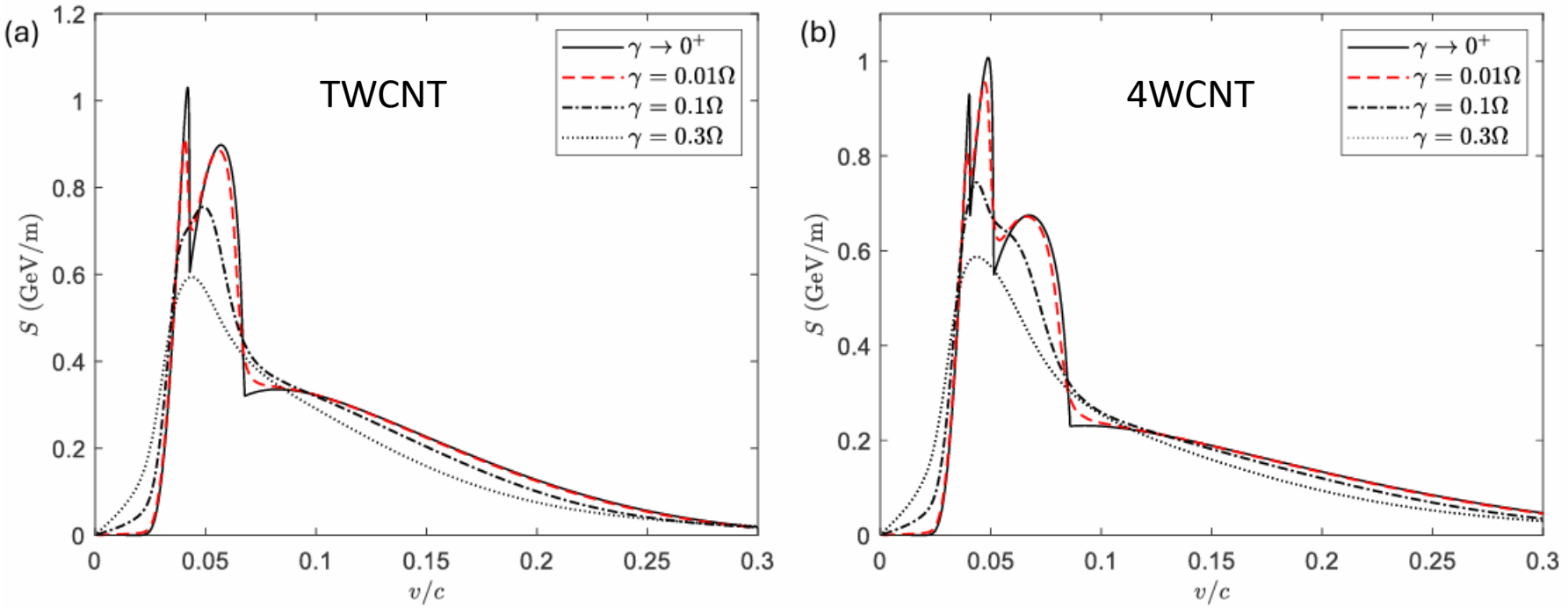


**Figure 14.** Stopping power for different damping parameters ($\Omega = \sqrt{4\pi n_g/a_1}$) for (a) a TWCNT with $a_1 = 1\,\mathrm{nm}$, $a_2 = 2\,\mathrm{nm}$ and $a_3 = 3\,\mathrm{nm}$, and (b) a MWCNT with $N = 4$ walls with $a_1 = 1\,\mathrm{nm}$, $a_2 = 2\,\mathrm{nm}$, $a_3 = 3\,\mathrm{nm}$ and $a_4 = 4\,\mathrm{nm}$. The following parameters are used: $n_{0j} = n_g$ and $r = r_0 = 0$.

# 3. Carbon nanotubes

Optimization of a SWCNT

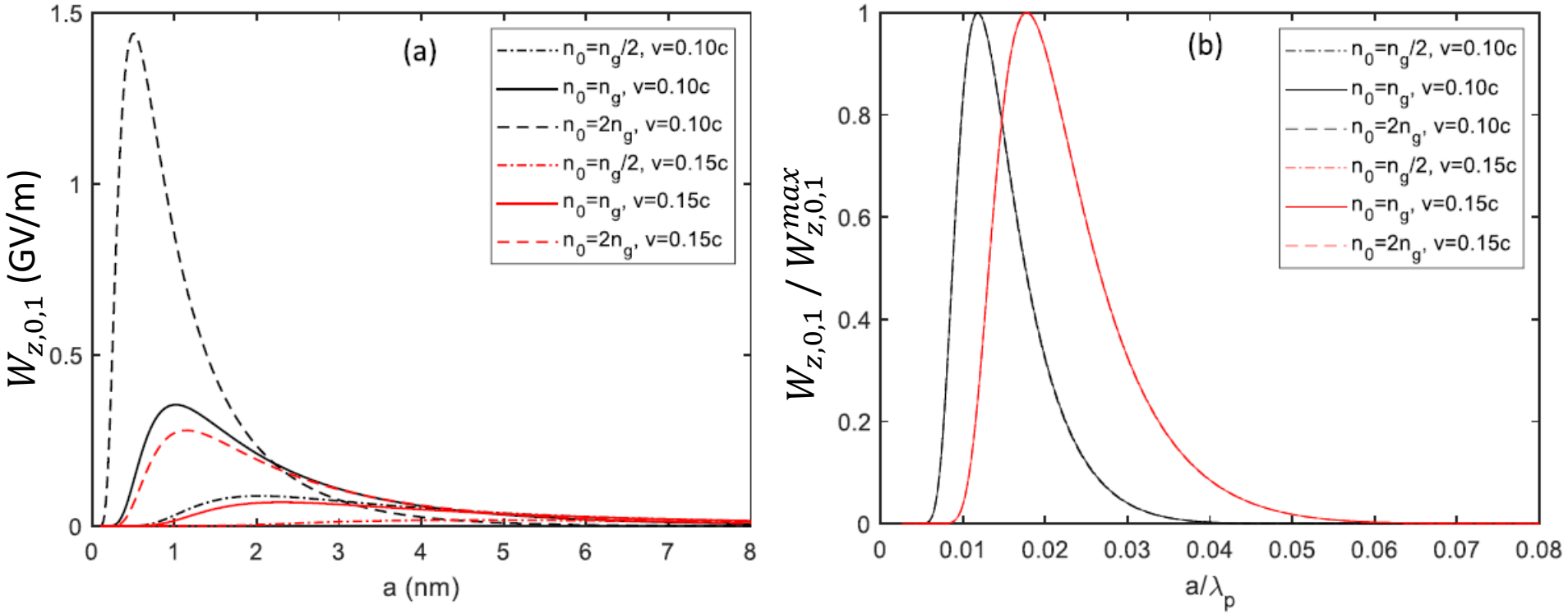


**Figure 8.** (a) Amplitude of $W_{z2}$ as a function of the radius $a$ for different values of $n_0$ and $v$ ($n_g = 1.53 \times 10^{20}$ m$^{-2}$ is the electron-gas density of a graphite sheet). (b) Amplitude of $W_{z2}$ (normalized to the maximum of figure (a)) as a function of $a/\lambda_p$.

$$\lambda_p = \frac{2\pi c}{\Omega_p}$$

Plasma frequency (2D): $\Omega_p = \sqrt{4\pi n_0/a}$

# 3. Carbon nanotubes

Optimization of a SWCNT

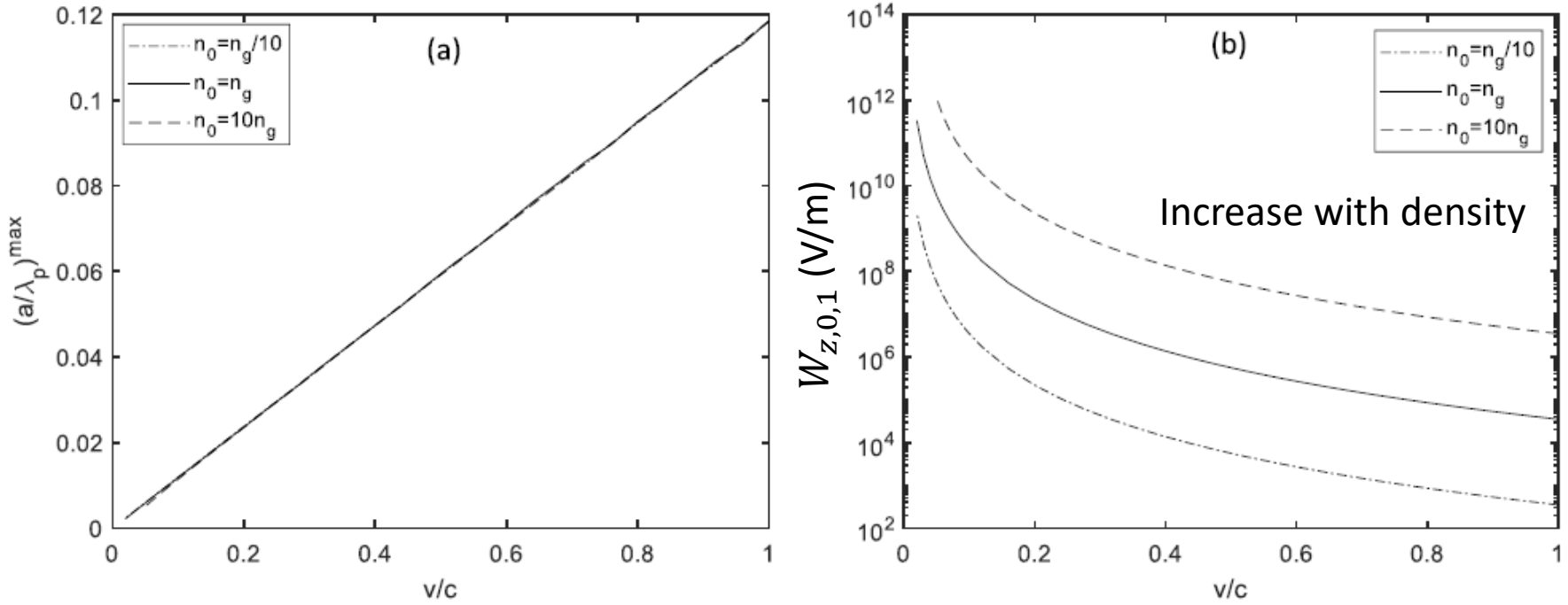


**Figure 9.** (a) Optimum radius and (b) maximum longitudinal wakefield associated as a function of $v$ for different surface densities ($n_g = 1.53 \times 10^{20}$ m$^{-2}$ is the electron-gas density of a graphite sheet).

$$a_{opt}[\mathrm{nm}] \approx 156.55 \frac{\beta_v^2}{n_0\left[10^{20}\,\mathrm{m}^{-2}\right]}$$

$$\beta_v = v/c$$

Conclusion: Higher wakefields can be excited from non-relativistic drivers, but they require CNT radius in the order of nm. For ultra-relativistic drivers, optimum CNT radius $\sim 100$ nm: better for beam acceptance.

# 3. Carbon nanotubes

How can you increase the density? Use MWCNTs with closer walls

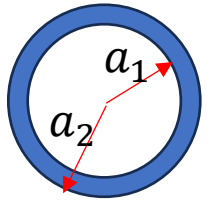


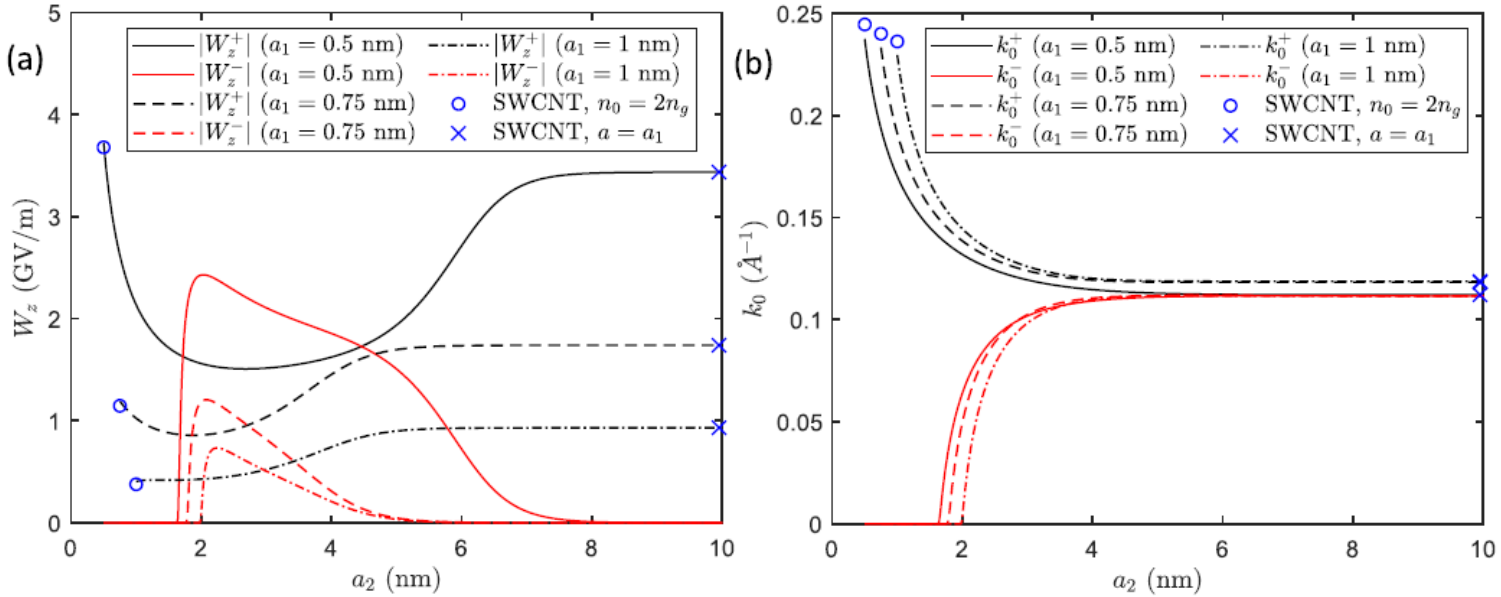


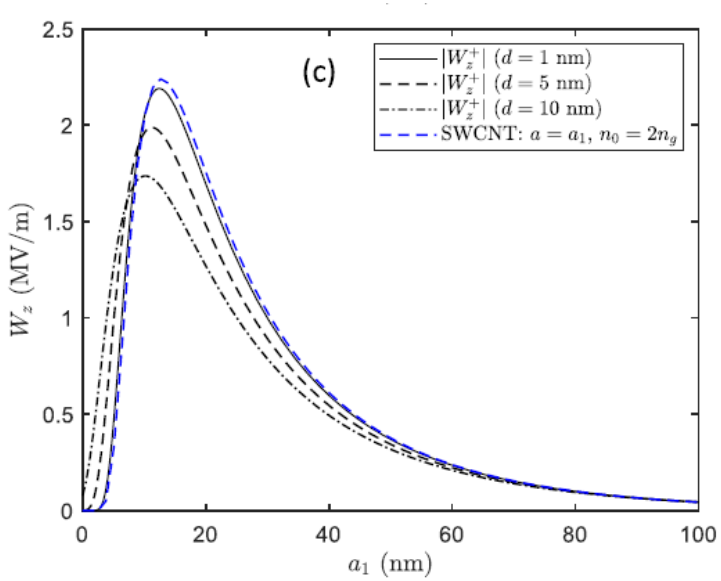


**Fig. 8.** (a) Amplitudes $W_z^{\pm}$ and (b) resonant wavenumbers $k_0^{\pm}$ as a function of the external radius $a_2$ for different $a_1$. The parameters used are: $v = 0.05c$ and $r = r_0 = 0$. The results are compared with the case of a SWCNT with $a = a_1$ and $n_0 = 2n_g$ (circles) and a SWCNT with $a = a_1$ and $n_0 = n_g$ (crosses) (Eq. (15) in [60]).

Conclusion: A MWCNT with N walls with small inter-wall distance compared to the inner radius can be approximated as a SWCNT with $n_0 = Nn_g$

# 3. Carbon nanotubes

For this reason, carbon nanostructures with a central aperture are being studying

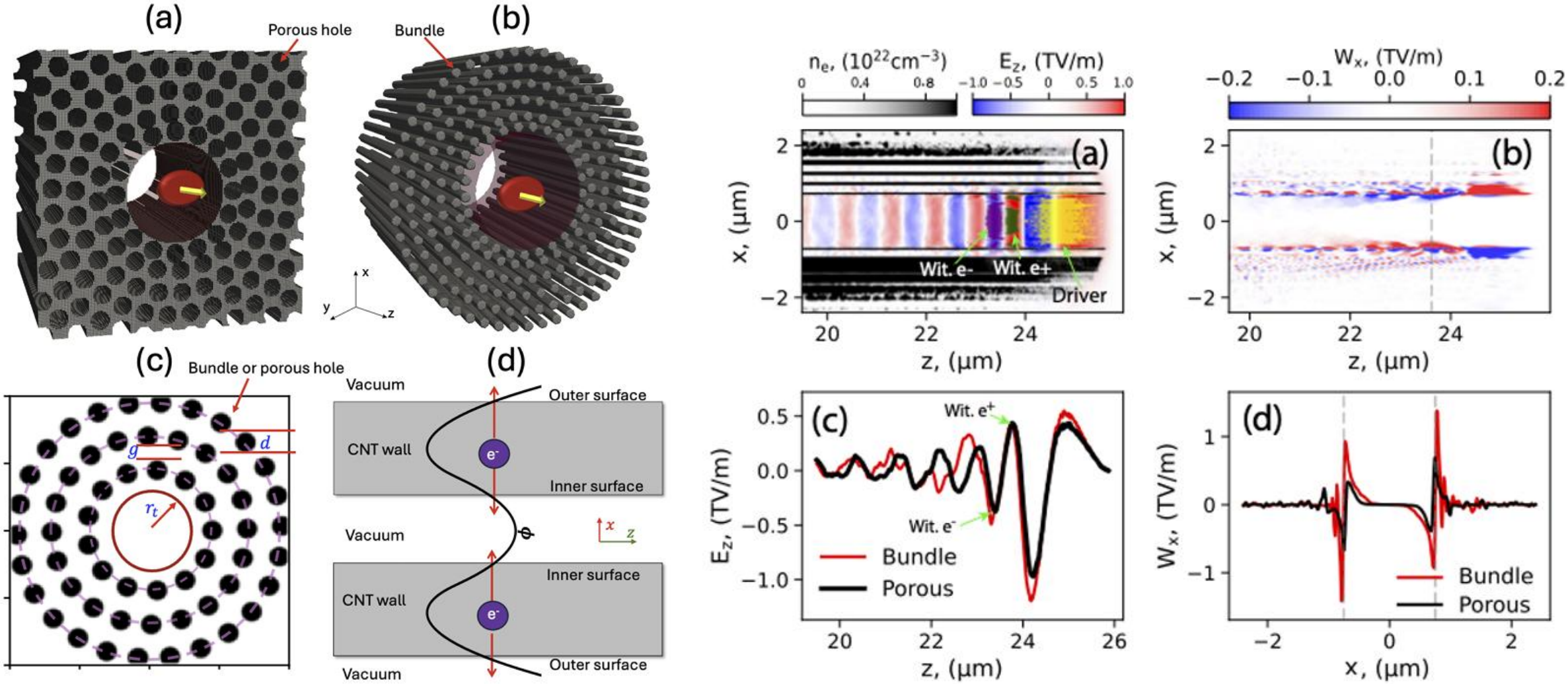


https://arxiv.org/pdf/2502.08498

# 3. Carbon nanotubes (comparison with PIC simulations)

- The longitudinal wakefield excited by a driver moving on-axis if $\gamma \to 0^+$ is given by:

$$W_z \approx W_z^{max} \cos(k_0 \zeta)$$

$$W_z^{max} = -4Qk_0^3 I_0(|k_0| r_0) I_0(|k_0| r) \Omega_p^2 a^2 K_0^2(|k_0| a) \left| \frac{\partial Z_0}{\partial k} \right|_{k=k_0}^{-1}$$

$r_0 = 0$ → 1

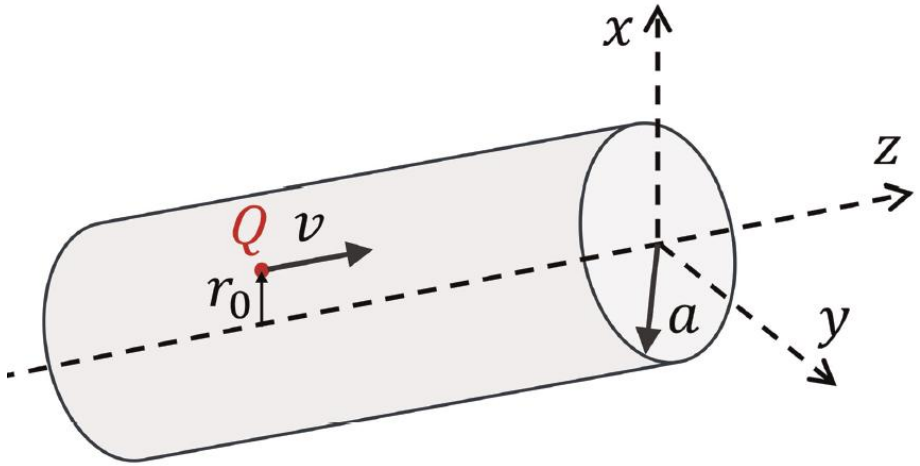


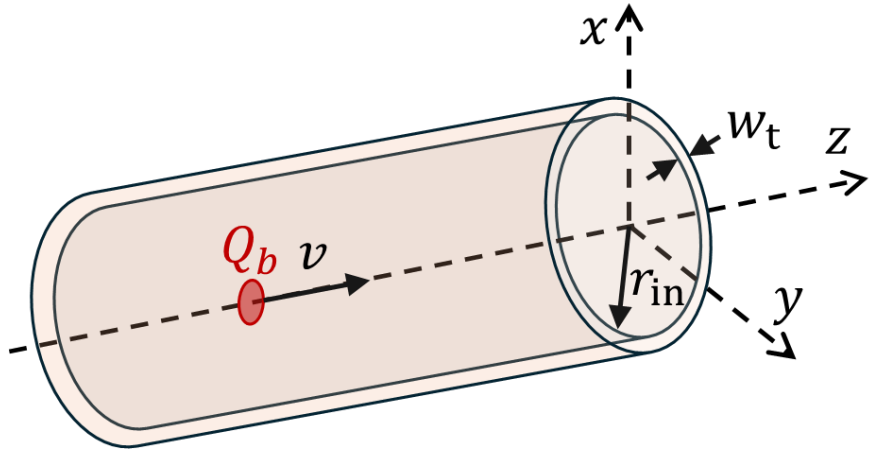

# 3. Carbon nanotubes (comparison with PIC simulations)

- The Fourier–Bessel Particle-in-Cell **(FBPIC)** code is used to perform the simulations using a cylindrical CNT hollow plasma channel model employing 2D radial grids.
- This code is based on a **collisionless** fluid model which **does not take into account the solid-state properties** related to the ionic lattice.
- We define a hollow plasma channel model with **inner radius** $\boldsymbol{r_{in}}$ and **wall thickness** $\boldsymbol{w_t}$ with a volumetric density $\boldsymbol{n_V = 10^{28}}$ **m$^{-3}$** of free electrons within this region.
- We will consider a **bi-Gaussian beam driver**, with $\sigma_\zeta = \sigma_r = 3.33$ nm, and charge $Q_b = -44$ fC travelling **on-axis**. The beam energy follows a Gaussian distribution (mean: 1 GeV, standard deviation: 0.005 GeV).

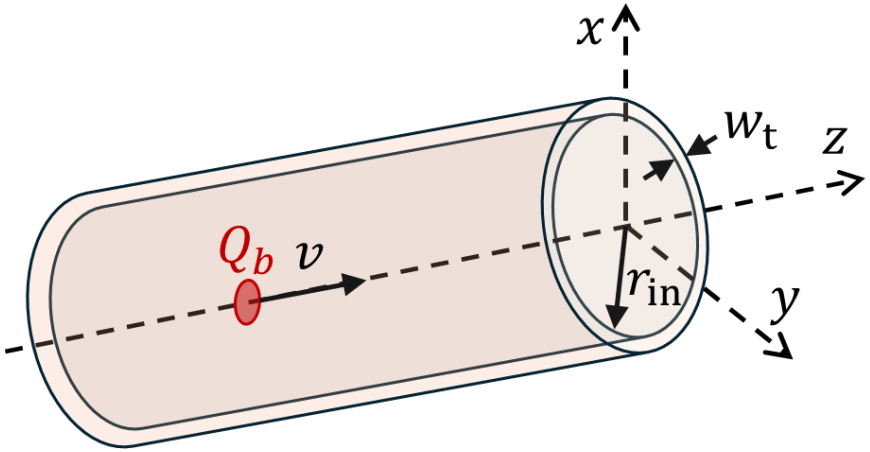

# 3. Carbon nanotubes (comparison with PIC simulations)

- To relate the surface density of the LHM and the volumetric density of PIC simulations, we will assume that the **number of free electrons** within the cylindrical surface of radius $a = r_{in}$ is **equal** to the number of free electrons in the wall thickness $w_t$.

$$n_0 = \frac{n_V w_t}{2r_{in}}(2r_{in} + w_t)$$

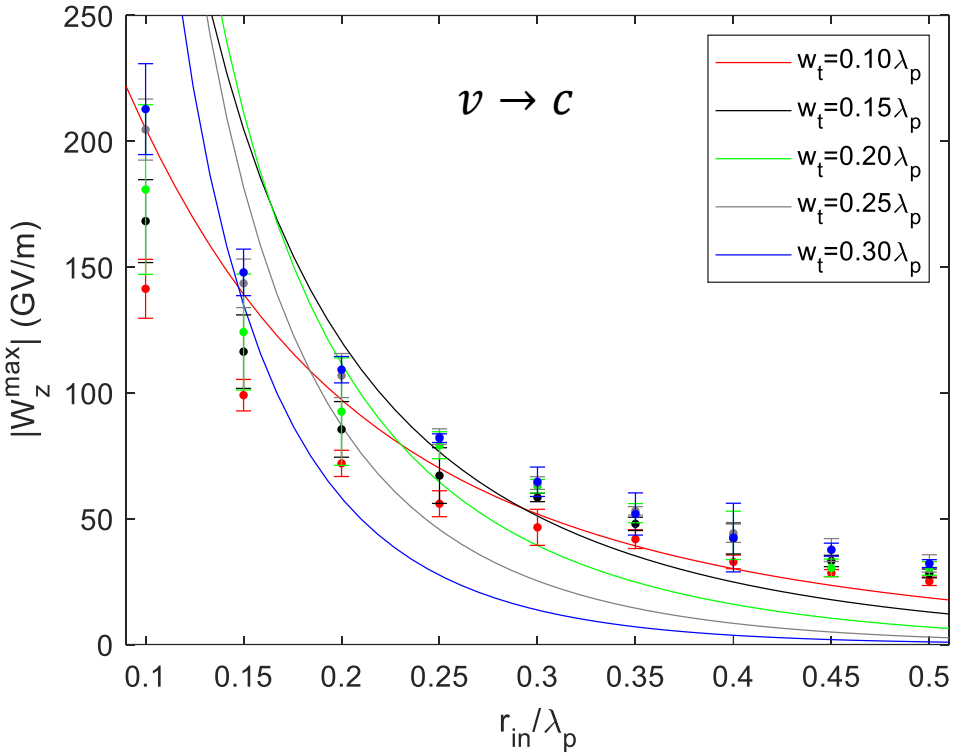


$\lambda_p = \frac{2\pi c}{\omega_p}$ is the plasma wavelength, where

$\omega_p = \sqrt{e^2 n_V / \varepsilon_0 m_e}$ is the plasma frequency.

Good qualitative agreement; quantitatively improves if $w_t$ is smaller.

# 3. Carbon nanotubes (comparison with PIC simulations)

- The comparison is better if we consider an **effective density** to take into account that not all free electrons of the wall thickness excite the wakefield effectively.

$$n_0 = \kappa \frac{n_V w_t}{2r_{in}}(2r_{in} + w_t)$$

$$\kappa \in (0, 1]$$

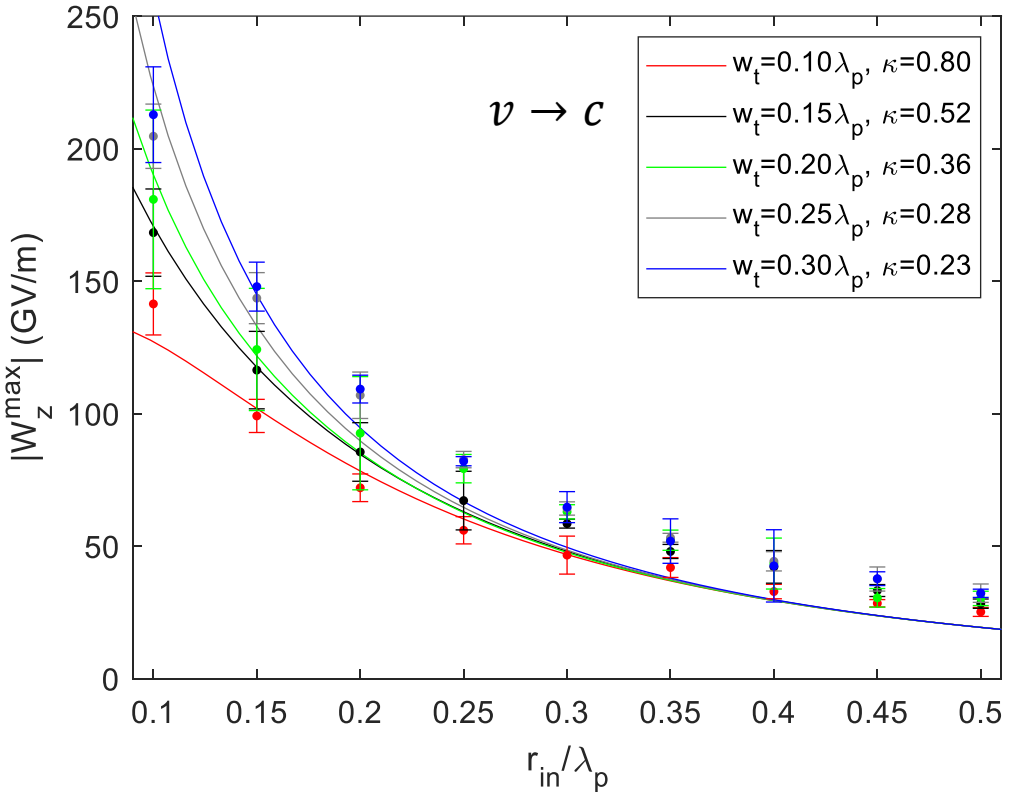


$\lambda_p = \frac{2\pi c}{\omega_p}$ is the plasma wavelength, where

$\omega_p = \sqrt{e^2 n_V / \varepsilon_0 m_e}$ is the plasma frequency.

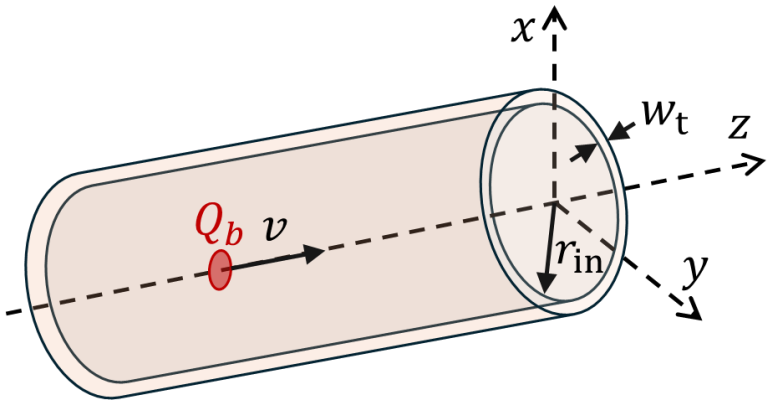

# 3. Carbon nanotubes (comparison with PIC simulations)

- Alternatively, we can consider an **effective wall thickness** $w_t^{\mathrm{eff}}$

$$n_0 = \frac{n_V w_t^{\mathrm{eff}}}{2r_{\mathrm{in}}}(2r_{\mathrm{in}} + w_t^{\mathrm{eff}})$$

$$w_t^{\mathrm{eff}} \leq w_t$$

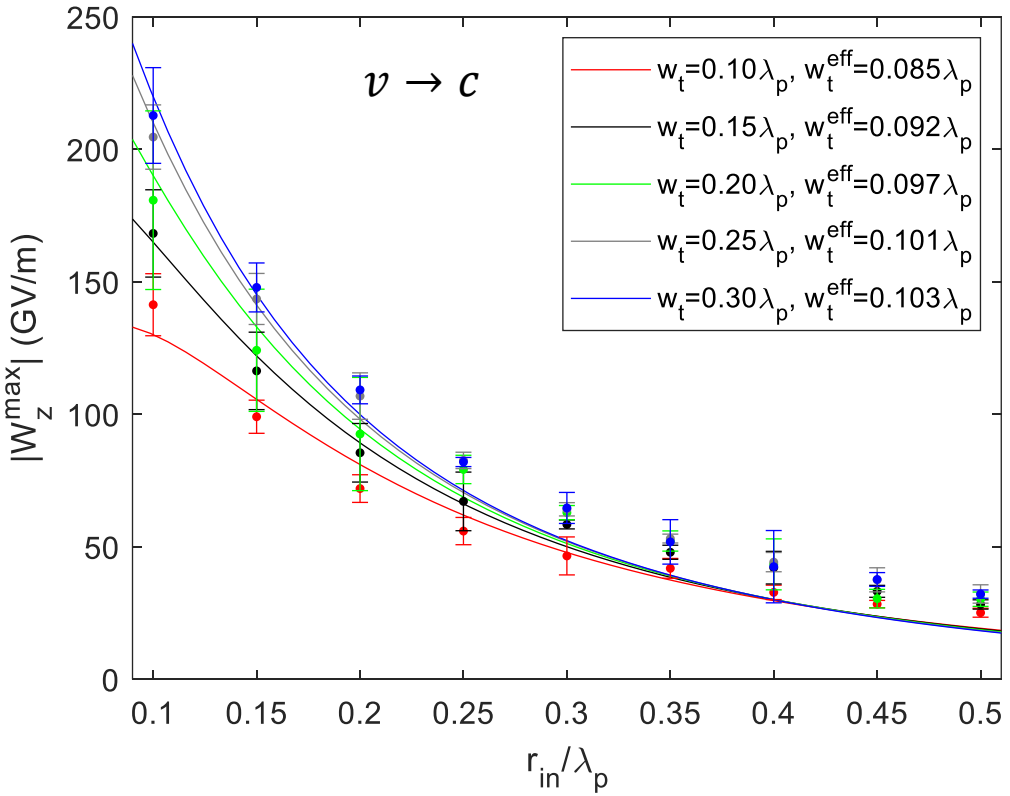


$\lambda_p = \frac{2\pi c}{\omega_p}$ is the plasma wavelength, where

$\omega_p = \sqrt{e^2 n_V / \varepsilon_0 m_e}$ is the plasma frequency.

# 3. Carbon nanotubes (comparison with PIC simulations)

- **Effective parameters.** As it is expected, $\kappa$ **decreases** and $w_t^{\mathrm{eff}}$ **increases** with the wall thickness.

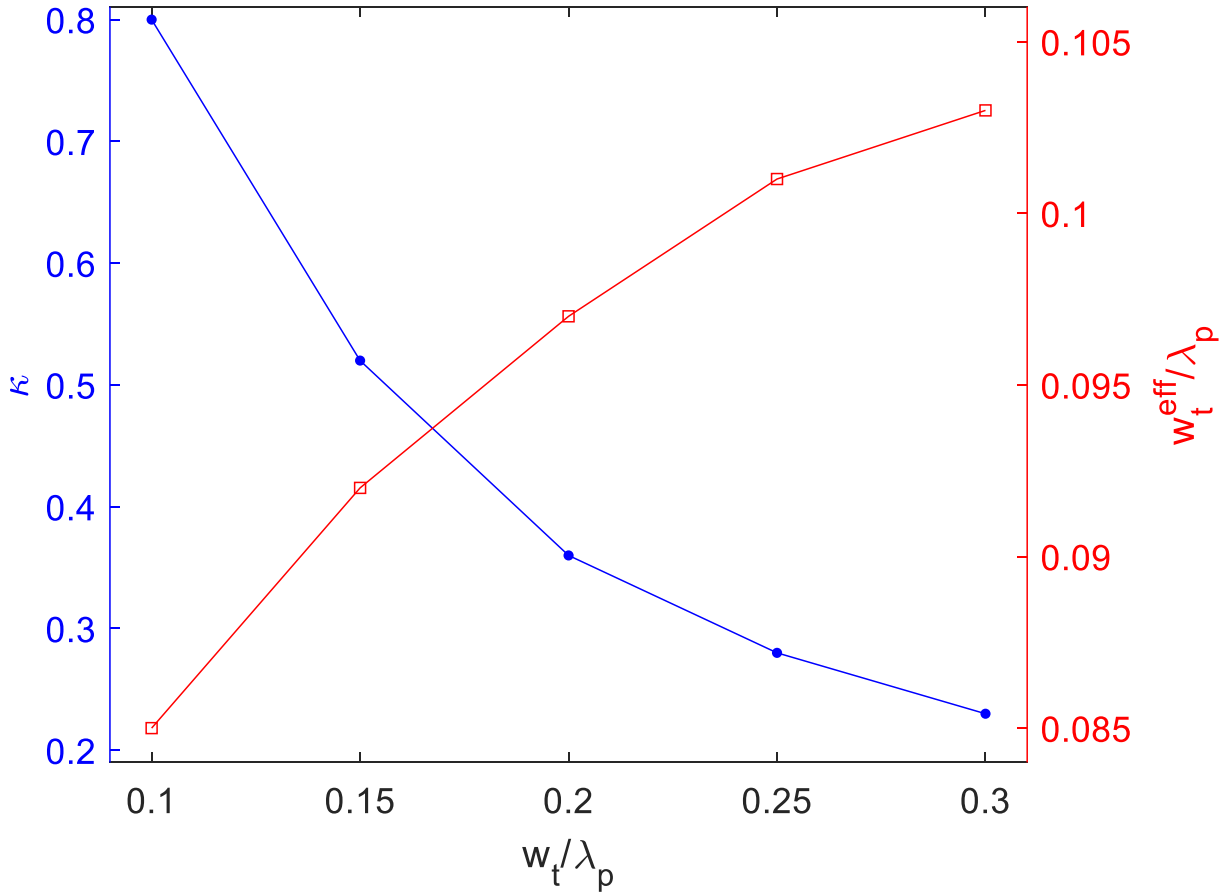

# 3. Carbon nanotubes (comparison with PIC simulations)

The discrepancies obtained between the linearized hydrodynamic model and the PIC simulations can be explained due to the differences between both approximations, such as:

- The **solid-state properties** cannot be taken into account in PIC codes, whereas these properties may be modelled with the parameters $\alpha$, $\beta$, and $\gamma$ in the linearized hydrodynamic model
- We are comparing a **3D region** with free electrons in PIC simulations with a **2D cylindrical surface** in the linearized hydrodynamic model
- The electrons and carbon ions comprising the CNT can **move in 3D in PIC simulations**, whereas they are assumed to be confined over the surface in the linearized hydrodynamic model
- The **driver interacts** with the surrounding medium (losing energy) in PIC codes, whereas in the linearized hydrodynamic model we assume a **constant velocity**
- The size of the driver beam in the PIC simulations **is not a point-like charge** as assumed in the linearized hydrodynamic model

| | LHM | PIC |
|---|---|---|
| Solid-state effects | YES $(\alpha, \beta, \gamma)$ | NO |
| Region with free electrons | 2D (cylindrical) | 3D |
| Movement of CNT particles | 2D (cylindrical) | 3D |
| Driver interaction | NO (constant v) | YES |
| Driver beam size | point-like | bi-Gaussian |

# 4. Graphene layers

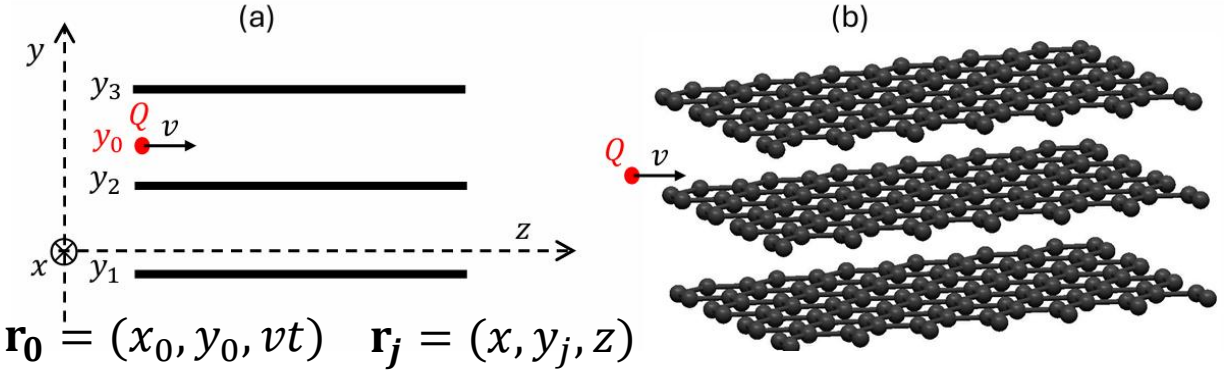


$\mathbf{r_0} = (x_0, y_0, vt) \quad \mathbf{r_j} = (x, y_j, z)$

- Fourier definition: $\mathbf{R} = (x, z) \rightarrow \mathbf{k} = (k_x, k_z)$

$$A(\mathbf{R}, y, t) = \frac{1}{(2\pi)^3} \int \tilde{A}(\mathbf{k}, y, \omega) e^{-i(\omega t - \mathbf{k}\cdot\mathbf{R})} d^2\mathbf{k} d\omega$$

- Using the relation:

$$\frac{1}{|\mathbf{r} - \mathbf{r}'|} = \frac{1}{2\pi} \int \mathrm{d}^2\mathbf{k} \frac{e^{ik(\mathbf{R}-\mathbf{R}')} e^{-k|y-y'|}}{k}$$

$$\Phi_0(\mathbf{r}, t) = \frac{Q}{|\mathbf{r} - \mathbf{r_0}|}$$

$$\Phi_{\mathrm{ind}}(\mathbf{r}, t) = -\sum_j \int \mathrm{d}^2\mathbf{r_j} \frac{n_j(\mathbf{r_j}, t)}{|\mathbf{r} - \mathbf{r_j}|}$$

$$\tilde{\Phi}_0(\mathbf{k}, y, \omega) = \frac{(2\pi)^2 Q \delta(\omega - \mathbf{k}\cdot\mathbf{v})}{k} e^{-k|y-y_0|}$$

$$\tilde{\Phi}_{\mathrm{ind}}(\mathbf{k}, y, \omega) = -\sum_{j=1}^{N} \frac{2\pi}{k} \tilde{n}_j(\mathbf{k}, \omega) e^{-k|y-y_j|}$$

# 4. Graphene layers

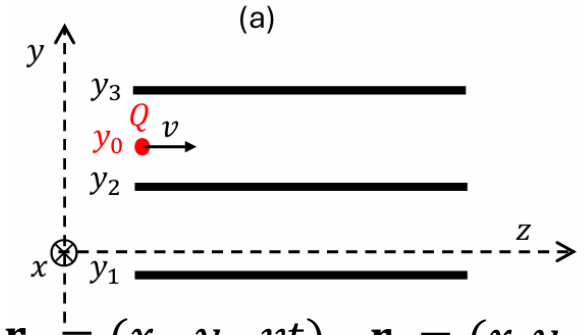


$\mathbf{r_0} = (x_0, y_0, vt) \quad \mathbf{r_j} = (x, y_j, z)$

- Matrix equation:

$$-\left(\frac{\partial^2}{\partial t^2} + \gamma_j \frac{\partial}{\partial t}\right) n_j(\mathbf{r_j}, t) = n_{0j} \nabla_j^2 \Phi(\mathbf{r_j}, t) - \alpha_j \nabla_j^2 n_j(\mathbf{r_j}, t) + \beta \nabla_j^2 \left[\nabla_j^2 n_j(\mathbf{r_j}, t)\right]$$

$$A(\mathbf{R}, y, t) = \frac{1}{(2\pi)^3} \int \widetilde{A}(\mathbf{k}, y, \omega) e^{-i(\omega t - \mathbf{k}\cdot\mathbf{R})} d^2\mathbf{k} d\omega$$

$\mathbf{R} = (x, z) \rightarrow \mathbf{k} = (k_x, k_z)$

$$\nabla_j^2 = \frac{\partial^2}{\partial x^2} + \frac{\partial^2}{\partial z^2}$$

$$\boxed{S_j(\mathbf{k}, \omega)\tilde{n}_j(\mathbf{k}, \omega) - \sum_l G_{jl}(\mathbf{k})\tilde{n}_l(\mathbf{k}, \omega) = B_j(\mathbf{k}, \omega)}$$

$$S_j(\mathbf{k}, \omega) = \omega(\omega + i\gamma_j) - \alpha_j k^2 - \beta k^4,$$

$$G_{jl}(\mathbf{k}) = 2\pi n_{0j} k e^{-k|y_j - y_l|},$$

$$B_j(\mathbf{k}, \omega) = -n_{0j} k^2 \widetilde{\Phi}_0(\mathbf{k}, y_j, \omega)$$

$$n_j(\mathbf{R}, y, t) = \frac{4}{(2\pi)^3} \int_0^\infty \int_0^\infty \mathrm{Re}[\widetilde{n}_j(\mathbf{k}, y, k_z v) e^{ik_z \zeta}] \cos(k_x x) dk_x dk_z,$$

$$\Phi_{\mathrm{ind}}(\mathbf{R}, y, t) = \frac{4}{(2\pi)^3} \int_0^\infty \int_0^\infty \mathrm{Re}[\widetilde{\Phi}_{\mathrm{ind}}(\mathbf{k}, y, k_z v) e^{ik_z \zeta}] \cos(k_x x) dk_x dk_z$$

# 4. Graphene layers (comparison with CNTs)

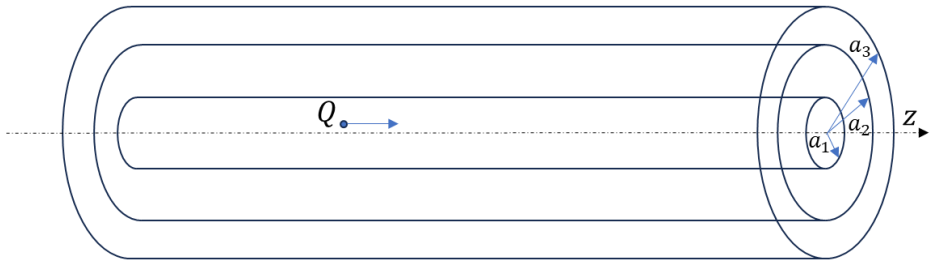


$\mathbf{r_0} = (\mathrm{r}_0, \varphi_0, vt) \quad \mathbf{r_j} = (a_j, \varphi, z)$

$$A(\varphi, z, t) = \sum_{m=-\infty}^{\infty} \int_{-\infty}^{\infty} \frac{\mathrm{d}k}{(2\pi)^2} \int_{-\infty}^{\infty} \frac{\mathrm{d}\omega}{2\pi} \mathrm{e}^{ikz+im\varphi-i\omega t} \widetilde{A}(m,k,\omega)$$

$$\boxed{S_j(m,k,\omega)\tilde{n}_j(m,k,\omega) - \sum_l G_{jl}(m,k)\tilde{n}_l(m,k,\omega) = B_j(m,k,\omega)}$$

$$S_j(m,k,\omega) = \omega(\omega + i\gamma_j) - \alpha_j\left(k^2 + \frac{m^2}{a_j^2}\right) - \beta\left(k^2 + \frac{m^2}{a_j^2}\right)^2,$$

$$G_{jl}(m,k) = n_{0j}a_l\left(k^2 + \frac{m^2}{a_j^2}\right) g\left(a_j, a_l; m, k\right),$$

$$B_j(m,k,\omega) = -n_{0j}\left(k^2 + \frac{m^2}{a_j^2}\right) \tilde{\Phi}_0\left(a_j, m, k, \omega\right).$$

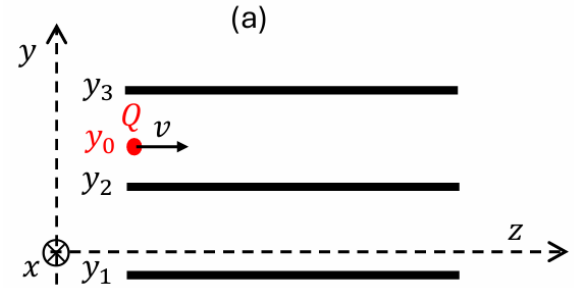


$\mathbf{r_0} = (x_0, y_0, vt) \quad \mathbf{r_j} = (x, y_j, z)$

$$A(\mathbf{R}, y, t) = \frac{1}{(2\pi)^3} \int \widetilde{A}(\mathbf{k}, y, \omega) e^{-i(\omega t - \mathbf{k}\cdot\mathbf{R})} d^2\mathbf{k} d\omega$$

$$\boxed{S_j(\mathbf{k},\omega)\tilde{n}_j(\mathbf{k},\omega) - \sum_l G_{jl}(\mathbf{k})\tilde{n}_l(\mathbf{k},\omega) = B_j(\mathbf{k},\omega)}$$

$$S_j(\mathbf{k},\omega) = \omega(\omega + i\gamma_j) - \alpha_j k^2 - \beta k^4,$$

$$G_{jl}(\mathbf{k}) = 2\pi n_{0j} k e^{-k|y_j - y_l|},$$

$$B_j(\mathbf{k},\omega) = -n_{0j} k^2 \widetilde{\Phi}_0(\mathbf{k}, y_j, \omega)$$

# 4. Graphene layers (comparison with CNTs)

- **Geometry.**

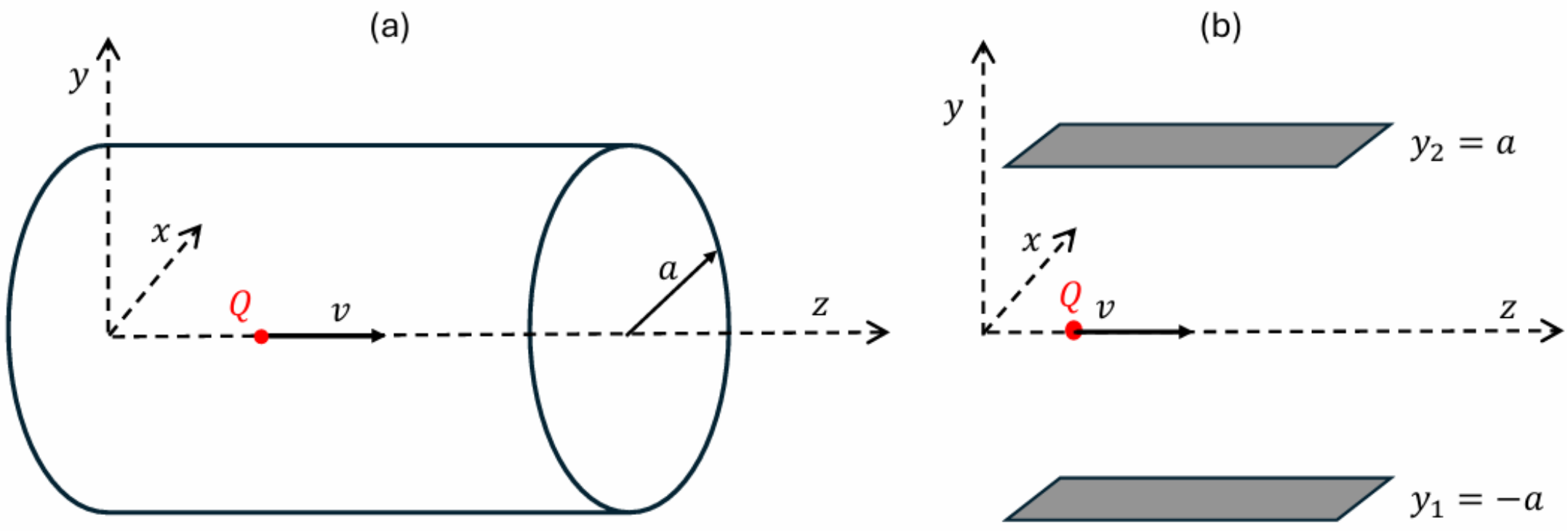

# 4. Graphene layers (comparison with CNTs)

- **Dispersion relation**

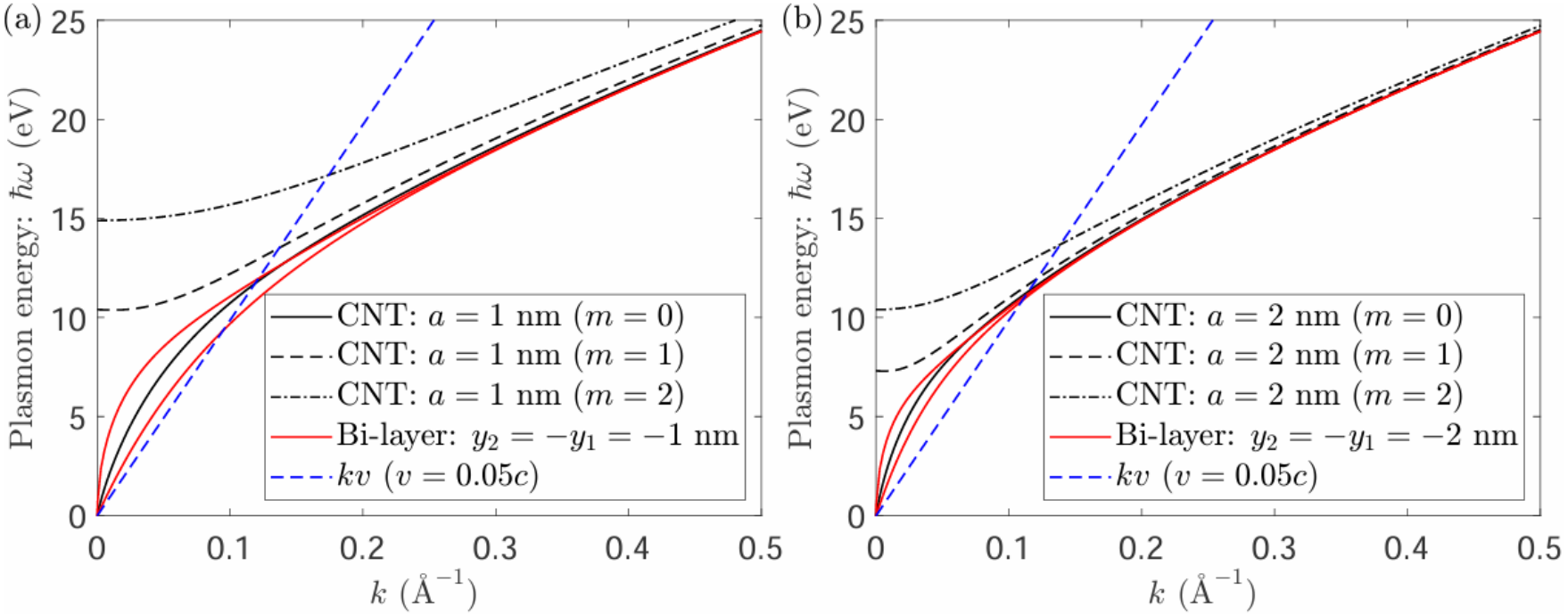


**Figure 4.**
*Plasmon dispersion relations $\omega_m(k)$ for different modes m for a CNT with (a) a = 1 nm and (b) a = 2 nm. The resonances $k_m$ are the intersection of a kv line (plotted for v = 0.05c) with the dispersion curves $\omega_m(k)$. For comparison, we include the dispersion relations for two graphene layers separated a distance 2a.*

# 4. Graphene layers (comparison with CNTs)

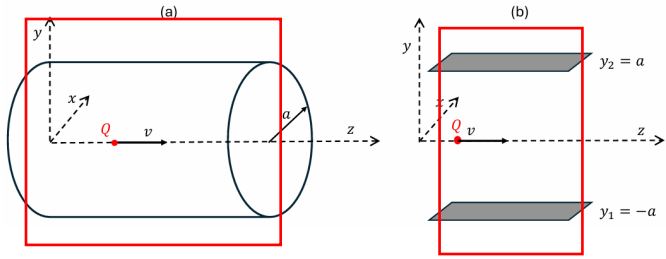


- **Wakefields**

Longitudinal

Transverse

CNT

Graphene

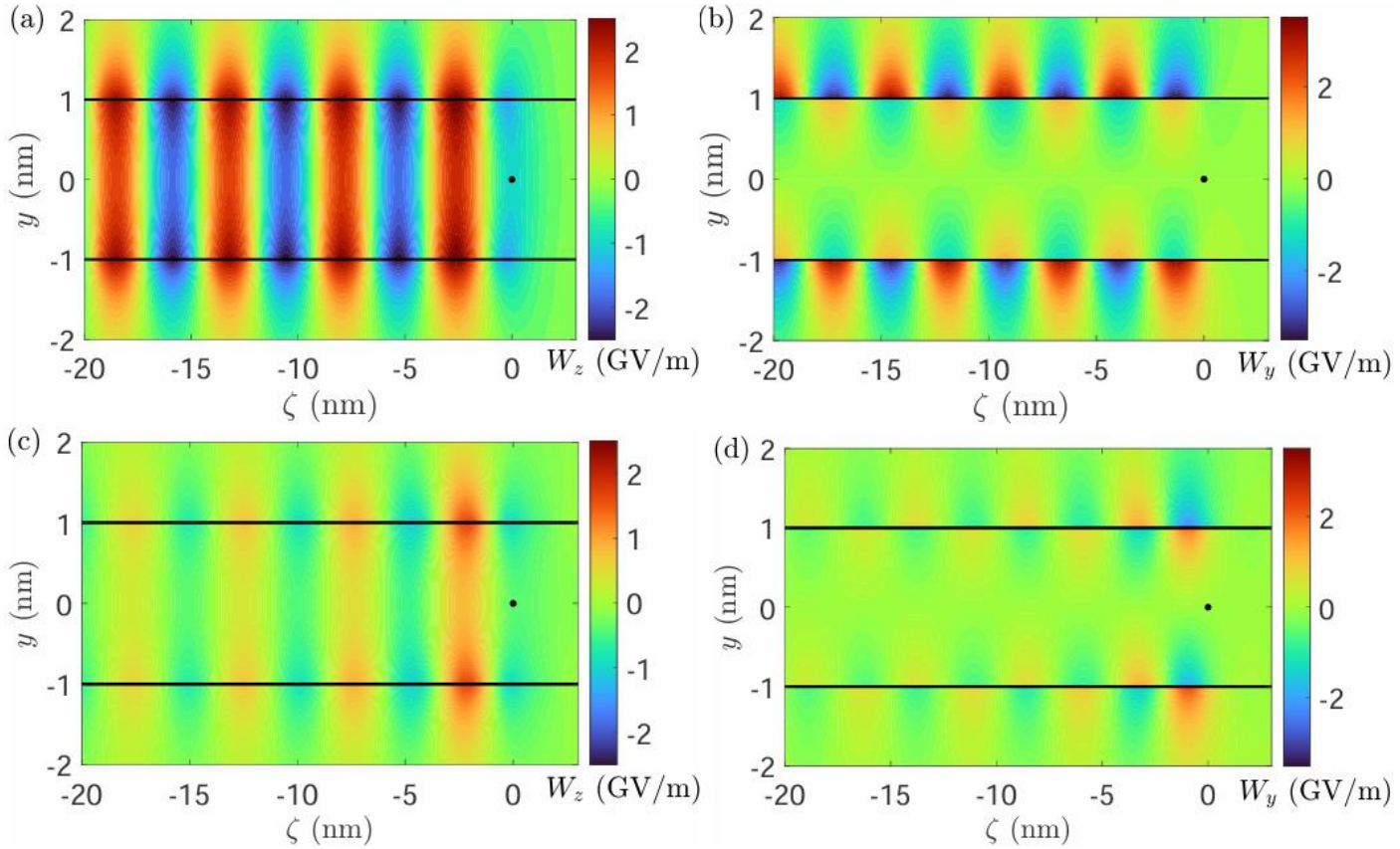


Decay

**Figure 5.**
*Induced wakefields (a) $W_z$ and (b) $W_y$ in the $y\zeta$-plane for a proton traveling on the z-axis with a velocity $v = 0.05c$ within a CNT with radius $a = 1$ nm. In (c) and (d) we consider two graphene layers located at $y_2 = -y_1 = a$. In both cases, the friction parameter is $\gamma = 10^{-3}$ a.u. $\approx 4.13 \times 10^{13}\,s^{-1}$. The wakefield $W_x$ is zero in the $y\zeta$-plane. The proton is indicated with a black point and the graphene layer with a black line.*

# 4. Graphene layers (comparison with CNTs)

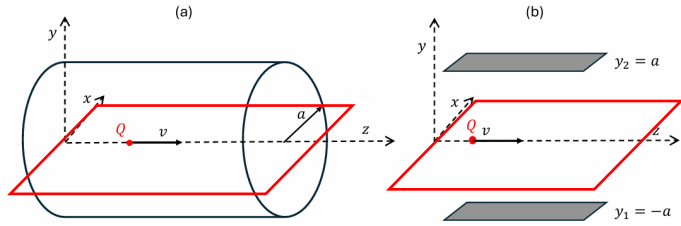


- **Wakefields**

Longitudinal

Transverse

CNT

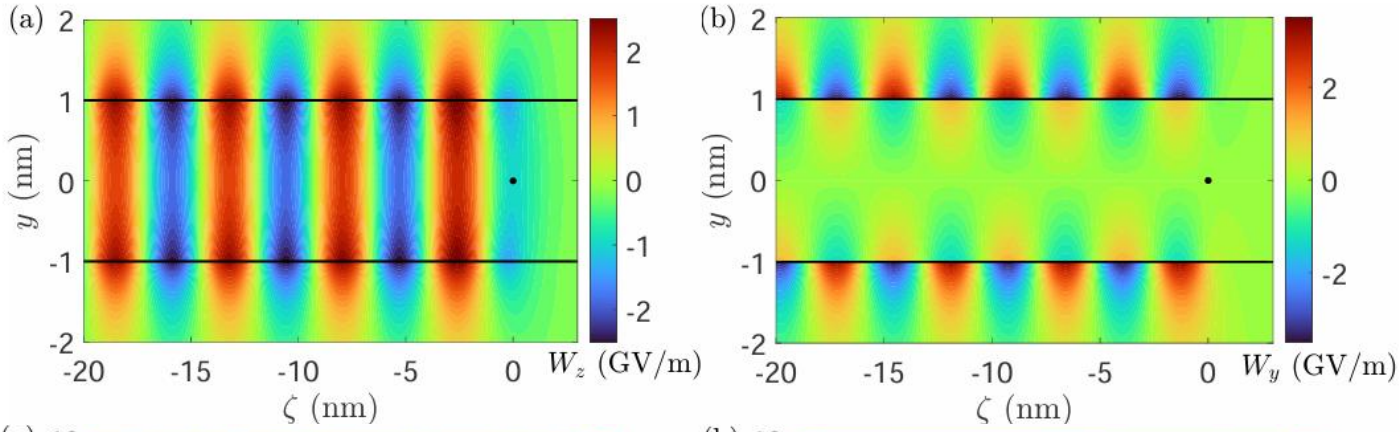


Graphene

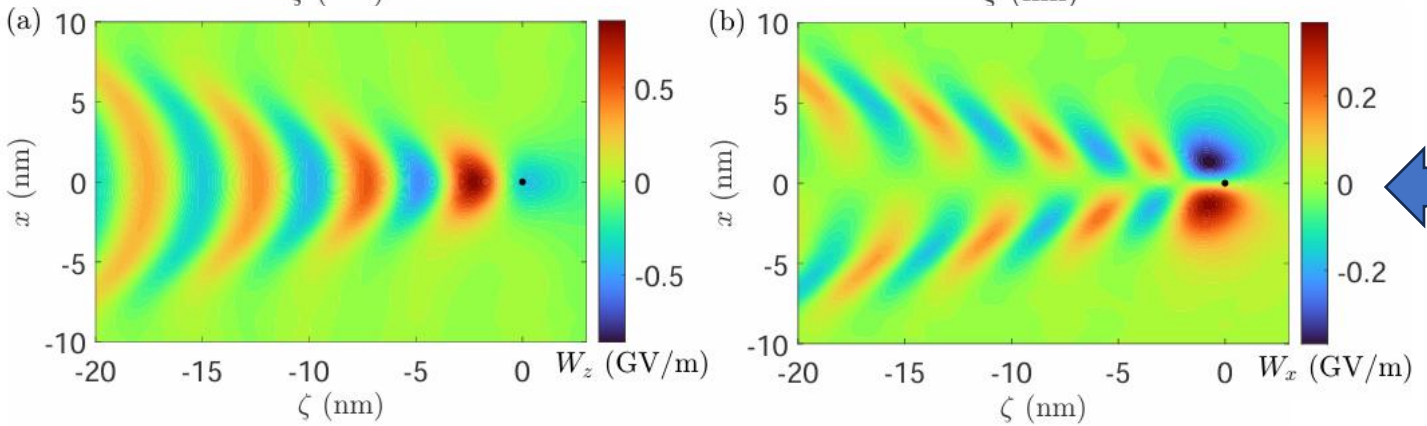


Decay due to spread in the plane

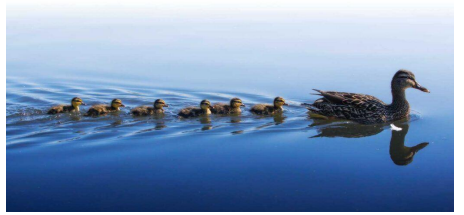

# 4. Graphene layers (comparison with CNTs)

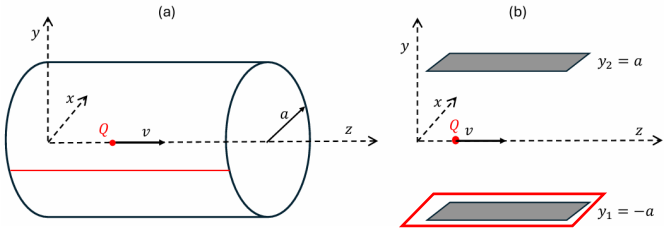


- **Perturbed density**

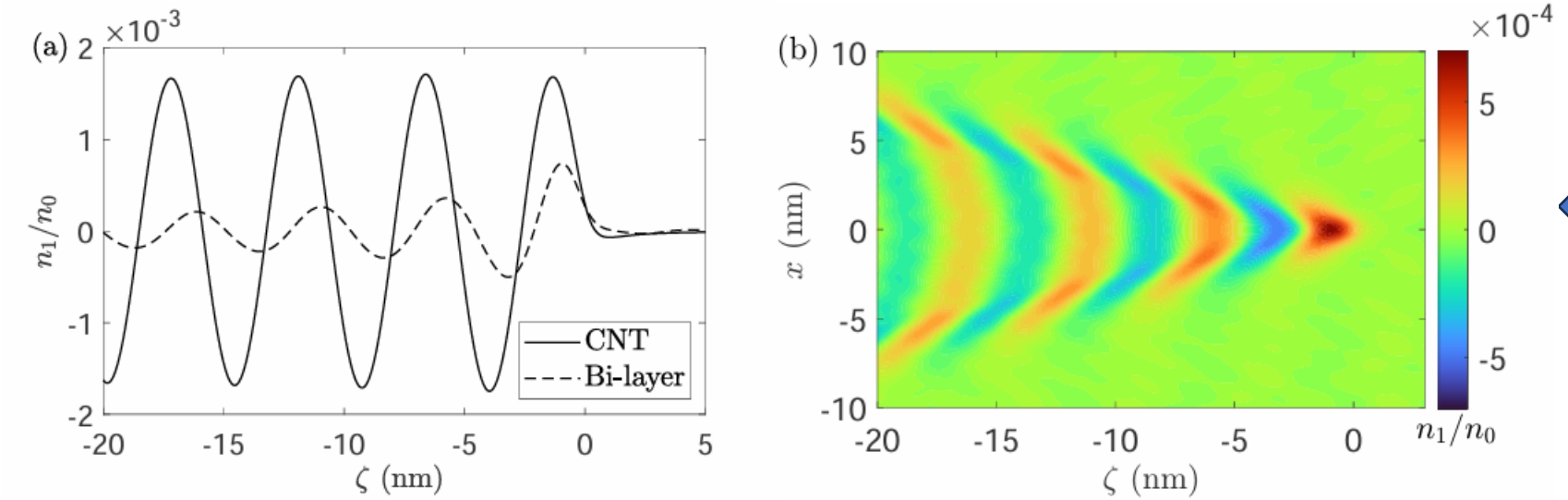


Decay due to spread in the plane

**Figure 7.**
*(a) Normalized perturbed density $n_1/n_0$ for a proton traveling on the z-axis with a velocity $v = 0.05c$ within a CNT with radius $a = 1\,nm$ and two graphene layers located at $y_2 = -y_1 = a$. In (b) we show the perturbed density in the layer plane, i.e. at $y_1 = -a$. Due to symmetry, the perturbed density in both layers is identical.*

# 4. Graphene layers (comparison with CNTs)

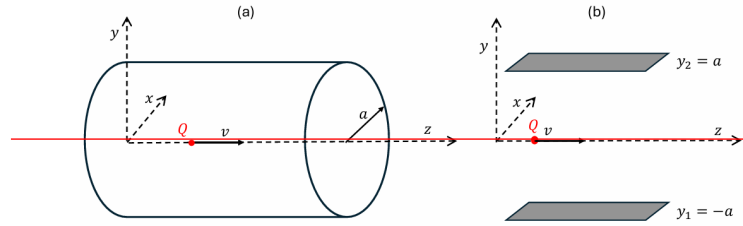


- **Wakefield along z-axis**

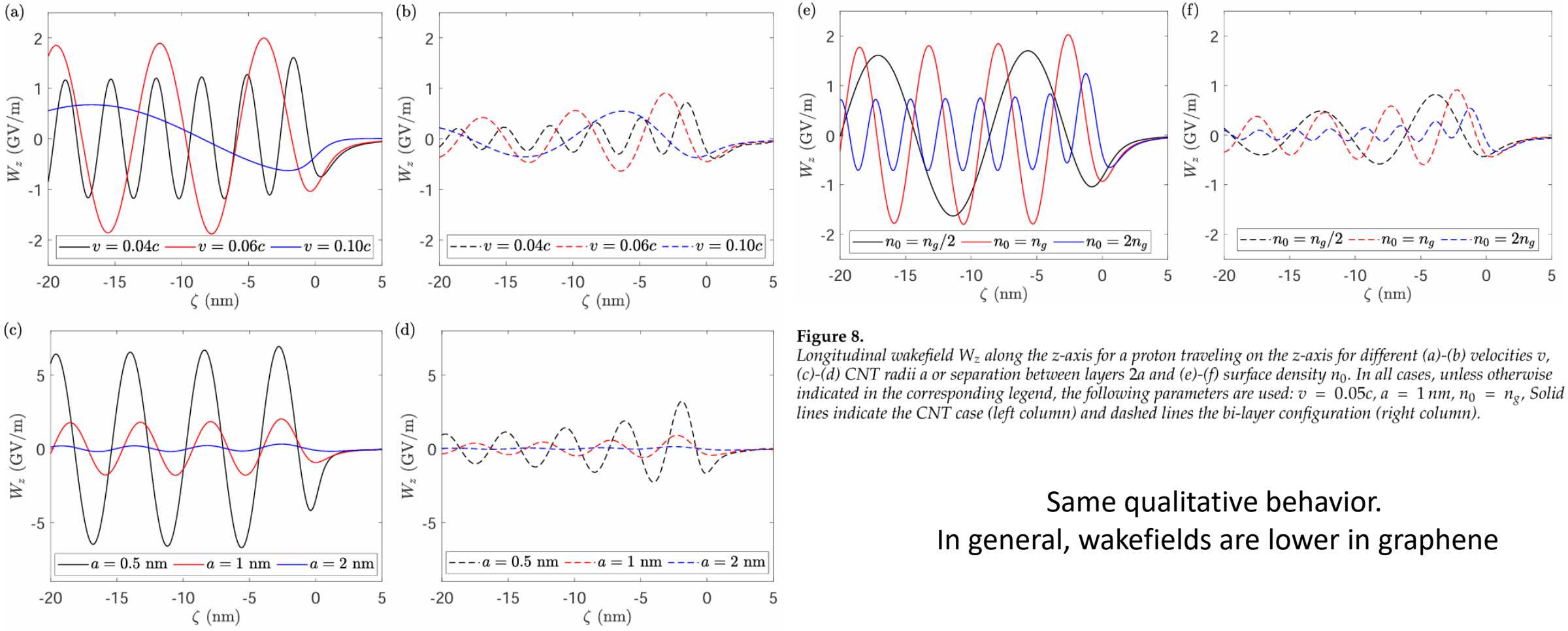


**Figure 8.**
*Longitudinal wakefield $W_z$ along the z-axis for a proton traveling on the z-axis for different (a)-(b) velocities v, (c)-(d) CNT radii a or separation between layers 2a and (e)-(f) surface density $n_0$. In all cases, unless otherwise indicated in the corresponding legend, the following parameters are used: $v = 0.05c$, $a = 1\,nm$, $n_0 = n_g$, Solid lines indicate the CNT case (left column) and dashed lines the bi-layer configuration (right column).*

Same qualitative behavior.
In general, wakefields are lower in graphene

# 4. Graphene layers (comparison with CNTs)

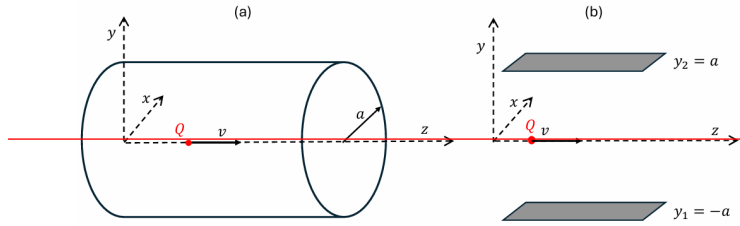


- **Maximum wakefield along z-axis and stopping power**

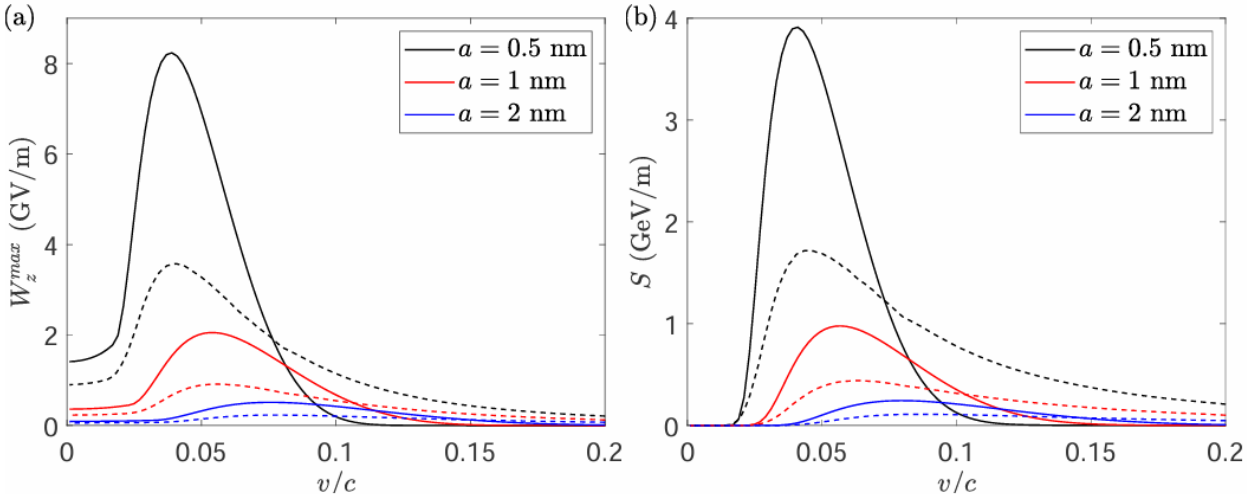


**Figure 9.**
*(a) Maximum longitudinal wakefield $W_z^{max}$ and (b) stopping power as a function of the driving velocity for different values of a. Solid lines indicate the CNT case and dashed lines the bi-layer configuration.*

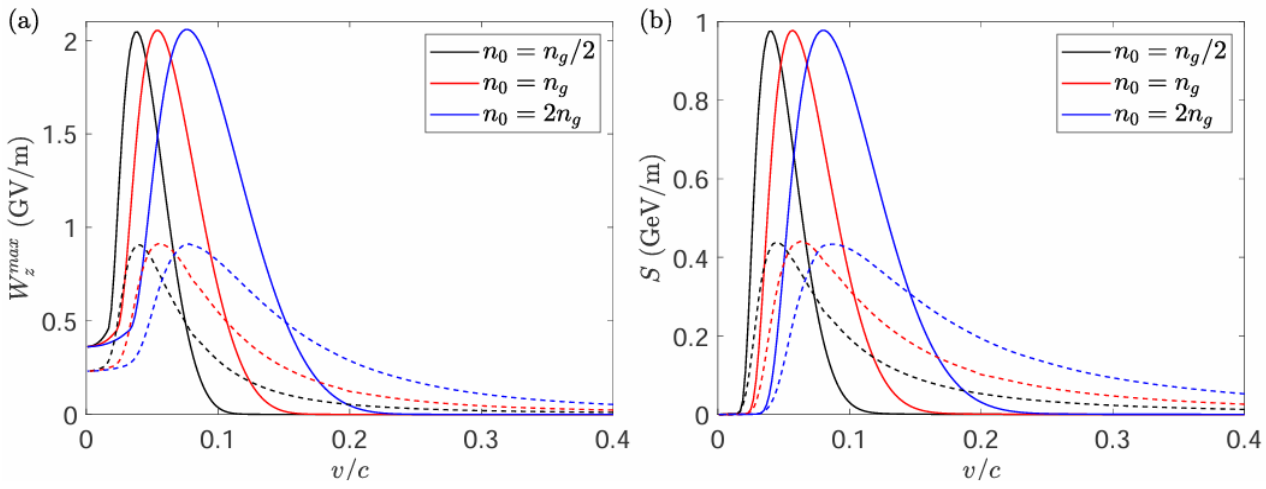


**Figure 10.**
*(a) Maximum longitudinal wakefield $W_z^{max}$ and (b) stopping power as a function of the driving velocity for different values of the surface density $n_0$ for a = 1 nm. Solid lines indicate the CNT case and dashed lines the bi-layer configuration.*

Same qualitative behavior. In general, wakefields are lower in graphene

# 4. Graphene layers (comparison with CNTs)

- **Maximum wakefield along z-axis and stopping power**

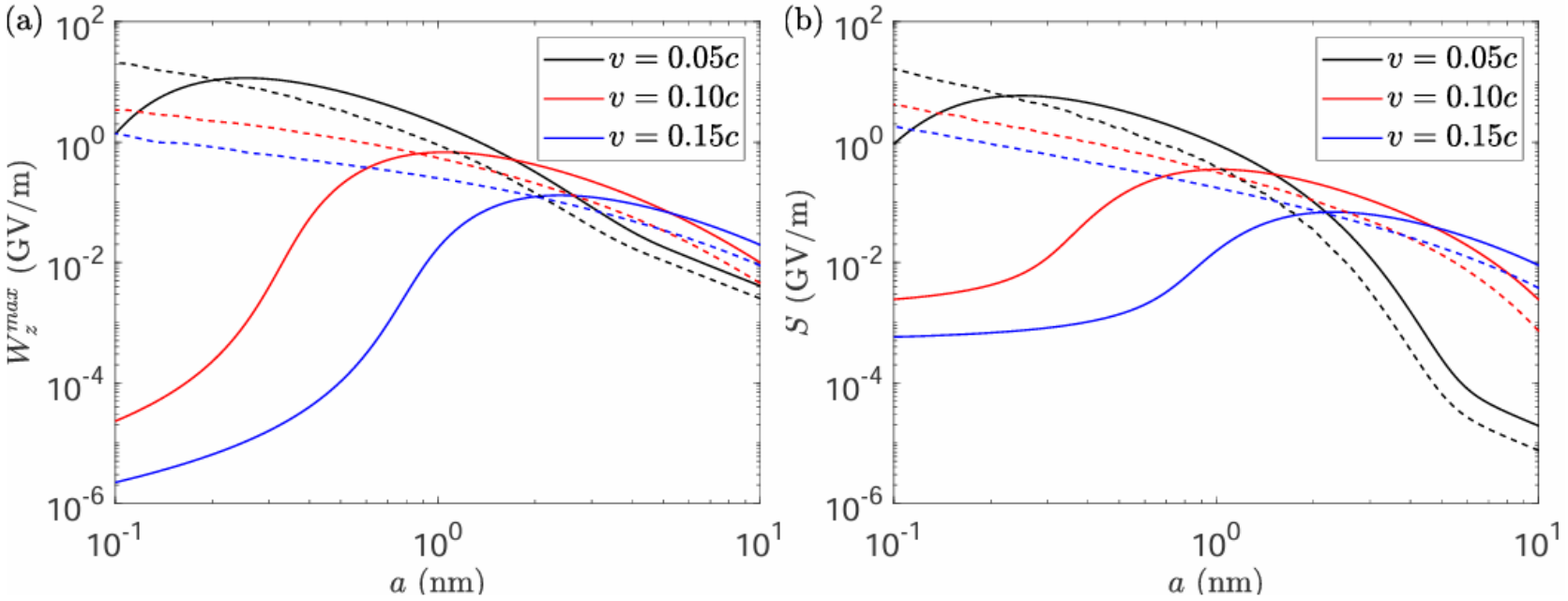


**Figure 11.**
*(a) Maximum longitudinal wakefield $W_z^{max}$ and (b) stopping power as a function of the CNT radius a (layers separated a distance 2a) for different values of the driving velocity. Solid lines indicate the CNT case and dashed lines the bi-layer configuration.*

In graphene layers, the wakefields increase as the separation between layer decreases contrary to CNTs where wakefields decrease rapidly for small radii.

# 4. Graphene layers (comparison with CNTs)

- **Acceleration and focusing**

Bi-layer graphene

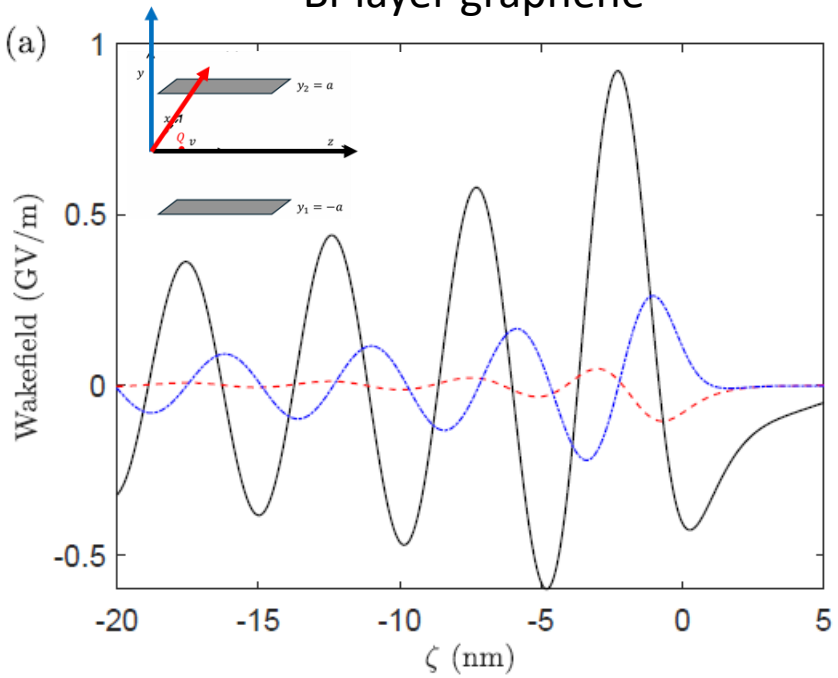


**Figure 12.** (a) Induced wakefields along the line $y = z = 0.2$ nm for a proton traveling on the $x$-axis with a velocity $v = 0.05c$. The graphene layers are located at $z_1 = -1$ nm and $z_2 = 1$ nm.

CNT

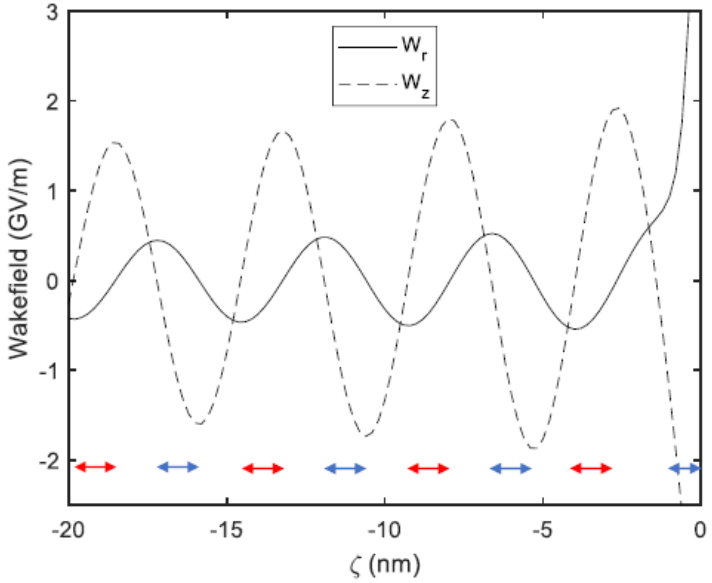


**Figure 7.** Wakefields (including the Coulomb term) at $r = a/2$ for $a = 1$ nm, $v = 0.05c$, $\gamma = 0.01\Omega_p$ and $r_0 = 0$. The red (blue) arrows indicate the regions where a positive (negative) witness charged particle would experience both acceleration and focusing simultaneously.

In CNTs, it is posible that a witness beam experiences **acceleration and focusing**, but in graphene layers is not possible

# 4. Graphene layers (comparison with PIC)

Work in progress

- **Longitudinal wakefield**

LHM model

PIC simulations (WarpX)

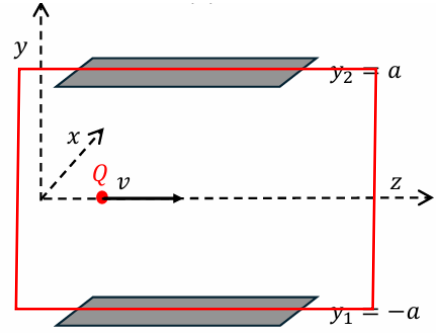


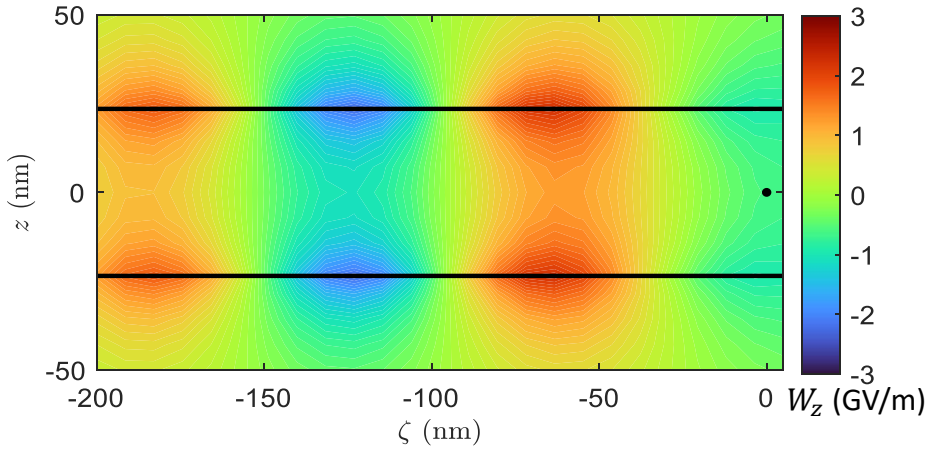


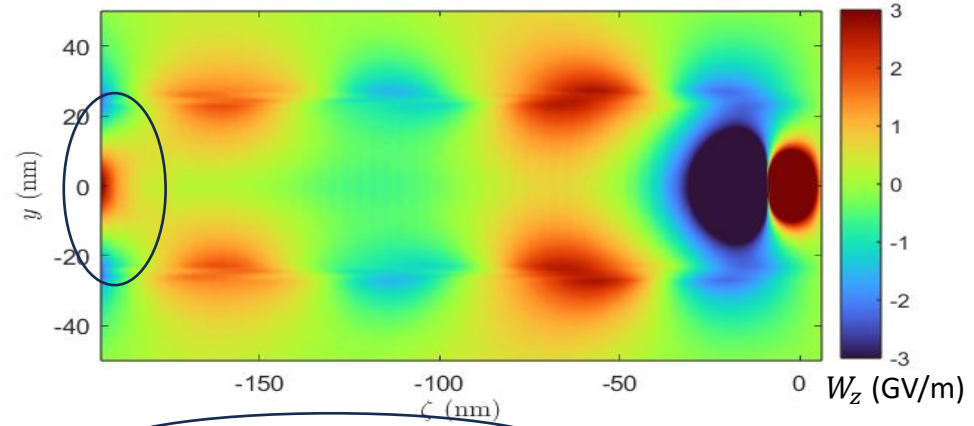


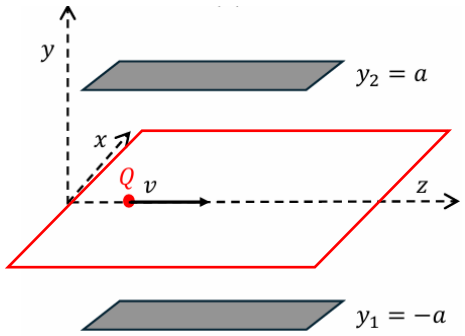


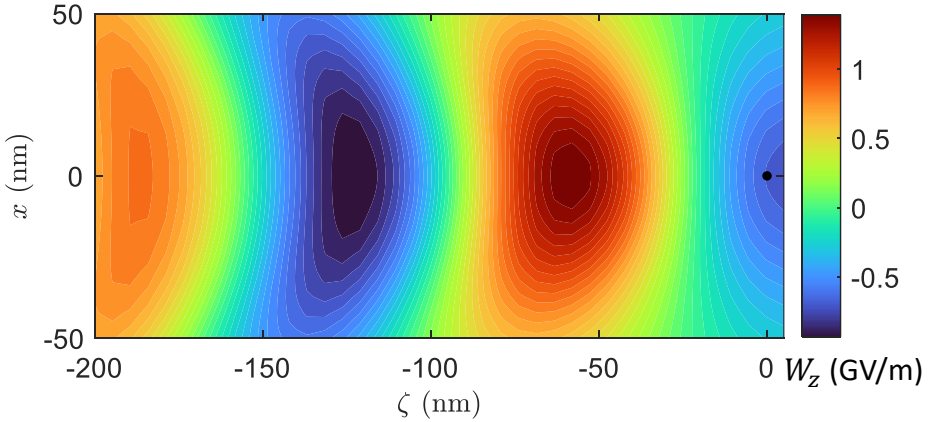


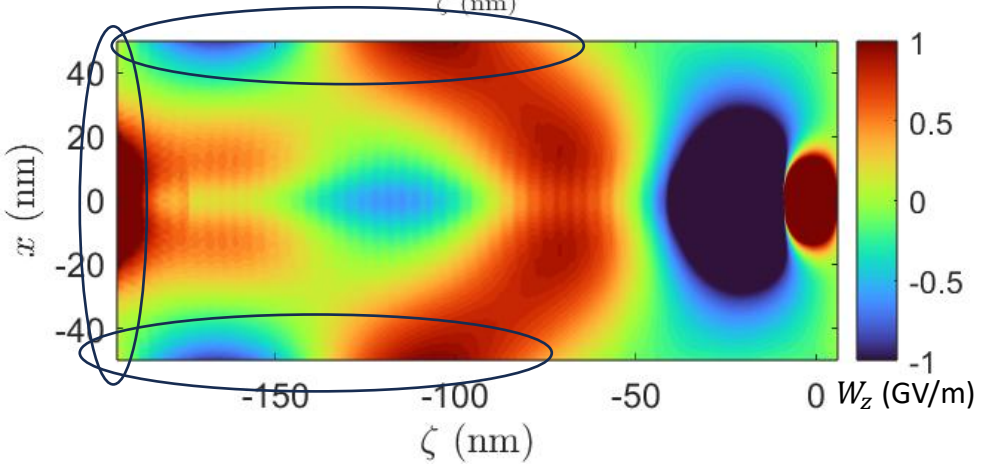


$Q = 1000, v = 0.25c, y_2 = -y_1 = 25$ nm

# 4. Graphene layers (with dielectrics)

Work in progress

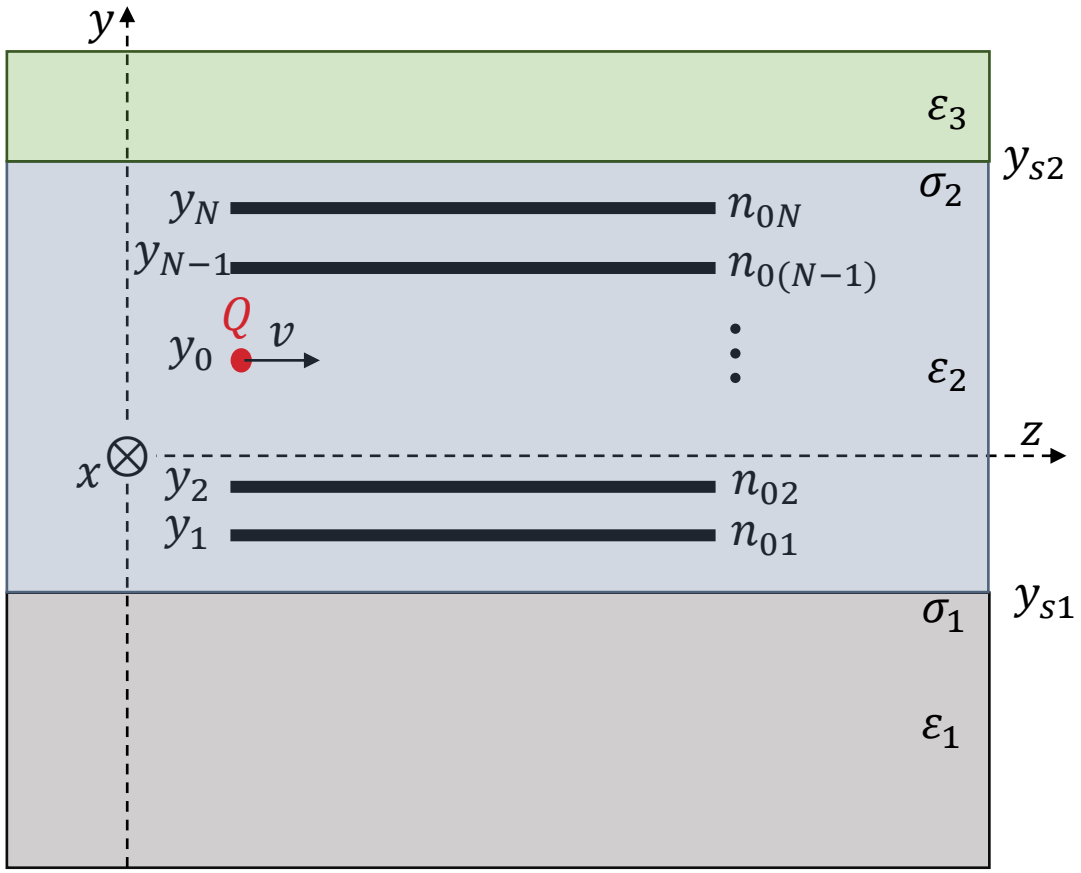


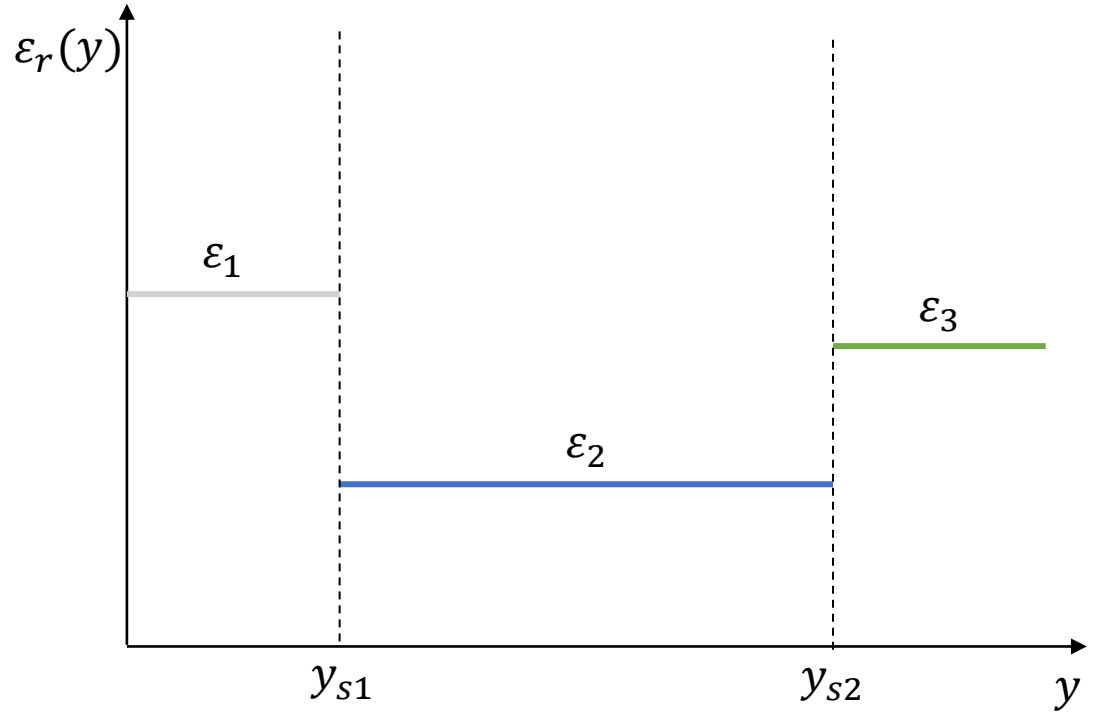


$$\boxed{Q + \sum_l n_l + \sum_p \sigma_p}$$

$$\nabla \cdot \vec{E} = \frac{\rho_{free} + \rho_{bound}}{\varepsilon_0}$$

# 4. Graphene layers (with dielectrics)

- Matrix equation:

$$-\left(\frac{\partial^2}{\partial t^2}+\gamma_j\frac{\partial}{\partial t}\right)n_j(\mathbf{r_j},t)=n_{0j}\nabla_j^2\underbrace{\Phi(\mathbf{r_j},t)}_{Q+\sum_l n_l+\sum_p \sigma_p}-\alpha_j\nabla_j^2 n_j(\mathbf{r_j},t)+\beta\nabla_j^2\left[\nabla_j^2 n_j(\mathbf{r_j},t)\right]$$

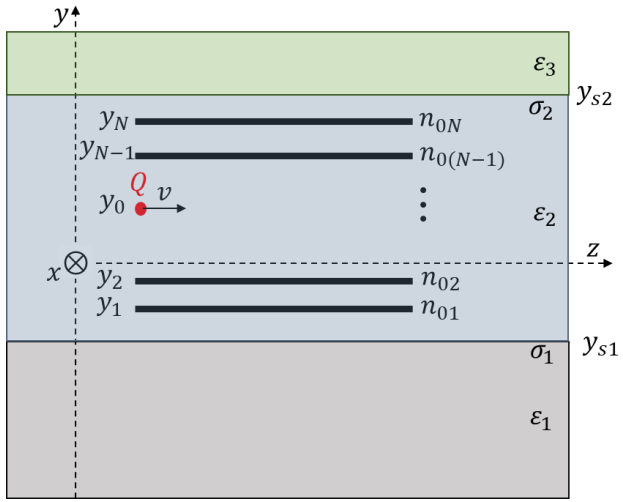


$$\mathbf{r_0}=(x_0,y_0,vt)\quad \mathbf{r_j}=(x,y_j,z)$$

$$\tilde{\Phi}_0(\mathbf{k},y,\omega)=\frac{(2\pi)^2Q\delta(\omega-\mathbf{k}\cdot\mathbf{v})}{k}e^{-k|y-y_0|}$$

$$\tilde{\Phi}_l=-\frac{2\pi}{k}\tilde{n}_l(\mathbf{k},\omega)\,e^{-k|y-y_l|}$$

$$\tilde{\Phi}_p=\frac{2\pi}{k}\tilde{\sigma}_p(\mathbf{k},\omega)\,e^{-k|y-y_{sp}|}$$

$$S_j(\mathbf{k},\omega)\tilde{n}_j(\mathbf{k},\omega)-\sum_l G_{jl}(\mathbf{k})\tilde{n}_l(\mathbf{k},\omega)+\sum_p F_{jp}(\mathbf{k})\tilde{\sigma}_p(\mathbf{k},\omega)=B_j(\mathbf{k},\omega)\propto Q$$

$$S_j(\mathbf{k},\omega)=\omega(\omega+i\gamma_j)-\alpha_j k^2-\beta k^4,$$

$$G_{jl}(\mathbf{k})=2\pi n_{0j}ke^{-k|y_j-y_l|},$$

$$F_{jp}(\mathbf{k})=2\pi n_{0j}ke^{-k|y_j-y_{sp}|}$$

$$B_j(\mathbf{k},\omega)=-n_{0j}k^2\tilde{\Phi}_0(\mathbf{k},y_j,\omega)$$

$$\left(\begin{array}{cccc|ccc} S_1-G_{11} & -G_{12} & \cdots & -G_{1N} & F_{11} & \cdots & F_{1S} \\ -G_{21} & S_2-G_{22} & \cdots & -G_{2N} & F_{21} & \cdots & F_{2S} \\ \vdots & \vdots & \ddots & \vdots & \vdots & \ddots & \vdots \\ -G_{N1} & -G_{N2} & \cdots & S_N-G_{NN} & F_{N1} & \cdots & F_{NS} \end{array}\right)\left(\begin{array}{c} \tilde{n}_1(\mathbf{k},\omega) \\ \vdots \\ \tilde{n}_N(\mathbf{k},\omega) \\ \hline \tilde{\sigma}_1(\mathbf{k},\omega) \\ \vdots \\ \tilde{\sigma}_S(\mathbf{k},\omega) \end{array}\right)=\left(\begin{array}{c} B_1(\mathbf{k},\omega) \\ \vdots \\ B_N(\mathbf{k},\omega) \end{array}\right)$$

N equations

N+S unknown functions

# 4. Graphene layers (with dielectrics)

- The boundary condition at the interfaces gives the other S eqs:

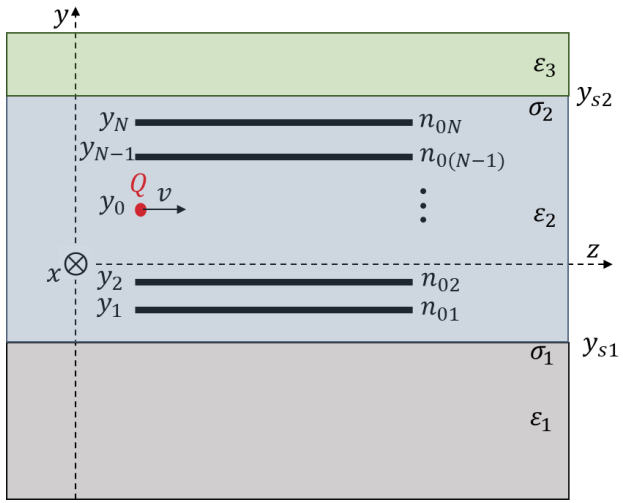


$\mathbf{r_0} = (x_0, y_0, vt) \quad \mathbf{r_j} = (x, y_j, z)$

Continuity of $\vec{D} \cdot \hat{n}$:

$$\varepsilon\left(y_{s_j}^-\right)\frac{\partial \Phi}{\partial y}\Big|_{y_{s_j}^-} = \varepsilon\left(y_{s_j}^+\right)\frac{\partial \Phi}{\partial y}\Big|_{y_{s_j}^+}, \qquad j = 1, \ldots, S$$

$$-\sum_l G'_{jl}(\mathbf{k})\tilde{n}_l(\mathbf{k},\omega) + \sum_p F'_{jp}(\mathbf{k})\tilde{\sigma}_p(\mathbf{k},\omega) = B'_j(\mathbf{k},\omega)$$

S linear equations

$$\frac{\partial e^{-k|y-a|}}{\partial y} = -k\,\mathrm{sign}(y-a)e^{-k|y-a|}$$

$$G'_{jl}(\mathbf{k}) = e^{-k\left|y_{s_j}-y_l\right|}\left(\varepsilon\left(y_{s_j}^-\right)\mathrm{sign}\left(y_{s_j}^- - y_l\right) - \varepsilon\left(y_{s_j}^+\right)\mathrm{sign}\left(y_{s_j}^+ - y_l\right)\right)$$

$$F'_{jp}(\mathbf{k}) = e^{-k\left|y_{s_j}-y_{s_p}\right|}\left(\varepsilon\left(y_{s_j}^-\right)\mathrm{sign}\left(y_{s_j}^- - y_{s_p}\right) - \varepsilon\left(y_{s_j}^+\right)\mathrm{sign}\left(y_{s_j}^+ - y_{s_p}\right)\right)$$

$$B'_j(\mathbf{k},\omega) = -2\pi Q\delta(\omega - \mathbf{k}\cdot\mathbf{v})e^{-k\left|y_{s_j}-y_0\right|}\left(\varepsilon\left(y_{s_j}^-\right)\mathrm{sign}\left(y_{s_j}^- - y_0\right) - \varepsilon\left(y_{s_j}^+\right)\mathrm{sign}\left(y_{s_j}^+ - y_0\right)\right)$$

# 4. Graphene layers (with dielectrics)

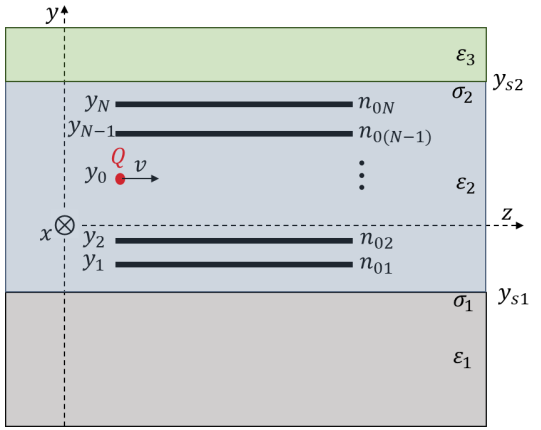


- Matrix equation:

$$\begin{matrix} \\ \text{N} \\ \\ \\ \\ \text{S} \\ \\ \\ \end{matrix}\begin{pmatrix} S_1 - G_{11} & -G_{12} & \cdots & -G_{1N} & F_{11} & \cdots & F_{1S} \\ -G_{21} & S_2 - G_{22} & \cdots & -G_{2N} & F_{21} & \cdots & F_{2S} \\ \vdots & \vdots & \ddots & \vdots & \vdots & \ddots & \vdots \\ -G_{N1} & -G_{N2} & \cdots & S_N - G_{NN} & F_{N1} & \cdots & F_{NS} \\ -G'_{11} & -G'_{12} & \cdots & -G'_{1N} & F'_{11} & \cdots & F'_{1S} \\ -G'_{21} & -G'_{22} & \cdots & -G'_{2N} & F'_{21} & \cdots & F'_{2S} \\ \vdots & \vdots & \ddots & \vdots & \vdots & \ddots & \vdots \\ -G'_{N1} & -G'_{N2} & \cdots & -G'_{NN} & F'_{N1} & \cdots & F'_{NS} \end{pmatrix} \begin{pmatrix} \tilde{n}_1(\mathbf{k},\omega) \\ \vdots \\ \tilde{n}_N(\mathbf{k},\omega) \\ \tilde{\sigma}_1(\mathbf{k},\omega) \\ \vdots \\ \tilde{\sigma}_S(\mathbf{k},\omega) \end{pmatrix} = \begin{pmatrix} B_1(\mathbf{k},\omega) \\ \vdots \\ B_N(\mathbf{k},\omega) \\ B'_1(\mathbf{k},\omega) \\ \vdots \\ B'_S(\mathbf{k},\omega) \end{pmatrix}$$

$\Rightarrow \tilde{n}_l(\mathbf{k},\omega), \tilde{\sigma}_p(\mathbf{k},\omega) \Rightarrow \tilde{\Phi}_{ind}(\mathbf{k},y,\omega) = -\sum_l \frac{2\pi}{k}\tilde{n}_l(\mathbf{k},\omega)\, e^{-k|y-y_l|} + \sum_l \frac{2\pi}{k}\tilde{\sigma}_p(\mathbf{k},\omega)\, e^{-k|y-y_{sp}|}$

$\Phi$ and wakefields as a function of time and position

Fourier transform

# 4. Graphene layers (with dielectrics)

- Single-layer

No substrate SiO2 Substrate

Longitudinal

Transverse

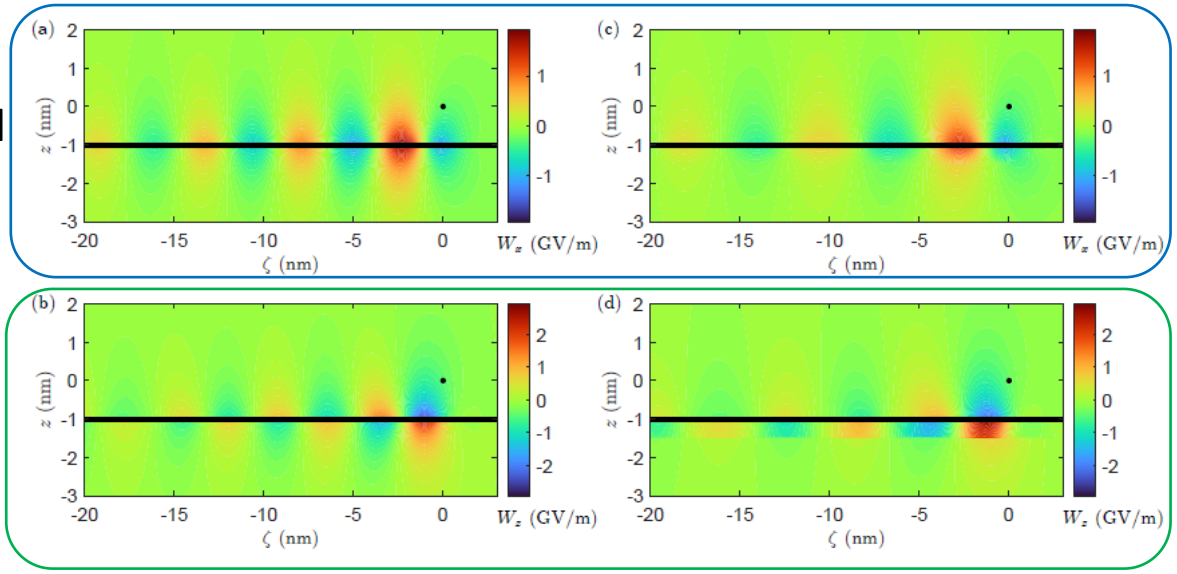


**Figure 3.** Induced wakefields (a) $W_x$ and (b) $W_z$ in the $\zeta z$-plane for a proton traveling on the $x$-axis with a velocity $v = 0.05c$ above a graphene layer located at $z_1 = -1$ nm. In (a) and (b) we do not consider a substrate; for comparison, in (c) and (d) a $SiO_2$ substrate ($\varepsilon_s = 3.9$) is located at $z \leq z_s = -1.5$ nm. The proton is indicated with a black point and the graphene layer with a black line.

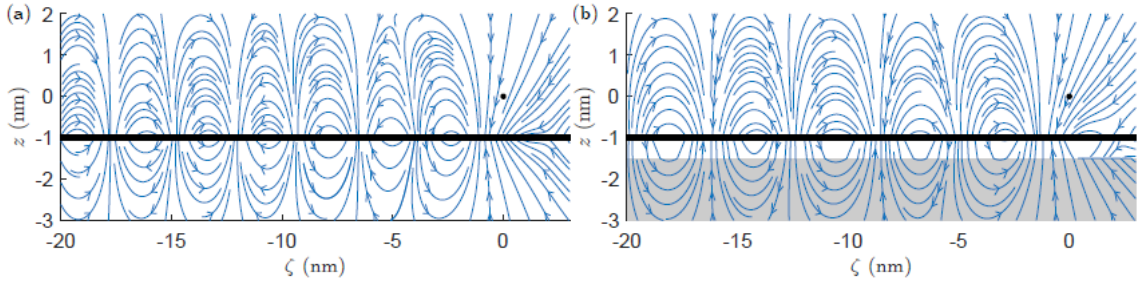


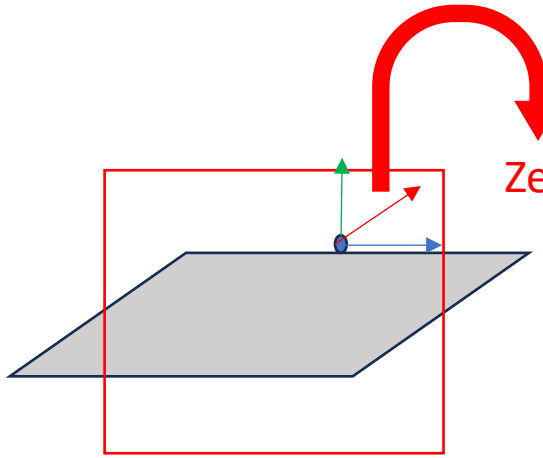

Zero due to symmetry

Infinite substrate

# 4. Graphene layers (with dielectrics)

- Single-layer

No substrate SiO2 Substrate

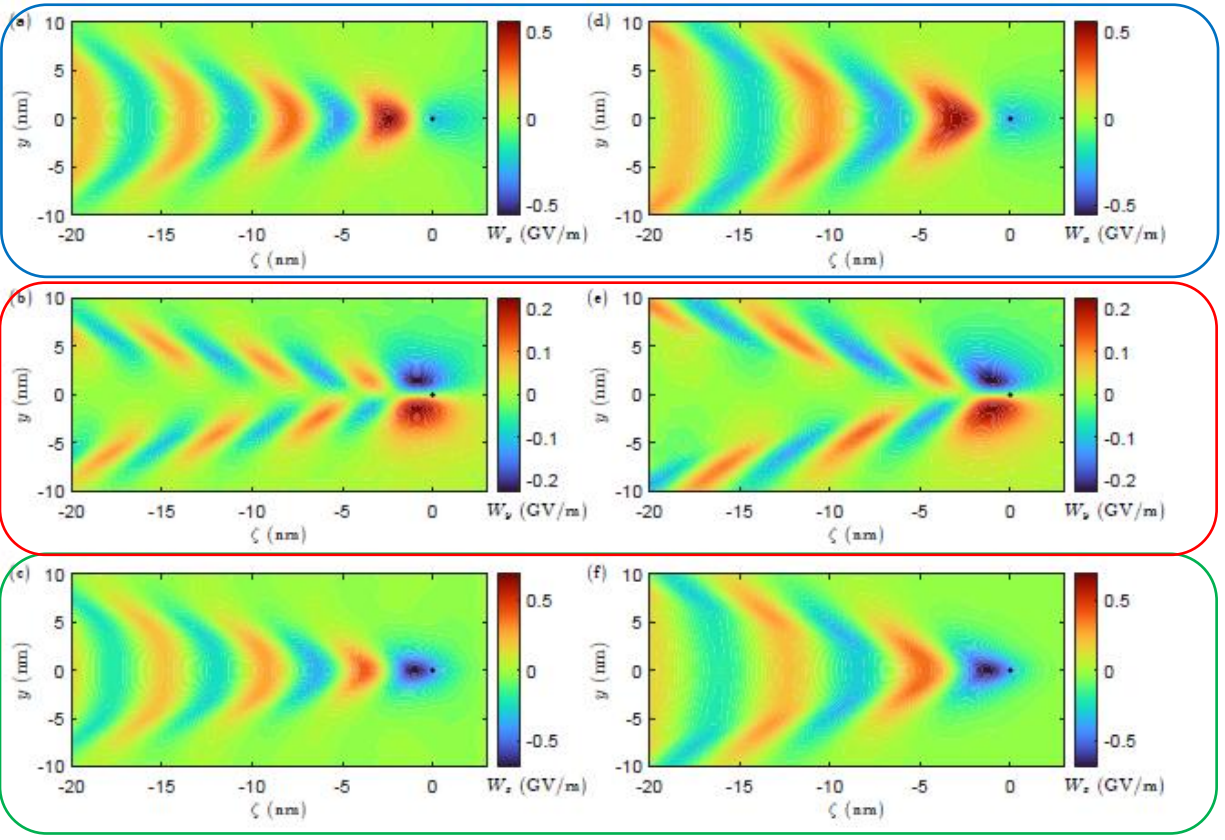


**Figure 5.** Induced wakefields (a) $W_x$, (b) $W_y$ and (c) $W_z$ in the $\zeta y$-plane for a proton traveling on the $x$-axis with a velocity $v = 0.05c$ above a graphene layer located at $z_1 = -1$ nm. In (a), (b) and (c) we do not consider a substrate; for comparison, in (d), (e) and (f) a $SiO_2$ substrate ($\varepsilon_s = 3.9$) is located at $z \leq z_s = -1.5$ nm. The proton is indicated with a black point.

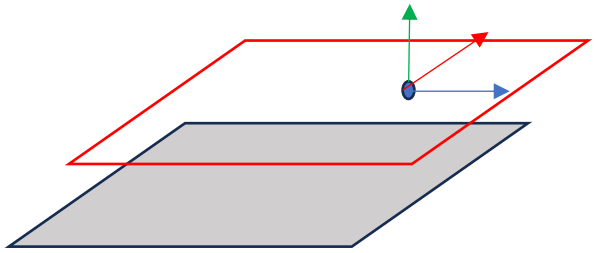

Perturbed density

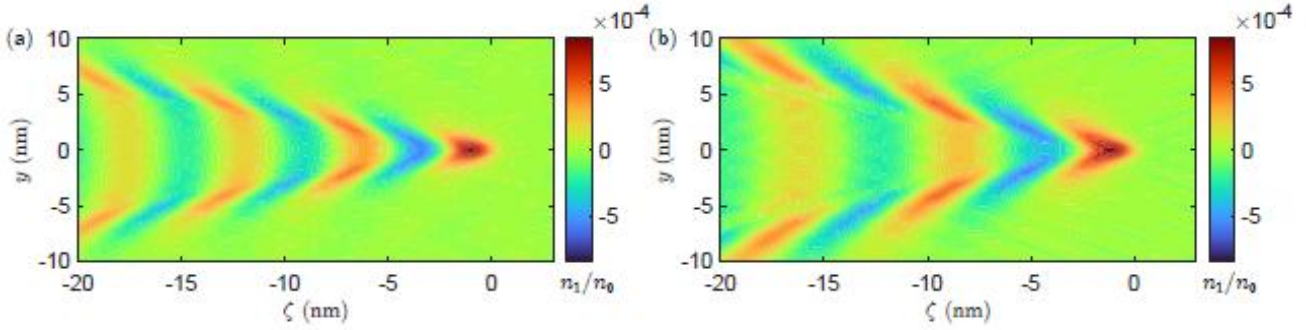


**Figure 6.** (a) Perturbed density $n_1/n_0$ in the graphene surface (i.e. at the plane $z_1 = -1$ nm) for a proton traveling on the $x$-axis with a velocity $v = 0.05c$. In (a) we do not consider a substrate; for comparison, in (b) a $SiO_2$ substrate ($\varepsilon_s = 3.9$) is located at $z \leq z_s = -1.5$ nm.

# 4. Graphene layers (with dielectrics)

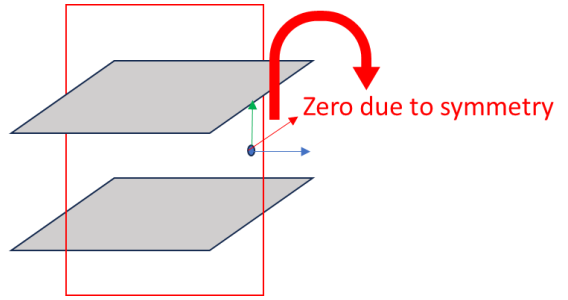


- Bi-layer

No substrate | Infinite substrate | Finite substrate | Two finite substrates

Longitudinal

Transverse

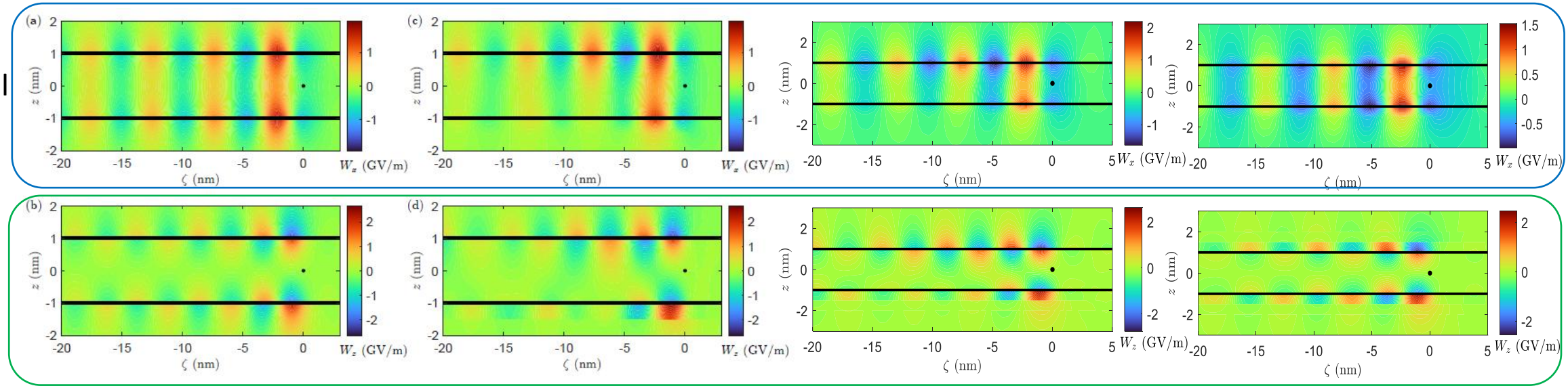


**Figure 10.** Induced wakefields (a) $W_x$ and (b) $W_z$ in the $\zeta z$-plane for a proton traveling on the $x$-axis with a velocity $v = 0.05c$. The graphene layers are located at $z_1 = -1$ nm and $z_2 = 1$ nm. In (a) and (b) we do not consider a substrate; for comparison, in (c) and (d) a $SiO_2$ substrate ($\varepsilon_s = 3.9$) is located at $z \leq z_s = -1.5$ nm. The proton is indicated with a black point and the graphene layers with black lines.

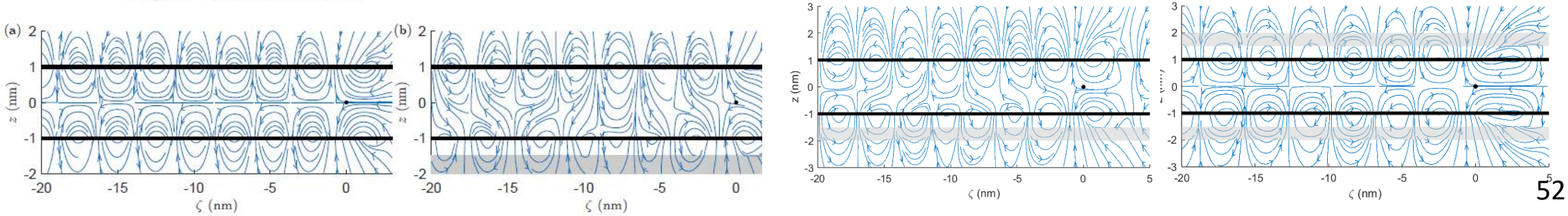

# 4. Graphene layers

- Multi-layer

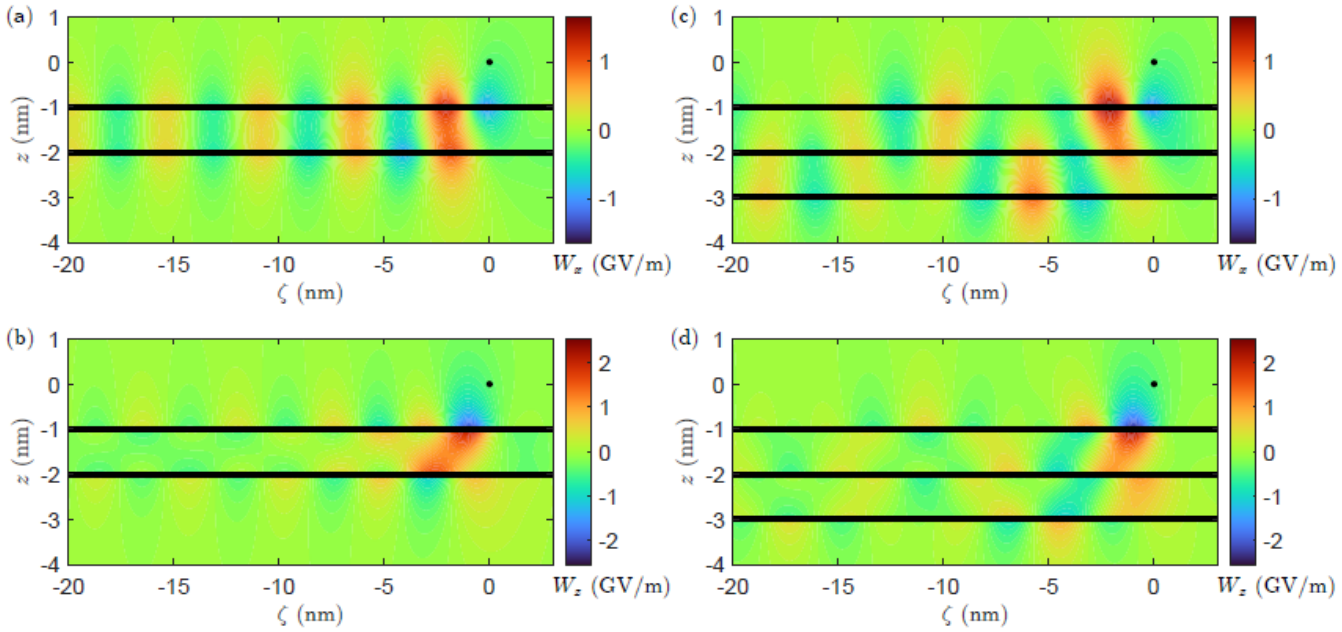


**Figure 18.** Induced wakefields (a) $W_x$ and (b) $W_z$ in the $\zeta z$-plane for a proton traveling on the $x$-axis with a velocity $v = 0.05c$ above two graphene layers located at $z_1 = -2\,\text{nm}$ and $z_2 = -1\,\text{nm}$. For comparison, in (c) and (d) we consider three layers at $z_1 = -3\,\text{nm}$, $z_2 = -2\,\text{nm}$, and $z_3 = -1\,\text{nm}$. The proton is indicated with a black point and the graphene layers with black lines.

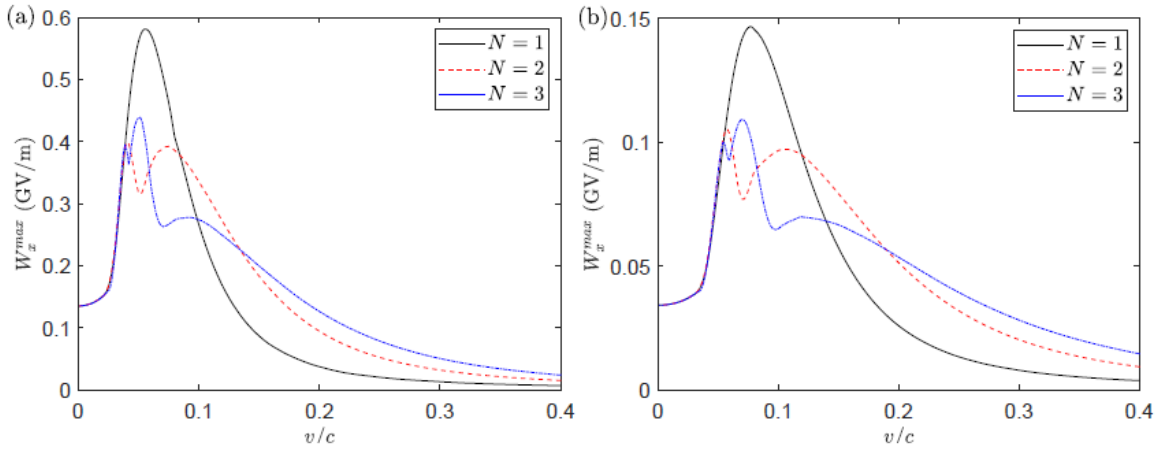


**Figure 19.** Maximum longitudinal wakefield $W_x^{max}$ as a function of the driving velocity for different number of graphene layers $N$. The graphene layers are located at $z_j = (j - 1 - N)d$, where $d$ is the inter-layer distance: (a) $d = 1\,\text{nm}$ and (b) $d = 2\,\text{nm}$.

Peaks similar to MWCNTs

# 4. Graphene layers

- Multi-layer

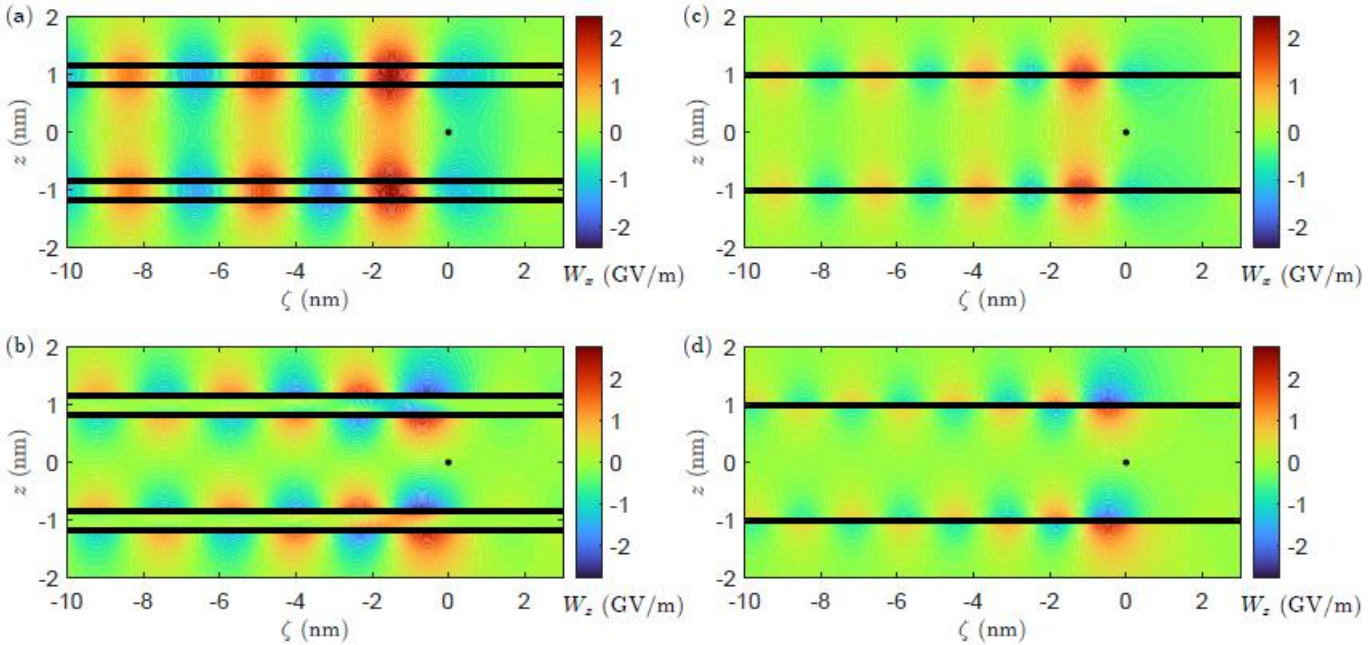


**Figure 20.** Induced wakefields (a) $W_x$ and (b) $W_z$ in the $\zeta z$-plane for a proton traveling on the $x$-axis with a velocity $v = 0.05c$. The graphene layers are located at $z_4 = -z_1 = 1.17$ nm and $z_3 = -z_2 = 0.83$ nm. For comparison, in (c) and (d) we consider two layers at $z_2 = -z_1 = 1$ nm with $n_0 = 2n_g$. The proton is indicated with a black point and the graphene layers with black lines.

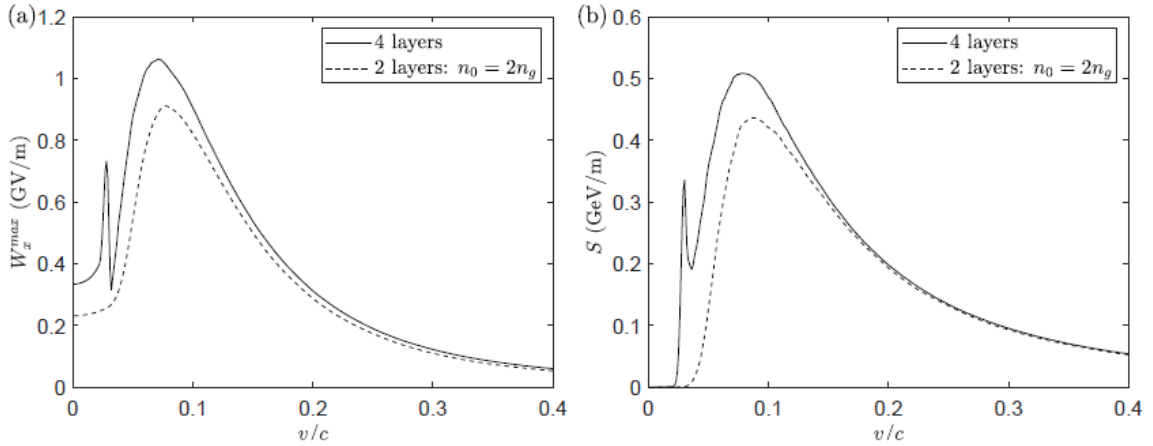


**Figure 21.** (a) Maximum longitudinal wakefield $W_x^{max}$ and (b) stopping power as a function of the driving velocity for the same configurations that Figure 20, i.e. 4 layers at $z_4 = -z_1 = 1.17$ nm and $z_3 = -z_2 = 0.83$ nm vs 2 layers at $z_2 = -z_1 = 1$ nm with $n_0 = 2n_g$.

Close graphene layer behave as single layer with higher surface density

# 5. Conclusions

- Plasmonic excitations in carbon nanostructures (CNT and graphene layers) have been studied using a linearized hydrodynamic model
- For a single-walled CNT, the optimum radius is given by $a_{opt}[\mathrm{nm}] \approx 156.55 \frac{\beta_v^2}{n_0\left[10^{20}\,\mathrm{m}^{-2}\right]}$
- For multi-walled CNTs (N walls) there is up to N resonant frequencies for each azimuthal mode *m*.
- The amplitudes have been related with the resonant frequencies.
- If the walls are very close, they behave as a SWCNT with $n_0 = N n_g$ and a higher wakefield can be obtained
- In **CNTs**, a witness beam could experience **simultaneously acceleration and focusing**, but in graphene layers is not posible (although the defocusing may be very low for a symmetric configuration, e.g. bi-layer)
- The maximum longitudinal wakeifeld in CNTs and bi-layer graphene has a similar qualitative behaviour, although lower for graphene because the field spreads in the layer planes
- Comparison with PIC simulations shows good agreement: **in progress**

# 6. Published works

- "Hydrodynamic Model for Particle Beam-Driven Wakefield in Carbon Nanotubes", Journal of Physics: Conference Series **2687** (2024), 042005. https://doi.org/10.1088/1742-6596/2687/4/042005 — Preliminaries
- "Excitation of wakefields in carbon nanotubes: a hydrodynamic model approach", New Journal of Physics **25** (2023), 123029. https://doi.org/10.1088/1367-2630/ad127 — SWCNT
- "Plasmonic excitations in double-walled carbon nanotubes", Results in Physics **60** (2024), 107698. https://doi.org/10.1016/j.rinp.2024.107698 — DWCNT
- "Excitation of Plasmonic Wakefields in Multi-Walled Carbon Nanotubes: A Hydrodynamic Approach", IntechOpen, 2024. http://dx.doi.org/10.5772/intechopen.114270 — SWCNT+DWCNT
- "Plasmonic Excitations in Carbon Nanotubes: PIC Simulations vs Hydrodynamic Model", IntechOpen, 2024. http://dx.doi.org/10.5772/intechopen.1006820 — PIC in CNTs
- "Wakefield excitation and stopping power in multi-walled carbon nanotubes: one- and two-fluid model", submitted to Journal of Physics D: Applied Physics (under review) — MWCNT
- "Plasmonic excitations in graphene layers", submitted to Chinese Journal of Physics (minor revision) — Graphene (with possible substrate)
- "Plasmonic excitations in carbon nanostructures: carbon nanotubes vs graphene", accepted at IntechOpen — CNT vs Graphene

Thank you for your attention

# BACKUP SLIDES

# 4. Graphene layers (restoring frequencies)

$$\ddot{\xi}_\nu + \omega_{\nu r}^2 \xi_\nu - s_\nu^2 \nabla_s^2 \xi_\nu = \frac{1}{m_\nu^*}[V_{\text{ext}}(\mathbf{r}_s, t) - e\Phi_{\text{ind}}(\mathbf{r}_s, t)]$$

Harmonic oscillator (interaction with ions)

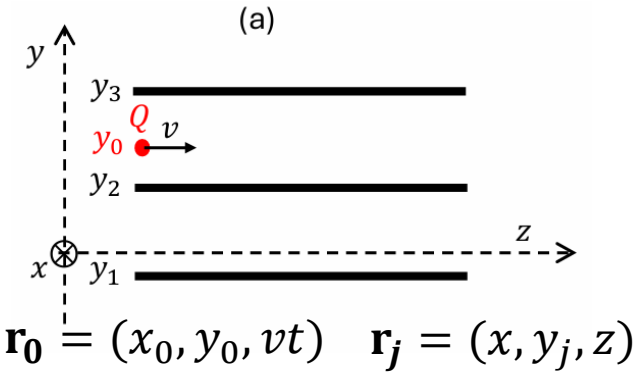


- Matrix equation:

$$S_j(\mathbf{k}, \omega)\tilde{n}_j(\mathbf{k}, \omega) - \sum_l G_{jl}(\mathbf{k})\tilde{n}_l(\mathbf{k}, \omega) = B_j(\mathbf{k}, \omega)$$

$$S_j(\mathbf{k}, \omega) = \omega(\omega + i\gamma_j) - \alpha_j k^2 - \beta k^4 - \omega_{r_j}^2$$

$$G_{jl}(\mathbf{k}) = 2\pi n_0 k e^{-k|y_j - y_l|},$$

$$B_j(\mathbf{k}, \omega) = -n_0 k^2 \tilde{\Phi}_0(\mathbf{k}, y_j, \omega)$$

$$n_j(\mathbf{R}, y, t) = \frac{4}{(2\pi)^3}\int_0^\infty \int_0^\infty \text{Re}[\tilde{n}_j(\mathbf{k}, y, k_z v)e^{ik_z\zeta}]\cos(k_x x)dk_x dk_z,$$

$$\Phi_{\text{ind}}(\mathbf{R}, y, t) = \frac{4}{(2\pi)^3}\int_0^\infty \int_0^\infty \text{Re}[\tilde{\Phi}_{\text{ind}}(\mathbf{k}, y, k_z v)e^{ik_z\zeta}]\cos(k_x x)dk_x dk_z$$

# 4. Graphene layers (restoring frequencies)

PHYSICAL REVIEW B **84**, 155416 (2011)

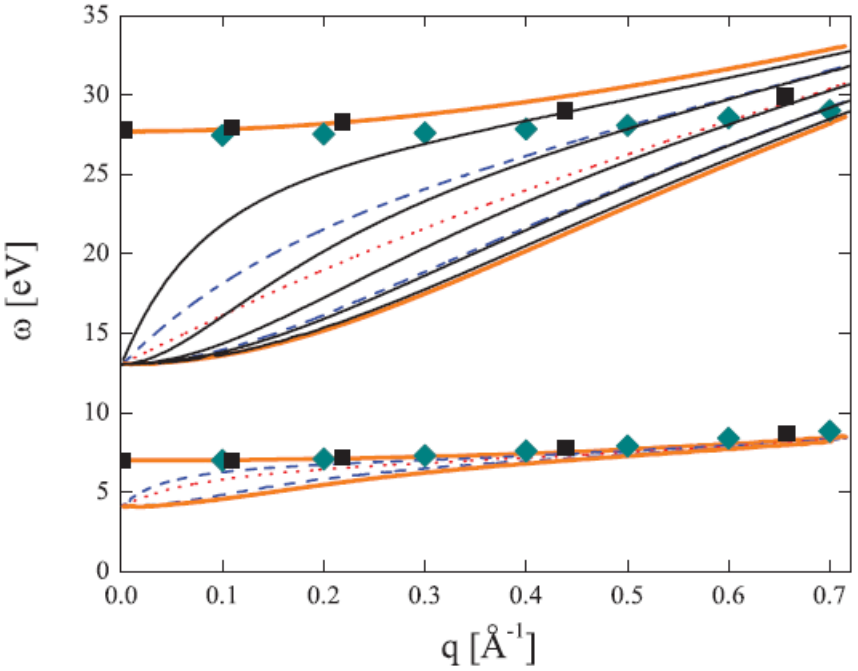


FIG. 3. (Color online) Dispersion curves for the $\pi$ (lower group) and $\sigma + \pi$ (upper group) plasmons in MLG, obtained from the LEG model with $N = 1$ [dotted (red) lines] and $N = 2$ [dashed (blue) lines], as well as $N = 5$ [only the upper group is shown by (black) solid lines]. The upper and the lower edges are shown for both the $\pi$ and $\sigma + \pi$ plasmon bands in HOPG [thick (orange) solid lines]. The (dark cyan) diamonds show the experimental plasmon peak positions in the EEL spectra of HOPG from Ref. 50, whereas the (black) squares show the peak positions obtained by *ab initio* calculations for graphite in Ref. 18.

Linearized hydrodynamic model

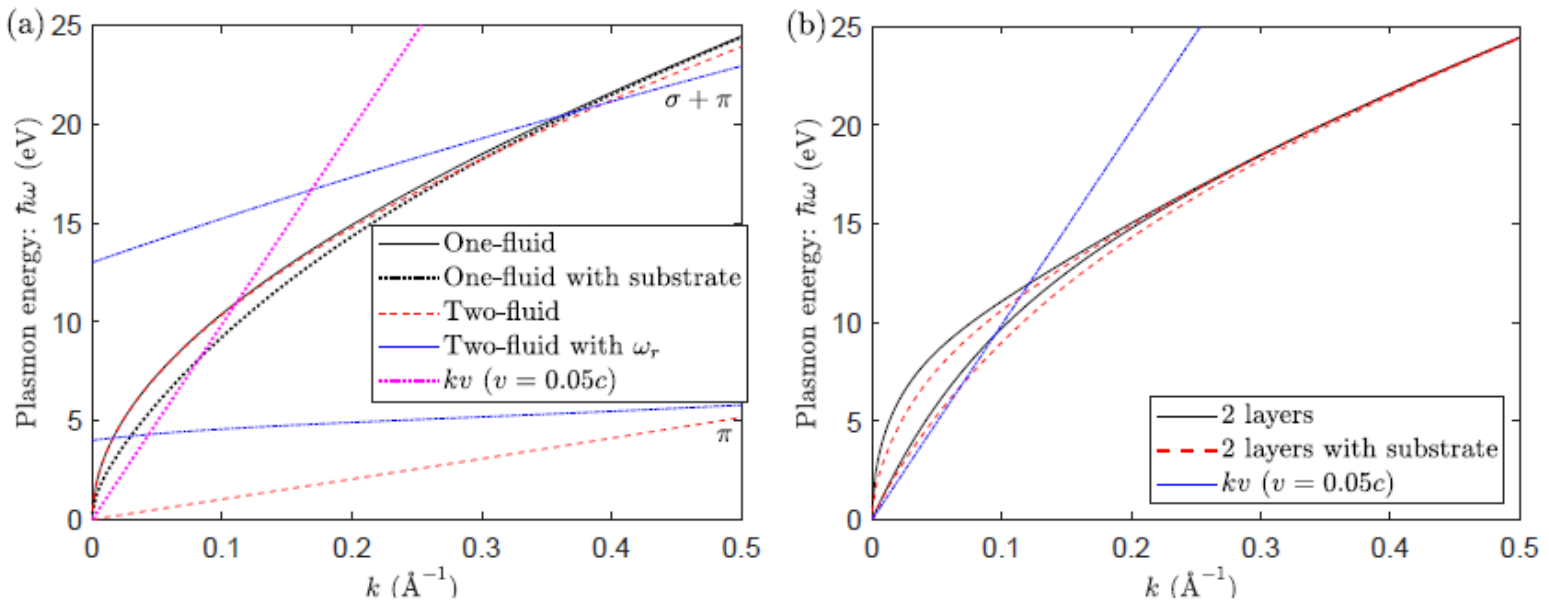


**Figure 2.** (a) Dispersion curves for a single graphene layer using a one-fluid model and a two-fluid model. In the case of the one-fluid we have plotted the dispersion relation if a $SiO_2$ substrate ($\varepsilon_s = 3.9$) is located 0.5 nm below the graphene layer. For completeness, we include the dispersion curves considering the two-fluid model with the restoring frequencies $\omega_{r_1} = \omega_{r_\pi} \approx 4\,\text{eV}$ and $\omega_{r_2} = \omega_{r_\sigma} \approx 13\,\text{eV}$ (see Appendix). The numerical values of $\omega_{r_j}$ are based on a fit to an experimental electron energy loss spectra [34]. (b) Dispersion curves for two graphene layers separated 2 nm ($z_2 - z_1 = 2\,\text{nm}$) without and with a $SiO_2$ substrate located 0.5 nm below the graphene layer (i.e. $z_1 - z_s = 0.5\,\text{nm}$). The intersection of the $kv$-line (depicted for $v = 0.05c$) with each dispersion curve indicates the minimum wavenumber that can be excited of that plasmonic mode.

# 4. Graphene layers (restoring frequencies)

Typical hydrodynamic model

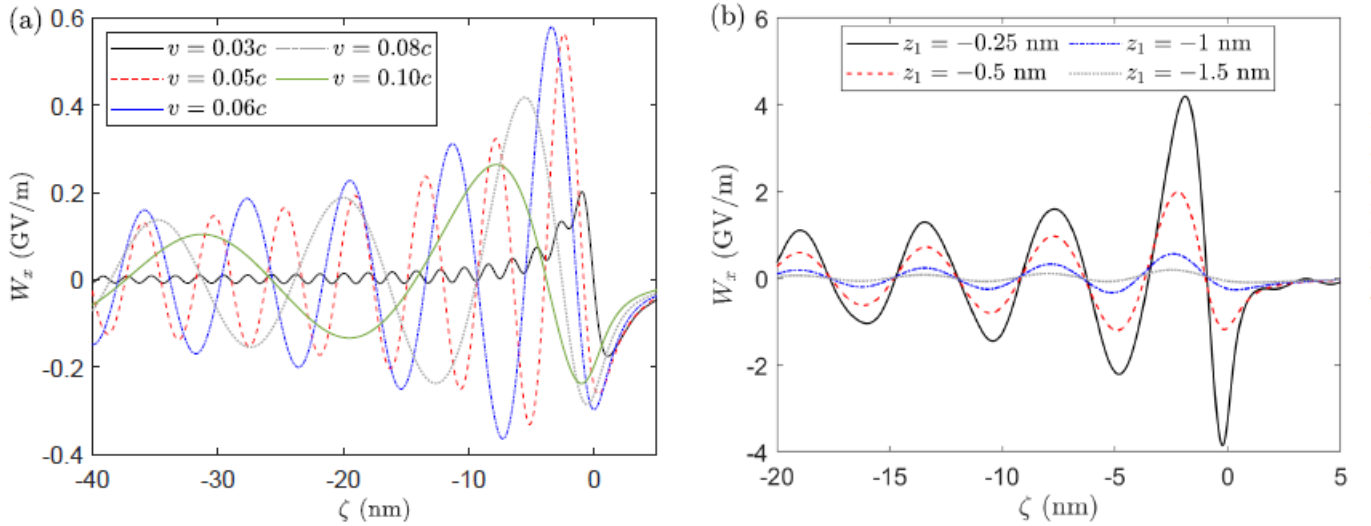


**Figure 7.** Induced longitudinal wakefield $W_x$ along the $x$-axis for a proton traveling on the $x$-axis for different (a) velocities $v$, (b) positions of the graphene layer $z_1$, (c) surface densities $n_{01}$ and (d) positions of the $SiO_2$ substrate with $\varepsilon_s = 3.9$. In all cases, unless otherwise indicated in the corresponding legend, we do not consider a substrate and use the following parameters: $v = 0.05c$, $z_1 = -1$ nm and $n_{01} = n_g$. In (c) it is also considered the two-fluid case where $\sigma$ and $\pi$ electrons are treated as separately fluids, i.e. we assume two layers with $z_1 = z_2$ and $n_{01} = 0.75n_g$, $n_{02} = 0.25n_g$.

Single layer with two-fluid model

Restoring frequencies

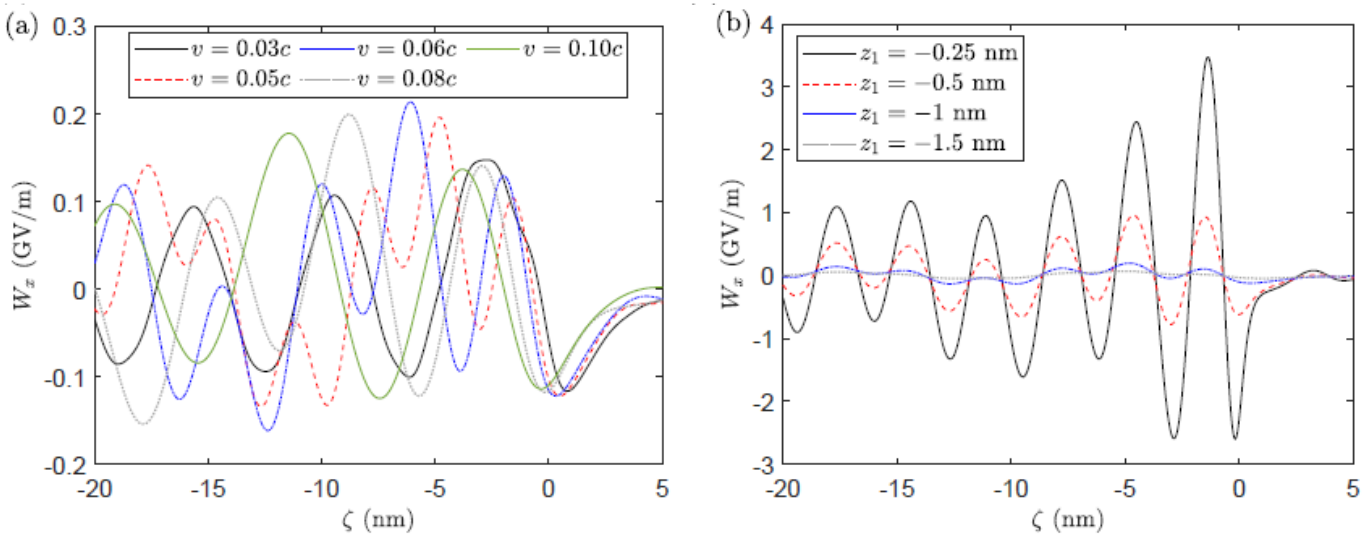


**Figure A.1.** Induced longitudinal wakefield $W_x$ along the $x$-axis for a proton traveling on the $x$-axis for different (a) velocities $v$, (b) positions of the graphene layer $z_1$ and (c) positions of the $SiO_2$ substrate with $\varepsilon_s = 3.9$ using the two-fluid model with restoring frequencies. In all cases, unless otherwise indicated in the corresponding legend, we do not consider a substrate and use the following parameters: $v = 0.05c$, $z_1 = z_2 = -1$ nm, $n_{01} \equiv n_\pi = 0.25n_g$, $n_{02} \equiv n_\sigma = 0.75n_g$, $\omega_{r_1} \equiv \omega_{r_\pi} = 4$eV and $\omega_{r_2} \equiv \omega_{r_\sigma} = 13$eV.

More complicated pattern because both frequencies are excited if restoring frequencies are taken into account

# 4. Graphene layers (restoring frequencies)

Typical hydrodynamic model

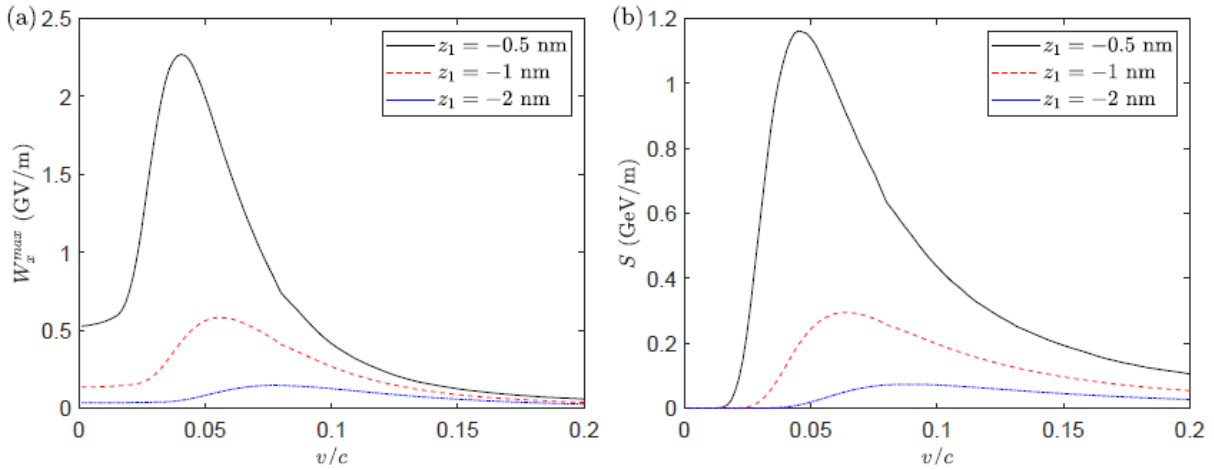


**Figure 8.** (a) Maximum longitudinal wakefield $W_x^{max}$ and (b) stopping power as a function of the driving velocity for different values of the position $z_1$ of the graphene layer.

Single layer with two-fluid model

First (low v) or second peak (high v) after driver

Restoring frequencies

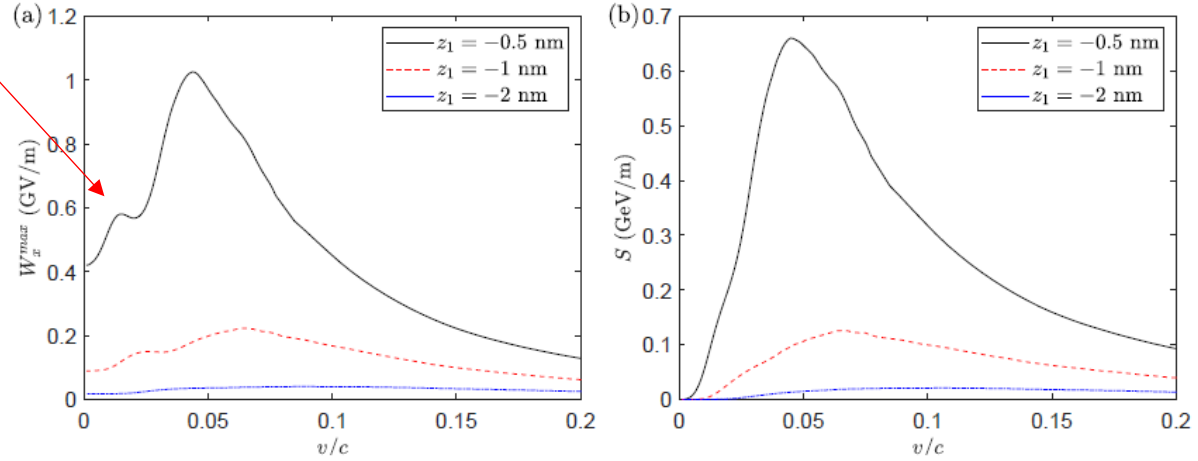


**Figure A.2.** (a) Maximum longitudinal wakefield $W_x^{max}$ and (b) stopping power as a function of the driving velocity for different values of the position $z_1$ of the graphene layer considering the two-fluid model with restoring frequencies.

Same behavior, but lower values

# 4. Graphene layers (restoring frequencies)

Typical hydrodynamic model

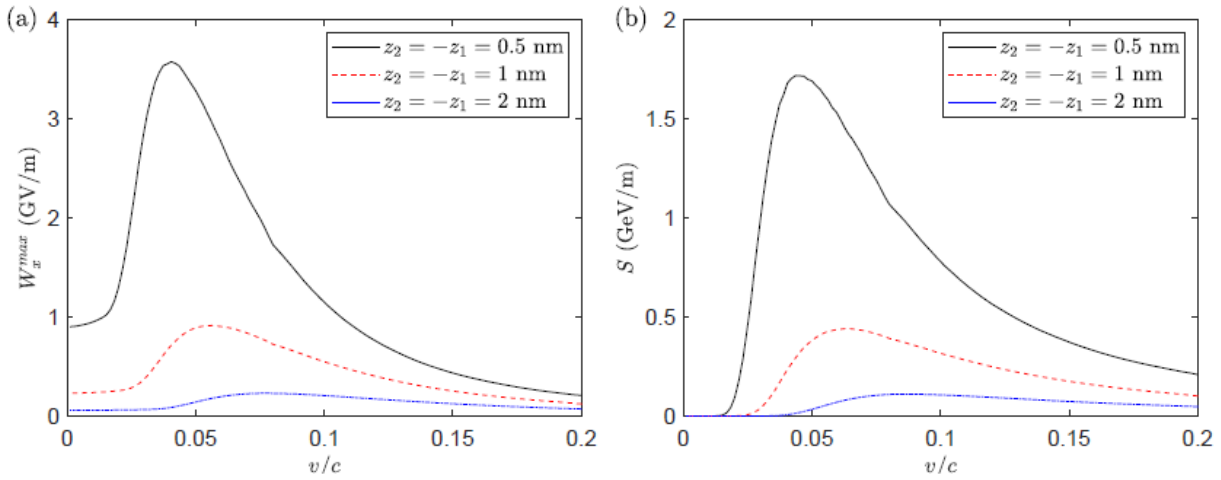


**Figure 16.** (a) Maximum longitudinal wakefield $W_x^{max}$ and (b) stopping power as a function of the driving velocity for different values of the position of the graphene layers.

First (low v) or second peak (high v) after driver

Restoring frequencies

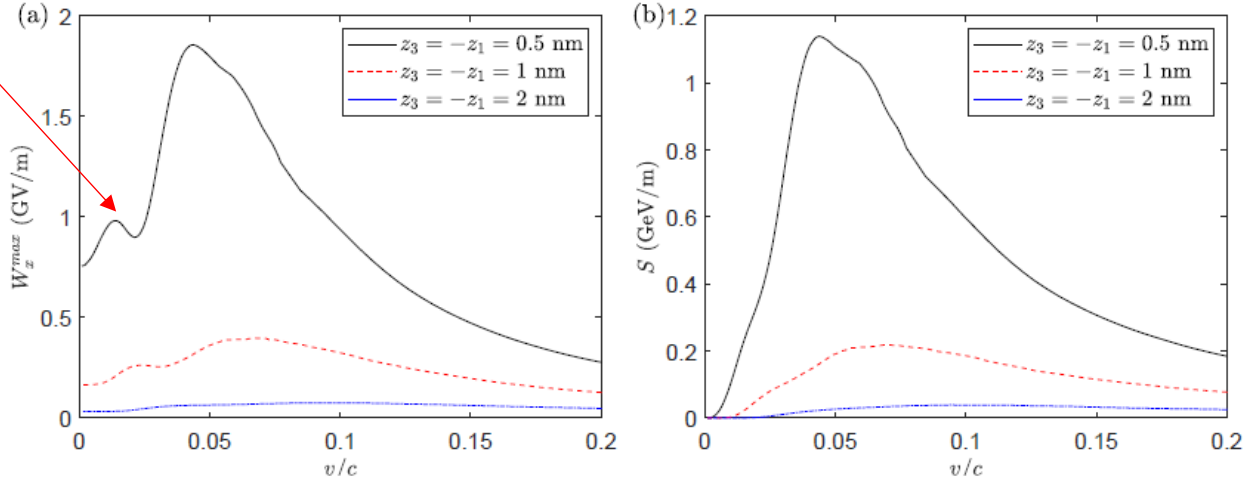


**Figure A.3.** (a) Maximum longitudinal wakefield $W_x^{max}$ and (b) stopping power as a function of the driving velocity for different values of the position of the graphene layers considering the two-fluid model with restoring frequencies in both graphene layers.

Bi-layer with two-fluid model

Same behavior, but lower values

# 4. Conclusions and outlook

- We have presented a **linear hydrodynamic model for wakefield excitation** by charges in multi-walled nanotubes.
- A driver particle can excite **plasmons** in nanotubes.
- In the **limit $\gamma \to 0^+$** we can **calculate easily the excited wakefield** and the dependences on the different parameters, which allows to perform a fast optimization of the CNT parameters.
- **All the calculations** have been made for the **mode m=0** (since if r0=0 is the only mode excited). **Higher modes are less important**, but they are not negligible if the driver is off-axis near to the surface.
- The results show **>GV/m fields** and are **qualitatively similar to the PIC simulations** and the order of magnitude is similar. Systematic comparisons with PIC simulations are ongoing.
- Published papers (SWCNTs): https://doi.org/10.1088/1367-2630/ad127c (New J. Phys.), https://iopscience.iop.org/article/10.1088/1742-6596/2687/4/042005/meta (*J. Phys.: Conf. Ser.)*
- Submitted paper to *Results in Physics* about DWCNTs: https://arxiv.org/abs/2401.08334